



QEX

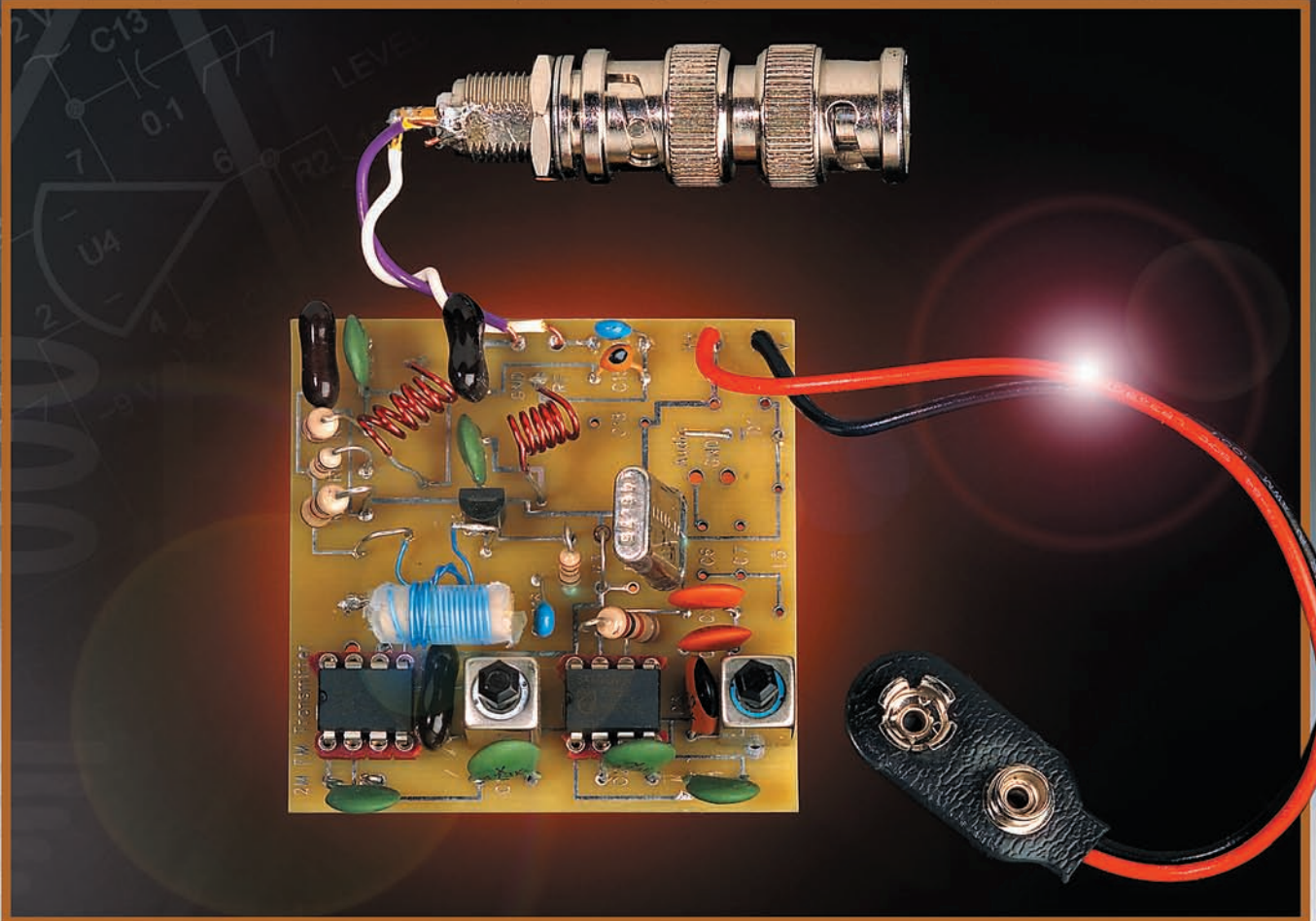
\$5

July/August 2008

www.arrl.org

A Forum for Communications Experimenters

Issue No. 249



KA5GSQ describes a crystal-controlled oscillator using SA602 ICs as frequency doublers to produce a 145.680 MHz output.

ARRL *The national association for*
AMATEUR RADIO

225 Main Street
Newington, CT USA 06111-1494



Two of the **LIGHTEST** and **MOST COMPACT** Amplifiers in the Industry!



HL-1.5KFX

HF/50MHz Linear Power

Features

- Solid State.
- The amplifier's decoder changes bands automatically with most ICOM, Kenwood, Yaesu.
- The amp utilizes an advanced 16 bit MPU (microprocessor) to run the various high speed protection circuits such as overdrive, high antenna SWR, DC overvoltage, band miss-set etc.
- Built in power supply.
- AC (200/220/235/240V) and (100/110/115/120V) selectable.
- Equipped with a control cable connection socket, for the HC-1.5KAT, auto antenna tuner by Tokyo Hy-Power Labs.

Specifications

Frequency:
1.8 ~ 28MHz all amateur bands including WARC bands and 50MHz

Mode:
SSB, CW, RTTY

RF Drive:
85W typ. (100W max.)

Output Power:
HF 1kW PEP max.
50MHz 650W PEP max.

Circuit:
Class AB parallel push-pull

Cooling Method:
Forced Air Cooling

AC Power:
AC 240V default (200/220/235) – 10 A max.
AC 120V (100/110/115) – 20 A max.

Dimensions:
10.7 x 5.6 x 14.3 inches (WxHxD)/272 x 142 x 363 mm

Weight:
Approx. 20kgs. or 45.5lbs.

Optional Items:
Auto Antenna Tuner (HC-1.5KAT)
External Cooling Fan (HXT-1.5KF for high duty cycle RTTY)

Accessories Included:
Band Decoder Cables included for Kenwood, ICOM and some Yaesu



HL-1.2KFX

750W PEP Desktop Linear

Features

- Solid State.
- This world-class compact 750W HF amplifier is the easiest to handle and operate.
- The amplifier's broadband characteristics require no further tuning once the operating band is selected.
- The amplifier allows operation in full break-in CW mode due to the use of the amplifier's high speed antenna relays
- Quiet operation allows for even the weakest DX signals
- The amp utilizes a sophisticated circuit to run the various high speed protection circuits.

Specifications

Frequency:
1.8 - 28MHz all amateur bands including WARC bands

Mode:
SSB, CW, RTTY

RF Drive:
75 - 90W

Output Power:
SSB 750W PEP max.,
CW 650W, RTTY 400W

Circuit:
Class AB parallel push-pull

Cooling Method:
Forced Air Cooling

AC Power:
1.4kVA max. when TX
AC 100/110/115/120V,
AC 200/220/230/240V

Dimensions:
9.1 x 5.6 x 14.3 inches (WxHxD)

Weight:
Approx. 33lbs.

More Fine Products from TOKYO HY-POWER



HC-1.5KAT

HF 1.5KW
Auto Tuner



HL-350V DX

VHF 330W
Amplifier



HC-200AT

HF/6m 200W
Auto Tuner
Lightning Tuning Speed



TOKYO HY-POWER LABS., INC. – USA
Technical Support
28301 Tomball Parkway, Suite #500-210
Tomball, TX 77375
Phone 713-818-4544
e-mail: thpsupport@airmail.net

TOKYO HY-POWER LABS., INC. – JAPAN
1-1 Hatanaka 3chome, Niiza Saitama 352-0012
Phone: +81 (48) 481-1211 FAX: +81 (48) 479-6949
e-mail: info@thp.co.jp
Web: <http://www.thp.co.jp>



Exclusively from Ham Radio Outlet!

www.hamradio.com

Western US/Canada 1-800-854-6046	Southeast 1-800-444-7927	Northeast 1-800-644-4476
Mountain/Central 1-800-444-9476	Mid-Atlantic 1-800-444-4799	New England/Eastern Canada 1-800-444-0047



QEX (ISSN: 0886-8093) is published bimonthly in January, March, May, July, September, and November by the American Radio Relay League, 225 Main Street, Newington, CT 06111-1494. Periodicals postage paid at Hartford, CT and at additional mailing offices.

POSTMASTER: Send address changes to: QEX, 225 Main St, Newington, CT 06111-1494 Issue No 249

Harold Kramer, WJ1B
Publisher

Larry Wolfgang, WR1B
Editor

Lori Weinberg, KB1EIB
Assistant Editor

L. B. Cebik, W4RNL (SK)

Zack Lau, W1VT

Ray Mack, W5IFS

Contributing Editors

Production Department

Steve Ford, WB8IMY
Publications Manager

Michelle Bloom, WB1ENT
Production Supervisor

Sue Fagan, KB1OKW
Graphic Design Supervisor

David Pingree, N1NAS
Senior Technical Illustrator

Advertising Information Contact:

Janet L. Rocco, W1JLR
Business Services

860-594-0203 – Direct

800-243-7768 – ARRL

860-594-4285 – Fax

Circulation Department

Cathy Stepina, QEX Circulation

Offices

225 Main St, Newington, CT 06111-1494 USA
Telephone: 860-594-0200

Fax: 860-594-0259 (24 hour direct line)

e-mail: qex@arrl.org

Subscription rate for 6 issues:

In the US: ARRL Member \$24, nonmember \$36;

US by First Class Mail:

ARRL member \$37, nonmember \$49;

International and Canada by Airmail: ARRL member \$31, nonmember \$43;

Members are asked to include their membership control number or a label from their QST when applying.

In order to ensure prompt delivery, we ask that you periodically check the address information on your mailing label. If you find any inaccuracies, please contact the Circulation Department immediately. Thank you for your assistance.



Copyright ©2008 by the American Radio Relay League Inc. For permission to quote or reprint material from QEX or any ARRL publication, send a written request including the issue date (or book title), article, page numbers and a description of where you intend to use the reprinted material. Send the request to the office of the Publications Manager (permission@arrl.org).

July/August 2008

About the Cover

John E. Post, KA5GSQ presents a crystal-controlled oscillator using a pair of SA602 ICs as frequency doublers to produce a 145.680 MHz output. The oscillator produces harmonics at least through 800 MHz, so higher-frequency output signals could be selected with the output filter.



In This Issue

Features

3 VHF Frequency Multiplication Using the SA602 IC
By John E. Post, KA5GSQ

6 Oscillator Noise Evaluation with a Crystal Notch Filter
By Wes Hayward, W7ZOI

13 Ground System Configurations for Phased Vertical Arrays
By Al Christman, K3LC

22 Observations on Ferrite Rod Antennas
By Jack R. Smith, K8ZOA

36 Some Thoughts on Crystal Parameter Measurement
By Jim Koehler, VE5FP

42 From Spark Generators to Modern VHF/UHF/SHF Voltage Controlled Oscillators
By Ulrich L. Rohde, PhD, N1UL

Columns

47 Tech Notes
By Eric P. Nichols, KL7AJ

61 Upcoming Conferences

50 Antenna Options
By L.B. Cebik, W4RNL

61 In the Next Issue of QEX

57 Letters to the Editor

Index of Advertisers

American Radio Relay League:.....	35, 60, 62, 63, 64, Cover III
Atomic Time:.....	56
Down East Microwave Inc:.....	56
Kenwood Communications:.....	Cover IV
National RF, Inc:	46
Nemal Electronics International, Inc:.....	5
RF Parts	59, 61
Teri Software:.....	46
Tokyo Hy-Power Labs, Inc:	Cover II
Tucson Amateur Packet Radio:	49

The American Radio Relay League



The American Radio Relay League, Inc. is a noncommercial association of radio amateurs, organized for the promotion of interest in Amateur Radio communication and experimentation, for the establishment of networks to provide communications in the event of disasters or other emergencies, for the advancement of the radio art and of the public welfare, for the representation of the radio amateur in legislative matters, and for the maintenance of fraternalism and a high standard of conduct.

ARRL is an incorporated association without capital stock chartered under the laws of the state of Connecticut, and is an exempt organization under Section 501(c)(3) of the Internal Revenue Code of 1986. Its affairs are governed by a Board of Directors, whose voting members are elected every three years by the general membership. The officers are elected or appointed by the Directors. The League is noncommercial, and no one who could gain financially from the shaping of its affairs is eligible for membership on its Board.

"Of, by, and for the radio amateur," ARRL numbers within its ranks the vast majority of active amateurs in the nation and has a proud history of achievement as the standard-bearer in amateur affairs.

A *bona fide* interest in Amateur Radio is the only essential qualification of membership; an Amateur Radio license is not a prerequisite, although full voting membership is granted only to licensed amateurs in the US.

Membership inquiries and general correspondence should be addressed to the administrative headquarters:

ARRL
225 Main Street
Newington, CT 06111 USA
Telephone: 860-594-0200
FAX: 860-594-0259 (24-hour direct line)

Officers

President: JOEL HARRISON, W5ZN
528 Miller Rd, Judsonia, AR 72081

Chief Executive Officer: DAVID SUMNER, K1ZZ

The purpose of *QEX* is to:

- 1) provide a medium for the exchange of ideas and information among Amateur Radio experimenters,
- 2) document advanced technical work in the Amateur Radio field, and
- 3) support efforts to advance the state of the Amateur Radio art.

All correspondence concerning *QEX* should be addressed to the American Radio Relay League, 225 Main Street, Newington, CT 06111 USA. Envelopes containing manuscripts and letters for publication in *QEX* should be marked Editor, *QEX*.

Both theoretical and practical technical articles are welcomed. Manuscripts should be submitted in word-processor format, if possible. We can redraw any figures as long as their content is clear. Photos should be glossy, color or black-and-white prints of at least the size they are to appear in *QEX* or high-resolution digital images (300 dots per inch or higher at the printed size). Further information for authors can be found on the Web at www.arrl.org/qex/ or by e-mail to qex@arrl.org.

Any opinions expressed in *QEX* are those of the authors, not necessarily those of the Editor or the League. While we strive to ensure all material is technically correct, authors are expected to defend their own assertions. Products mentioned are included for your information only; no endorsement is implied. Readers are cautioned to verify the availability of products before sending money to vendors.

Larry Wolfgang, WR1B

lwolfgang@arrl.org

Empirical Outlook

The day after I turned in for typesetting the Antenna Options column for this issue, we received word that L. B. Cebik, W4RNL, had passed away. This was quite a shock, especially since L. B. and I had exchanged e-mails only a few days earlier. It's always sad to hear that one of our authors became a silent key, and L. B. had to be one of Amateur Radio's most prolific authors, not only for *QEX* and *QST*, but for other publications as well. Please see my introduction to this Antenna Options column in this issue for a few more words about L. B.

K1SFA Photo

On a happier note, in early June at ARRL Headquarters we celebrated with Paul Rinaldo, W4RI, to mark his 25th anniversary as a member of the ARRL staff! This was also a retirement party, although Paul will continue to work for ARRL in a variety of capacities.

Long-time *QEX* readers, will, of course, recognize Paul as the first editor of our little publication! Paul started *QEX* with issue number 1 in December 1981. With a few typewritten pages, those early issues established the standards for publishing technical material that we try to maintain with *QEX* today.

Paul moved from the Washington, DC area to Newington, CT, in 1983 to work at ARRL Headquarters as Manager of the ARRL Technical Department after M. F. "Doug" DeMaw, W1FB, retired. He went on to become the Publications Manager and Editor of *QST*. Paul was named Chief Technology Officer, and returned to the DC area to open the ARRL Technology Office. Paul has worked with the IARU on ITU World Radio Conference preparations, and has been a member of the US delegation to numerous ITU Conferences. Paul has chaired several Working Groups at those conferences over the years.

Your current editor was a young Assistant Technical Editor with about two years of experience on the ARRL Staff when Paul became Technical Department Manager. It seems to me that Paul's greatest influence at that time was one of communications. There were frequent meetings during which staff members brainstormed ideas and planned the direction of various publications.

During that time the FCC implemented the Volunteer Examiner program and I became "ARRL License Manuals Editor." I was also tasked with writing a book that had been discussed on various levels for many years, even before I had come to ARRL Headquarters. Eventually that book became *Understanding Basic Electronics*. We spent many hours gathering ideas about what Amateur Radio operators at the various license levels should know, and how to present that information in our *License Manuals* series. Likewise, the "formula" for *UBE* was hashed out with a number of significant refinements.

It was great to work for Paul during the years he was my direct supervisor and then as Publications Manager. Thanks Paul, and best wishes for a long and happy "retirement!"

This year marked my second official trip to the Dayton Hamvention. What a great time I had there! It was wonderful to meet so many *QEX* readers as well as some hams who wanted to learn more about the magazine. I also had the opportunity to meet with some of our authors for the first time, and that was also great. I don't want to tip my hand just yet on the specifics, but I am looking forward to some very interesting articles for future issues, based on some of the contacts I made there!

Of course there was so much to see and so many forums to attend. I wasn't able to attend all of the forums I would have liked to attend (after all, I had to spend *some* time in the ARRL Expo area and several interesting forums were held simultaneously), but I did manage to take in a few excellent presentations.

If I didn't get to meet you at Hamvention, I'm sorry I missed you. I hope we have another opportunity to meet during some of my other travels. If you did not have the opportunity to attend Hamvention this year, I hope you will be able to put it on your schedule for next year. Even if you aren't looking for new equipment or gadgets (and there are *plenty* of both) the opportunity to meet other hams and learn what they are doing with this great hobby of ours is wonderful.



Founding *QEX* Editor Paul Rinaldo, W4RI, and current Editor Larry Wolfgang, WR1B, share a moment to reminisce during Paul's 25 anniversary/retirement party.

VHF Frequency Multiplication Using the SA602 IC

How about a simple technique for VHF frequency generation and multiplication? Here is another application for the NE602/SA602 IC!

For a while I have wanted to build an overtone crystal oscillator/multiplier circuit in order to generate VHF signals, particularly in the 2 m band. Searching for inspiration one day, I came upon an application note produced by Philips Semiconductors in December, 1991: AN1983 *Crystal Oscillators and Frequency Multipliers Using the NE602 and NE5212*.¹ The final section of this note presents a method to employ the NE602 (now the SA602) as a frequency doubler. The circuit shown in the note produced the second harmonic by coupling the fundamental signal produced by the internal oscillator into both the LO and RF ports of the SA602 internal mixer. The mixer output contains the sum and difference of the input frequencies, in this case the second harmonic

and a dc term. The note claims that additional SA602 frequency doublers allow generation of signals up to about 500 MHz. The note also claims that a distinct advantage of this approach is that the conversion gain of the SA602 produces a second harmonic that is 10 to 15 dB higher in amplitude than the fundamental. This is much better than a passive doubler — so this circuit seemed like an excellent place to begin!

Upon reflection, I found several faults with the implementation provided in the application note. First, they used an RC network to provide a 90° phase shift between the input signals of the multiplier in order to eliminate the dc offset at the mixer output. This seems unnecessary, since capacitive coupling between the stages automatically blocks any dc. Second, although the SA602 is designed for double-ended operation, the suggested circuit was single-ended, resulting in an output power reduction of 3 dB.

A Better Approach

Overcoming these objections produced the circuit shown in Figure 1. In this circuit components Y1, C4, C5, and U1 form a simple Colpitts crystal oscillator. Diode D1 reduces the 9 V supply voltage in order to avoid exceeding (by much) the 8 V supply voltage rating for the SA602. The series resonant circuit consisting of C3 and L1 connected to the emitter of the internal transistor in the SA602 reduces the loop gain of the oscillator at the fundamental frequency and forces oscillation at the third overtone frequency of the crystal. The internal oscillator transistor is current starved, so resistor R1 is necessary to increase the bias current in order to provide sufficient loop gain at the third harmonic. This ensures that the oscillator will start. Capacitors C1 and C2 couple the fundamental frequency into the mixer RF port, while coupling to the LO port from the oscil-

¹Philips Semiconductors Applications Note AN1983, *Crystal Oscillators and Frequency Multipliers using the NE602 and NE5212*, Dec, 1991.

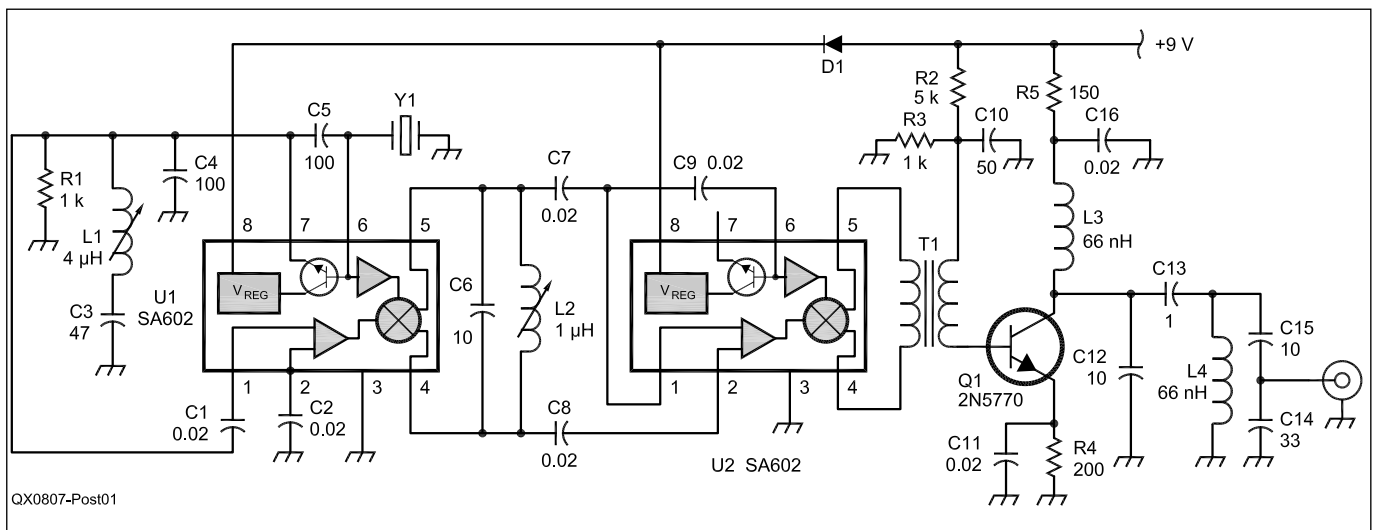


Figure 1 — VHF overtone crystal oscillator/doubler circuit.

lator is handled internally to the IC. Finally, inductor L2 and C6 form a 72 MHz bandpass filter at the mixer output. This is tuned to select the second harmonic of the oscillator, while attenuating other frequencies.

When this portion of the overtone oscillator was constructed and placed in operation a -5.7 dBm, 36.416 MHz third overtone signal was observed at pin7 of the SA602, while a -20.2 dBm, 72.849 MHz second harmonic component was observed across the bandpass filter formed by C8 and L2 across pins 4 and 5. There was no sign of the promised 10 to 15 dB conversion gain at this point!

Other harmonics of the third overtone were also observed, including the -42.0 dBm fourth harmonic at 145.680 MHz. All of these measurements are reduced by the loading effect of the 50Ω input resistance of the spectrum analyzer, but they do give some idea of the relative amplitude of the signals produced by the first SA602 oscillator/doubler circuit.

Next, components U2, C7, C8, C9, and T1 were installed and placed in operation. Transformer T1 converts the double-ended signal that is present at pins 4 and 5 of U2 to a single-ended signal required to drive the amplifier stage. Capacitively coupling the LO input of U2 (pin 6) to pin 1 seemed to provide slightly more power than capacitively coupling to either pin 2 or ground. Spectrum analyzer measurements at the secondary of T1 revealed a -12.6 dBm, 145.680 MHz fourth harmonic, while the 72.849 MHz second harmonic was down to -22.5 dBm, and the 36.416 MHz third overtone (which is the fundamental) was measured at -32.7 dBm. This equates to about 8 dB of conversion gain for the second doubler (-20.2 dBm input at 72.849 MHz and -12.6 dBm output at 145.680 MHz) — somewhat less than the 10 to 15 dB that was expected. Additional harmonics were noted at integer multiples of the 36.416 MHz third overtone, signal extending up to about 500 MHz.

The final stage in the circuit is a bandpass amplifier designed to boost the desired signal to the milliwatt level while attenuating undesired harmonic energy. Resistors R2 to R4 provide base-emitter forward bias sufficient to establish about 4 mA of collector current. Capacitor C11 bypasses the emitter resistor to avoid amplifier degeneration. Capacitor C10 was selected experimentally in order to form a series resonant circuit with the inductance of the secondary of T1 to minimize the impedance between ground and the base of Q1 and maximize output power. Inductors L3 and L4 along with capacitors C12 to C15 form a two-pole Chebyshev top-coupled bandpass filter. The top-coupled topology provides 18 dB/octave attenua-

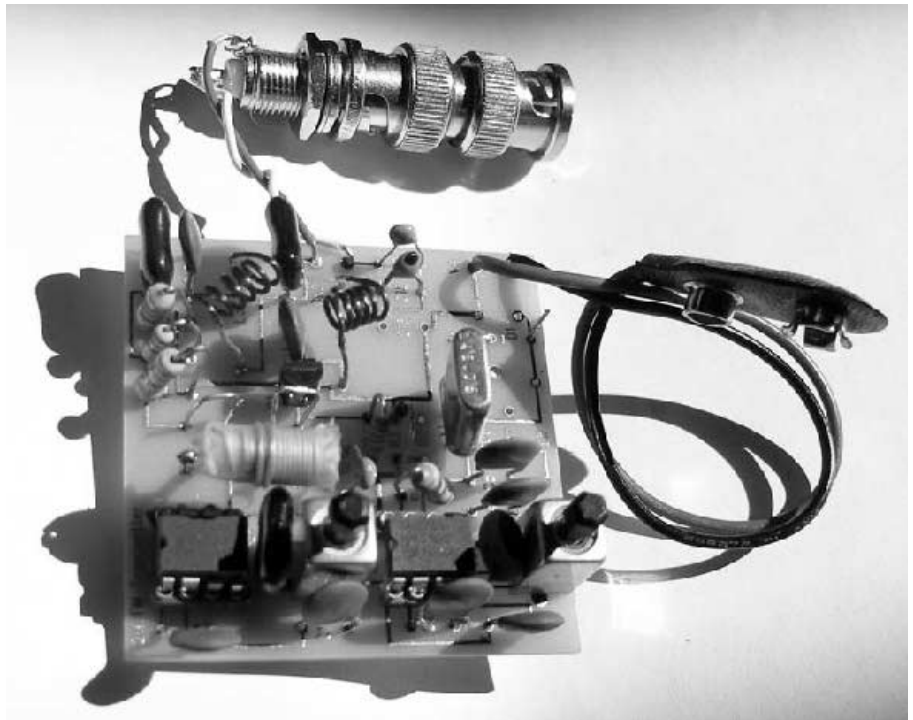


Figure 2 — This photo shows the circuit board implementation of the oscillator/doubler circuit.

tion for signals below the passband, but only 6 dB/octave attenuation for signals above the passband. Since the harmonic energy at the mixer output is highest for frequencies below the desired signal the additional attenuation provided by this filter is beneficial. Finally, Resistor R5, along with capacitor C16, decouple the amplifier from the power supply line.

Circuit Development, Construction, and Alignment

Initial experimentation was conducted by constructing the circuit on a protoboard. This makes for rapid construction and the circuits seemed to work satisfactorily, even though these boards are not recommended for use much above HF. This approach facilitated exploration of different alternatives for driving the LO and RF ports on the SA602 in order to determine which configuration maximized output power at 145.680 MHz. Once the best alternative was identified a prototype was constructed on a section of copper clad circuit board material as a ground plane, using the “dead bug” or “ugly” construction technique. For the final circuit a printed circuit board was fabricated by a commercial supplier and the parts were installed, as shown in Figure 2.

All parts except for T1, L3, L4, and Y1 are available from [\[sandkits.net\]\(http://sandkits.net\). Overtone crystals for the 2 m band are available from Ken Simpson, W8EK for \\$5 each. Contact Ken at \[w8ek@speakeasy.net\]\(mailto:w8ek@speakeasy.net\). The primary of transformer T1 was constructed by wrapping 15 turns of 30 gauge wire-wrap wire around a \$\frac{3}{8}\$ inch wooden form and securing it with tape. The T1 primary contains sufficient inductance so that when combined with the output capacitance found at pins 4 and 5 of U2 a parallel resonant circuit is formed, further suppressing harmonic energy. The T2 secondary is formed from two turns of 30 gauge wire-wrap wire wrapped around the primary coil. Inductors L2 and L3 were formed from five turns of 20 gauge copper magnet wire, sized using a \$\frac{1}{4}\$ inch form.](http://www.danssmallpart-</p></div><div data-bbox=)

Final alignment is straightforward, especially if a spectrum analyzer is available to monitor the power output. Upon power-up, adjust the slug on inductor L1 until the oscillator output is at the overtone frequency, if it is not already. The shift between fundamental and overtone modes as L1 is adjusted is quite dramatic and makes for interesting viewing on the analyzer. Next, adjust the slug on inductor L2 to maximize output power. Finally, adjust the turn spacing for L3 and L4 slightly to “tune” the bandpass filter and maximize the output power at the selected frequency.

Table 1
Output Power for the Circuit

Frequency (MHz)	Output power (dBm)
36.42	-33.6
72.84	-30.0
109.25	-37.3
145.69	-0.5
182.12	-33.5
218.54	-33.5
254.95	-58.0

Circuit Performance and Applications

The circuit produces approximately 0.9 mW of output power at 145.680 MHz while consuming 18 mA from a 9 V source, or 162 mW of power. Table 1 shows the measurement results at the output of the circuit obtained using the spectrum analyzer. Harmonic energy measures at 1 μ W or less, well below the 10 μ W FCC requirement for sources of this power level. Thus, when connected to a suitable antenna this circuit is usable as a miniature 2 m transmitter for fox hunting applications. Other applications could include a VHF signal source for use in transmitter and receiver projects. I hope this article inspires you to think about other new applications for the SA602!

[When KA5GSQ sent his oscillator to us for the cover photo, we took that opportunity to look at the oscillator output in the ARRL Lab. ARRL Lab Test Engineer, Bob Allison, WB1GCM, powered up the oscillator and fed the output to the spectrum analyzer, then captured the display as Figure 3. The 0 dB reference level was set to 0 dBm, with no input attenuation. The 145.680 MHz desired output signal is about 2 mW. Harmonic energy at frequencies above and below the 145.680 MHz output signal is less than 1 μ W, well below the 10 μ W FCC spectral output requirement for sources at this power level. — Ed.]

John E. Post is an assistant professor of electrical and computer engineering with Embry-Riddle Aeronautical University in Prescott, AZ. He holds an Amateur Extra class license, KA5GSQ, and has BS, MS, and PhD degrees in electrical engineering.

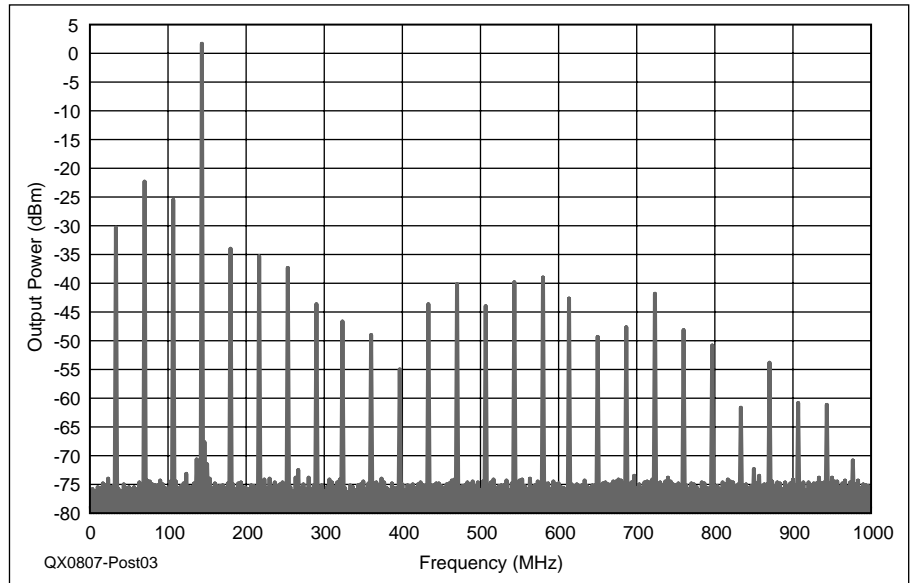


Figure 3 — The oscillator spectral output as measured in the ARRL Lab. Notice the harmonic-rich output, with signals stronger than -55 dBm through at least 800 MHz. We did not “tweak” the author’s filter tuning for this measurement.



We Design And Manufacture To Meet Your Requirements

***Prototype or Production Quantities**

800-522-2253

This Number May Not Save Your Life...

But it could make it a lot easier! Especially when it comes to ordering non-standard connectors.

RF/MICROWAVE CONNECTORS, CABLES AND ASSEMBLIES

- Specials our specialty. Virtually any SMA, N, TNC, HN, LC, RP, BNC, SMB, or SMC delivered in 2-4 weeks.
- Cross reference library to all major manufacturers.
- Experts in supplying “hard to get” RF connectors.
- Our adapters can satisfy virtually any combination of requirements between series.
- Extensive inventory of passive RF/Microwave components including attenuators, terminations and dividers.
- No minimum order.



NEMAL ELECTRONICS INTERNATIONAL, INC.

12240 N.E. 14TH AVENUE
NORTH MIAMI, FL 33161

TEL: 305-899-0900 • FAX: 305-895-8178

E-MAIL: INFO@NEMAL.COM

BRASIL: (011) 5535-2368

URL: WWW.NEMAL.COM

Oscillator Noise Evaluation with a Crystal Notch Filter

*Do you need to characterize the noise performance of an oscillator project?
Read on to learn how.*

Among the most common projects built by radio amateurs are oscillators and frequency synthesizers. These are often parts for a larger project. A critical performance specification of any oscillator system is noise. Many contemporary synthesizers use direct digital methods which are plagued by spurious outputs. Yet noise and spurs are rarely evaluated by the builders, for they are both difficult to measure. This article presents a simple and inexpensive method that will allow almost any experimenter to examine the oscillator systems that he or she creates. Although limited in frequency, the method takes that first step toward meaningful evaluation.

The Problem

The output of a high quality traditional LC oscillator is shown in Figure 1. This figure is not an output from an actual measurement. Rather, it is a sketch of what we would see if a *real circuit* was evaluated with an *ideal* spectrum analyzer. The resolution bandwidth for the analyzer is arbitrarily set to 500 Hz. The data of Figure 1 could also be obtained with an ideal receiver. The *ideal* analyzer or receiver has an unbounded dynamic range not found in real-world instruments. The oscillator has an output power of a few milliwatts with noise that is over 125 dB lower in a 500 Hz bandwidth.

It is vitally important that some bandwidth information be included with any signal to noise measurement. We often see statements such as "The noise was 90 dB below the carrier." This statement means nothing without bandwidth information, for the power related to noise is directly proportional to the bandwidth of observation. If we examine noise with a spectrum analyzer, the displayed noise will increase by 10 dB if the bandwidth is

increased by 10. In the same sense, if we are listening to noise in a receiver, the noise we hear will decrease when we switch from a SSB to a narrower CW bandwidth. The usual practice with the noise measurement of oscillators is to normalize the results to a 1 Hz bandwidth. The oscillator data of Figure 1 will be normalized later when the measurement is described.

As we will learn later in the paper, the Figure 1 example is not an exotic special purpose synthesizer, but a fundamental, very practical circuit that many of us have built, a JFET Hartley oscillator using an LC resonator. Yet it easily exceeds the noise performance found in most commercially built ham equipment.

Oscillator noise would be much easier to measure if we merely attenuated the very strong carrier. An 80 dB reduction of the carrier strength in Figure 1 would leave the

carrier and noise of Figure 2. A spectrum analyzer or receiver with a dynamic range of a mere 50 dB could now perform the measurement.

Virtually all of the schemes that we normally use to measure oscillator noise are nothing more than clever methods to eliminate or attenuate the carrier. These often elegant and interesting methods are found in the literature.¹ Even though oscillator noise is difficult to measure, it can present major practical limitations to our ham gear.² Local oscillator noise is probably the defining limitation in most of the equipment we now use for communications.

The devoted experimenter striving for the best possible oscillator performance can certainly build his or her own system for noise evaluation.³ But this is a difficult and time

¹Notes appear on page 12.

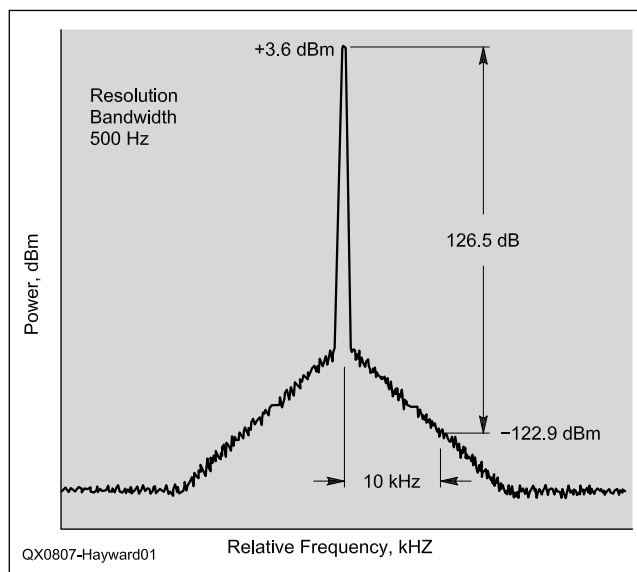


Figure 1 — The signal from an oscillator as viewed in an ideal spectrum analyzer with a bandwidth of 500 Hz. There is nothing special about that bandwidth; it was chosen as a common, practical value typically found in receivers.

consuming chore. We seek a solution that is simple enough for the more casual experimenter to use to evaluate oscillator noise.

A Crystal Notch Filter

A strong carrier can be significantly attenuated with a narrow bandwidth notch filter. The filter must be narrow, for we wish to measure noise that is close to the carrier. But the notch must be deep, for considerable carrier attenuation is needed. A suitable circuit is possible if quartz crystals are used. One route to designing a crystal notch filter is outlined in Figure 3. The simplest such filter is realized by inserting a crystal as a shunt element in a 50 Ω system, shown in Figure 3A. The notch depth is limited in this topology. Greater depth is realized if several crystals are used. Several crystals can be paralleled in the simplest filter. A much more effective scheme, however, isolates the crystals with sections of transmission line, shown in Figure 3B where three crystals are applied. Transmission line sections are impractical at the frequencies where we would normally use crystals. But a quarter wavelength of line is easily synthesized with a pi network as shown in Figure 3C. Recall that a symmetrical pi network operating at one frequency with $Q = 1$ ($X_L = X_C = R_0$) exhibits a 90° phase shift and most other properties of a quarter wave line. Finally, a deeper null is possible with a given crystal if we transform upward from 50 Ω.

The first experimental notch filter that I built at 5 MHz is shown in Figure 4. A filter impedance of 471 Ω allowed the use of 15 μH inductors from the junk box in the phase shifting π networks. The filter was terminated with L-networks that transformed the 471 Ω to 50 Ω, also realized with available RF chokes. The measured transfer function for the filter is shown in Figure 5. The notch depth is 75 dB, but the 1 dB width is well under 1 kHz. I used crystals within 10 Hz of each other in this design, but good results can be expected with a greater spread. Computer circuit simulation is useful.

Although this filter is useful for close-in measurements, it presents a problem far away from 5 MHz, as seen in Figure 6.⁴ The composite low pass filter cutoff at about 7 MHz is close to the 5 MHz notch. In addition, the end L-networks introduce passband ripple which compromise low frequency data when evaluating direct digital synthesizers for low frequency spurious responses.

Higher Order Notch Filters

Figure 7 shows a 10 MHz notch filter with 5 crystals. The circuit uses 200 Ω synthetic transmission line sections between crystals. Ferrite transformers match the ends to 50 Ω.

This 10 MHz filter is useful to almost 20 MHz and has a notch that is 85 dB deep with transfer characteristics shown in Figure 8.

A modified filter expands the performance of the circuit of Figure 7 by adding five more crystals. See Figure 9. The added 11.06 MHz crystals are in a batch with a spread of 140 Hz and yielded a notch depth

of 85 dB around 11.06 MHz. The dual frequency filter is shown in Figure 9. A photo of the filter is presented in Figure 10.

Noise Measurements with a Spectrum Analyzer and a Notch Filter

Our first experiment examines noise from

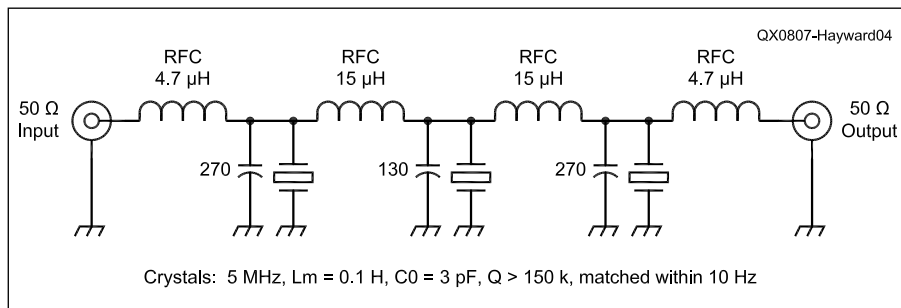
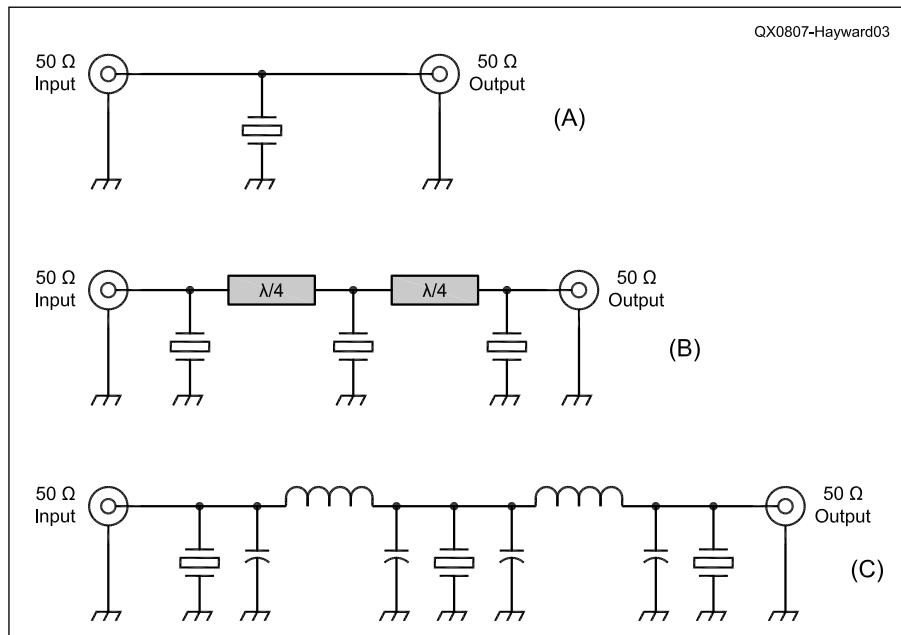
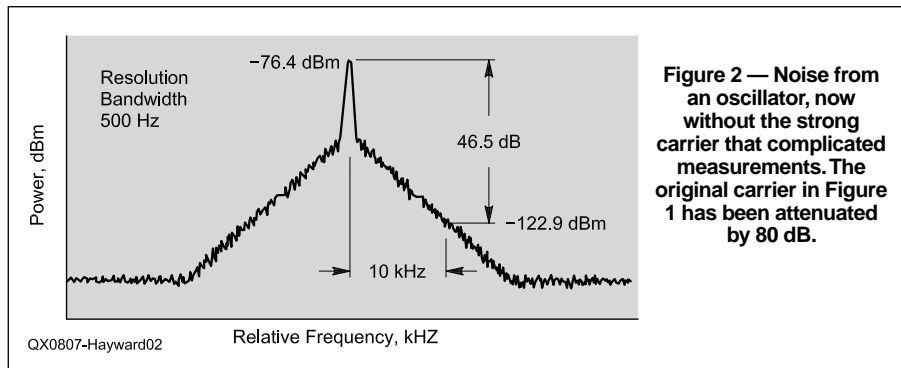


Figure 4 — Schematic diagram for a 5 MHz crystal notch filter. The crystal parameters listed are not critical, but are just those of the crystals used in this experiment.

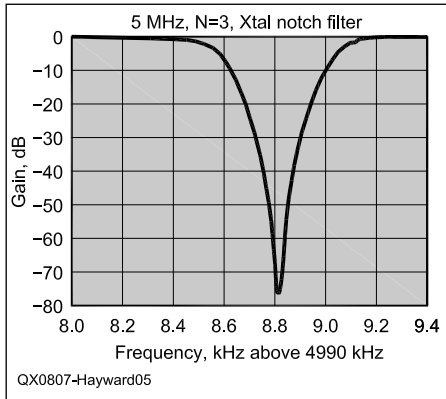


Figure 5 — Measured response for the three crystal 5 MHz notch filter. The left most frequency in the graph is 4998 kHz. Gain measurements were done with a DDS source and a spectrum analyzer.

a Direct Digital Synthesizer with a spectrum analyzer and notch filter. The DDS uses the popular AD-9850 which is useful, but now far removed from the state of the art. A borrowed HP8558B spectrum analyzer completed the measurement suite. The normally high noise figure of the spectrum analyzer is improved with a homebrew high gain low noise amplifier.⁵

The first data photo (Figure 11) shows the output of the DDS when set to 10.008 MHz, which is about 10 kHz above the null frequency of the 10 MHz crystal notch filter. The DDS output is +3.4 dBm. However, I attenuated the DDS output by 60 dB before it reached the LNA. Our goal in this case was to set the analyzer gain to put the signal at the top of the screen, which is the spectrum analyzer reference level.

The DDS was then tuned downward in frequency. When it got to about 9.9985 MHz, I took the photo of Figure 12. The signal is close to, but still not completely in the filter notch where there is maximum attenuation. I didn't tune the DDS all the way into the "rabbit hole," for it would then have been into background noise. The noise that we see, incidentally, results from the LNA preceding the spectrum analyzer. There is still 60 dB of attenuation between the DDS and the notch

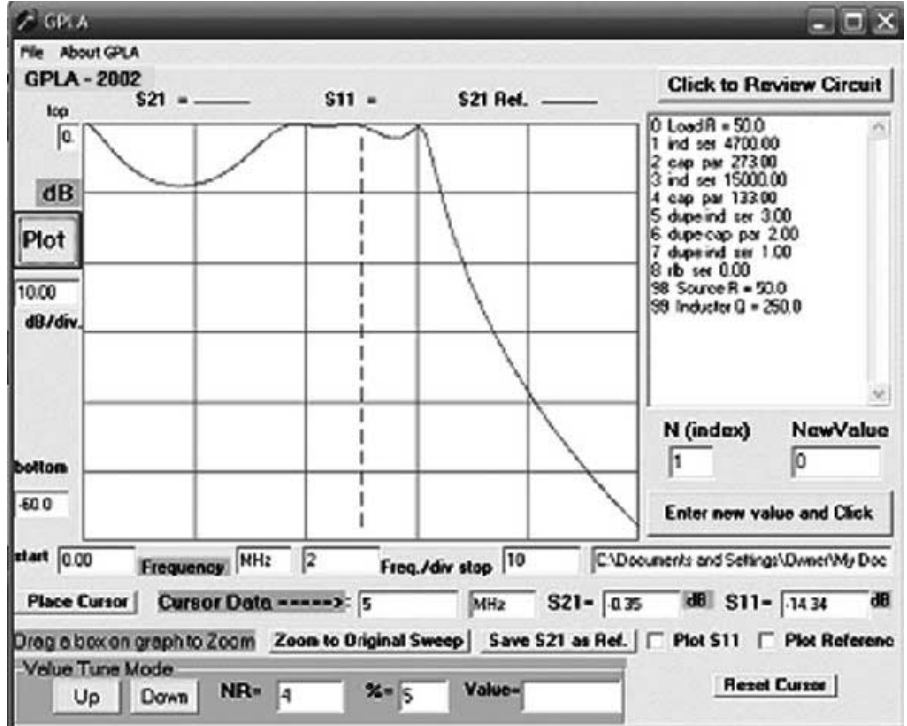


Figure 6 — Simulation of the 5 MHz notch filter well away from 5 MHz. In this computer analysis, the crystals were replaced with 3 pF capacitors.

filter input.

Next, the DDS was tuned down to 9.9983 MHz, completely into the notch. The 60 dB of attenuation was removed from the DDS output, causing both the DDS carrier

and noise to increase. The notch filter still removes enough of the signal to guarantee that the LNA and spectrum analyzer were not overloaded. RBW was decreased to 3 kHz and the span was set to 50 kHz per division.

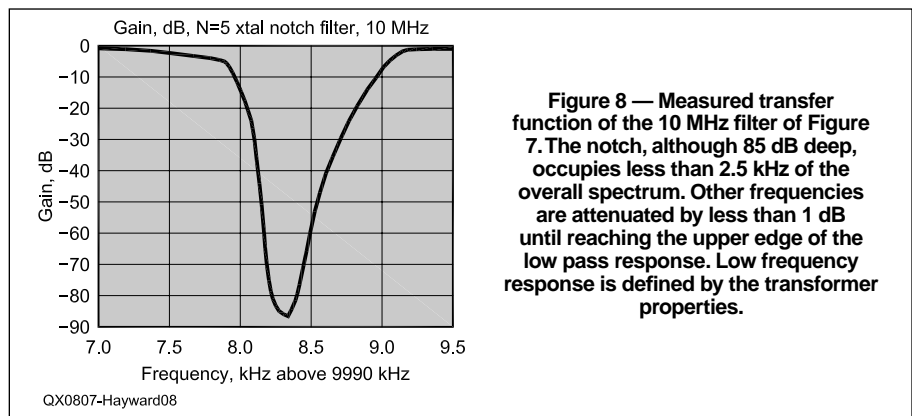


Figure 8 — Measured transfer function of the 10 MHz filter of Figure 7. The notch, although 85 dB deep, occupies less than 2.5 kHz of the overall spectrum. Other frequencies are attenuated by less than 1 dB until reaching the upper edge of the low pass response. Low frequency response is defined by the transformer properties.

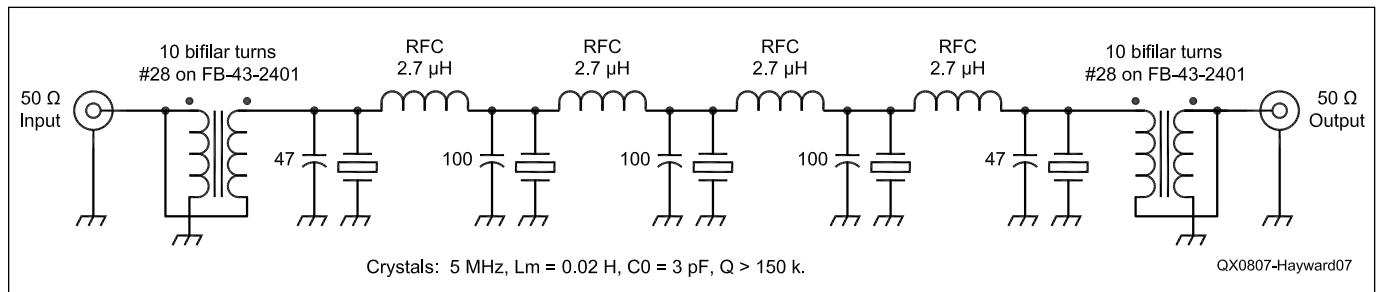


Figure 7 — 10 MHz crystal notch filter with five crystals.

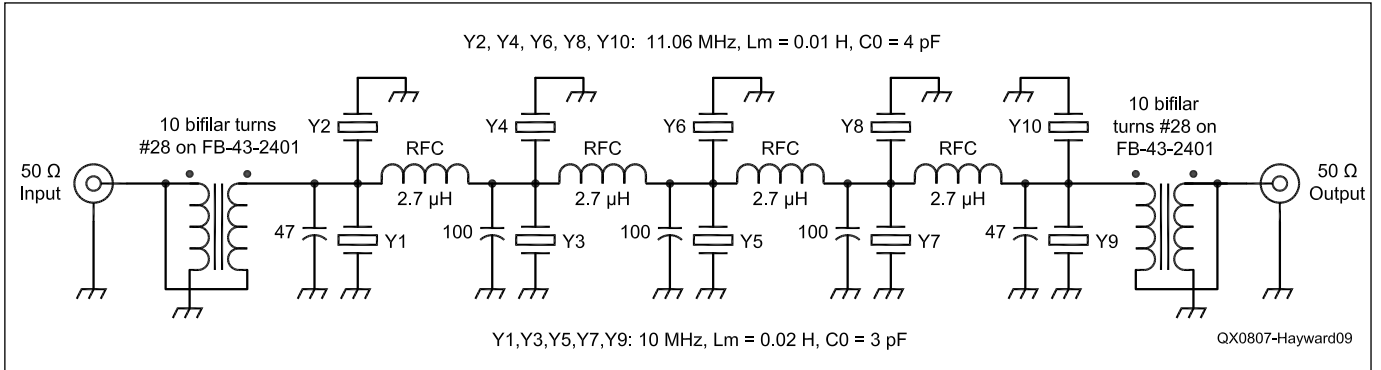


Figure 9 — A crystal filter with notches at both 10 and 11.06 MHz.

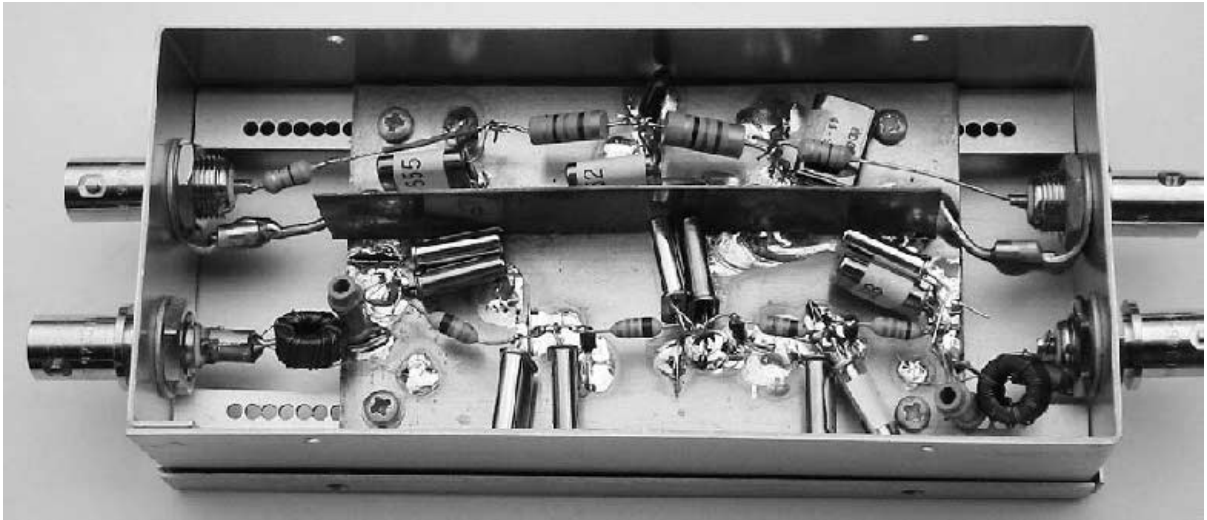


Figure 10 — Two crystal notch filters are contained in one box. The upper filter is the 5 MHz filter with three crystals. The lower filter has deep notches at 10 and 11.06 MHz with five crystals for each frequency.

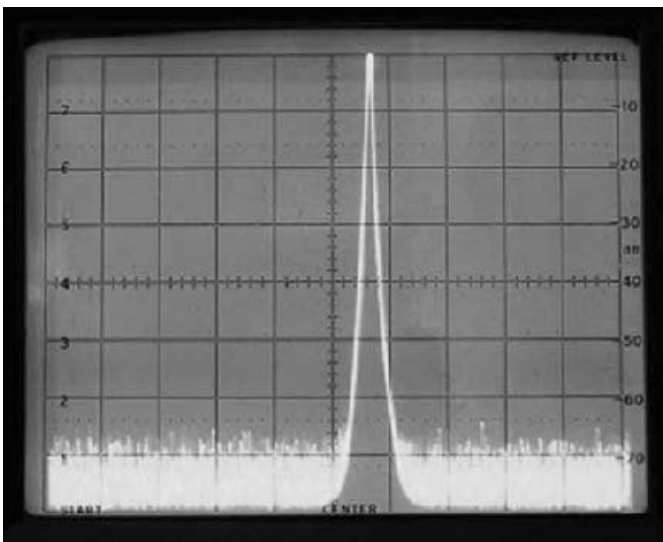


Figure 11 — Photo showing the output of a DDS. The spectrum analyzer resolution bandwidth (RBW) was 10 kHz with a span of 200 kHz/div. The signal was attenuated by 60 dB for this measurement. The homebrew spectrum analyzer at W7ZOI has a narrowest RBW of 30 kHz, making it unsuitable for these noise measurements.

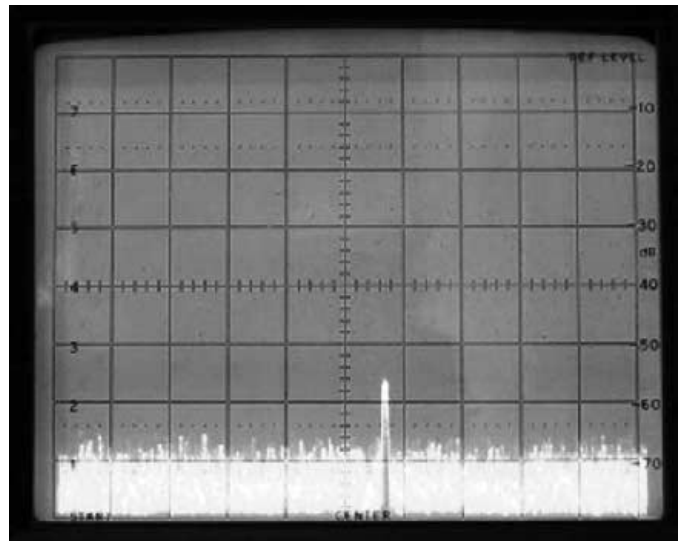


Figure 12 — The response with the DDS tuned part way into the notch of the crystal filter. The DDS is still attenuated by 60 dB. The strong signal is now attenuated an additional 55 dB by the notch filter.

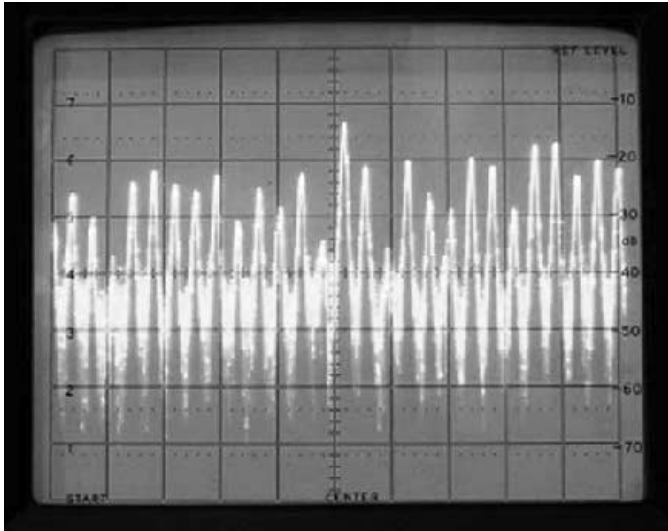


Figure 13 — The DDS output spectrum around 10 MHz. The strongest signal near the center is the actual DDS carrier. The many other signals are spurs characteristic of a DDS. Most of these are 75 to 80 dB below the original, unattenuated carrier. See text. RBW = 3 kHz and span = 50 kHz/div.

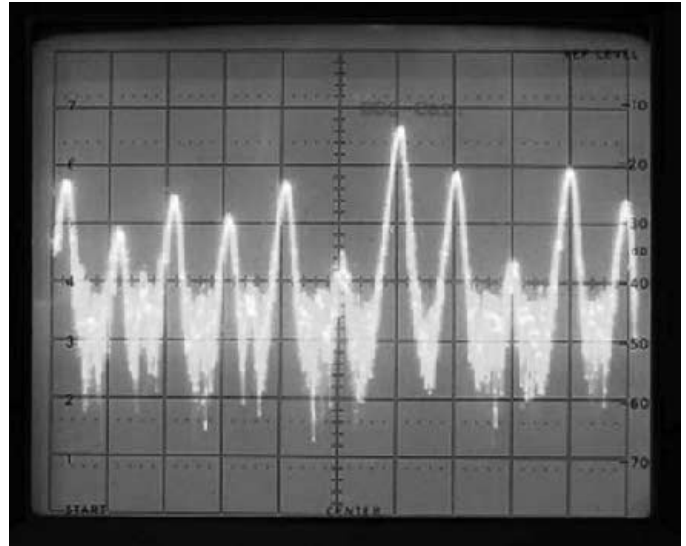


Figure 14 — This plot is the same as Figure 13 except that the span has been dropped to 20 kHz/div, allowing the noise level to be estimated.

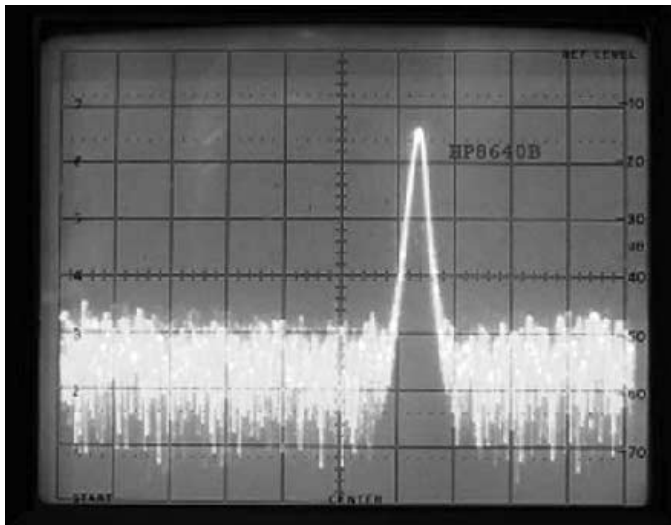


Figure 15 — Noise from HP-8640B. We could get a viable number for the noise by adding video filtering.

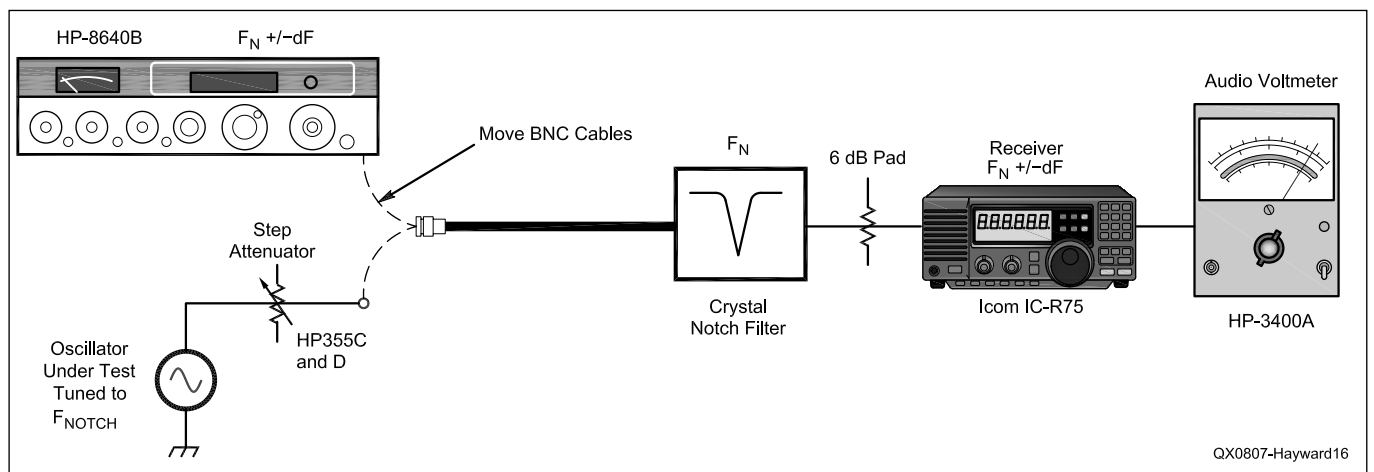


Figure 16 — Test set up for oscillator noise measurements with a crystal notch filter and a communications receiver. A general purpose signal generator (here a HP-8640B) provides calibration. An external LNA is not required with a typical receiver. See text.

This yielded Figure 13, which clearly shows a proliferation of spurious signals.

The span was decreased further to 20 kHz per division for Figure 14. The noise (away from the spurs) is now well below the reference level. This can be better observed with the addition of more video filtering in the spectrum analyzer. But more video filtering causes the sweep speed to decrease to the point that it was not possible to obtain a digital photo.

We could estimate noise performance from the analyzer display, but we are then depending upon the accuracy of the analyzer circuitry. A more conservative approach to noise evaluation uses a signal generator in a substitution measurement. The noise is first observed with the analyzer with ample video filtering (smoothing). The DDS was then disconnected and replaced with an HP-8640B set to a frequency 10 kHz above the notch and injected through the filter which guarantees that the loss of the filter is taken into account. The HP-8640B had an output of -105 dBm when it produced the same signal as the noise at the low point between spurs. The DDS carrier power was +3.4 dBm, so the Carrier to Noise Ratio is $CNR=108.4$ dBc. If we normalize this to 1 Hz bandwidth by adding a factor of $10 \text{ Log (BW)}=34.8$ dB to obtain a wideband spectral noise density of $CNR_n = 143.2$ dBc/Hz.⁶

We might ask how this DDS compares with a good signal generator. I set up the HP-8640B for the same output power as the DDS and tuned it into the notch to produce Figure 15. The noise floor here is oscillator rather than LNA noise, for it drops by 10 dB if you insert 10 dB of attenuation at the *input* to the crystal notch filter.

There are a couple of significant details that should be emphasized about these results. First, they are approximations. The filter shape factor in the spectrum analyzer is okay for most situations, but the lack of skirt selectivity makes it difficult to see the noise between lines. The wideband DDS noise may be even better than the number quoted above.

The other important detail is that the HP8640B noise is clearly lower than the measured synthesizer noise by an observable margin. This is why this generator is so highly prized.

Noise Measurements with a Communications Receiver

Although a spectrum analyzer is the preferred instrument for many lab measurements, effective results can also be obtained with a general coverage receiver. The receiver may be nothing more than the usual station transceiver. My receiver-based test setup is shown in Figure 16.

Having evaluated a DDS, we will now consider a different example, an oscillator presented in the literature as one that was especially noisy.⁷ We begin by measuring the power output of the *oscillator under test* (OUT) with an AD-8307 based power meter.⁸ This could also be done with other 50 Ω instruments. The OUT is then attached to the step attenuator, which is set for fairly high attenuation. The OUT and the receiver are now tuned to the frequency of the crystal notch filter. Listen to the receiver output to get the OUT tuned for minimum carrier signal at the receiver. The attenuator can then be reduced to yield a reasonable level for measurement. In this example, the available power from the OUT was +15.0 dBm. An attenuation of 20 dB was picked, yielding a power of -5 dBm available to the notch filter. See Figure 16.

These measurements were done at 7.373 MHz. A new crystal notch filter was built with some available crystals. The filter schematic is identical to that of Figure 7.⁹

The receiver was set for CW with a relatively wide bandwidth of 2.2 kHz. The receiver was tuned 10 kHz above the carrier, the receiver AGC was turned off, and the speaker was muted by attaching an audio voltmeter to the earphone output.^{10, 11} The meter level was observed while the OUT was temporarily disconnected to confirm that the measured noise resulted from the OUT. The voltmeter level with the OUT connected (a few mV) was recorded. The “switch” of Figure 16 was then changed

to connect the signal generator in place of the OUT. The generator was tuned to the receiver frequency, 10 kHz above the OUT, and the amplitude was adjusted to produce the same meter response that was observed with noise. In my measurement, this happened with a signal generator level of -93.5 dBm. Recall that the available carrier power is -5 dBm. The carrier-to-noise ratio (CNR) is then the difference, 88.5 dB, also called 88.5 dBc for “dB with respect to the carrier.” This result occurred in a relatively wide bandwidth of 2200 Hz. Different receiver bandwidths will produce different results. We normalize the data to 1 Hz bandwidth by adding 10 Log (BW) to the CNR, bringing the normalized ratio to $CNR=121.9$ dBc/Hz at a spacing of 10 kHz. The signal generator energy was injected through the notch filter and following attenuation, so filter losses are removed from the measurement. Both OUT carrier and noise powers are reduced by the step attenuator, leaving the ratio unchanged. While this is not a great oscillator, it is not as bad as I suspected that it might be.

The oscillator circuit was then modified. The current and voltage starved differential bipolar pair was replaced with a JFET operating as a traditional Hartley oscillator.¹² The same oscillator resonator and buffer amplifier were used, leaving the available output power unchanged at -5 dBm. The CNR from this circuit was 146.4 dBc/Hz at a spacing of 10 kHz, a 24.5 dB improvement over the “noisy” oscillator.

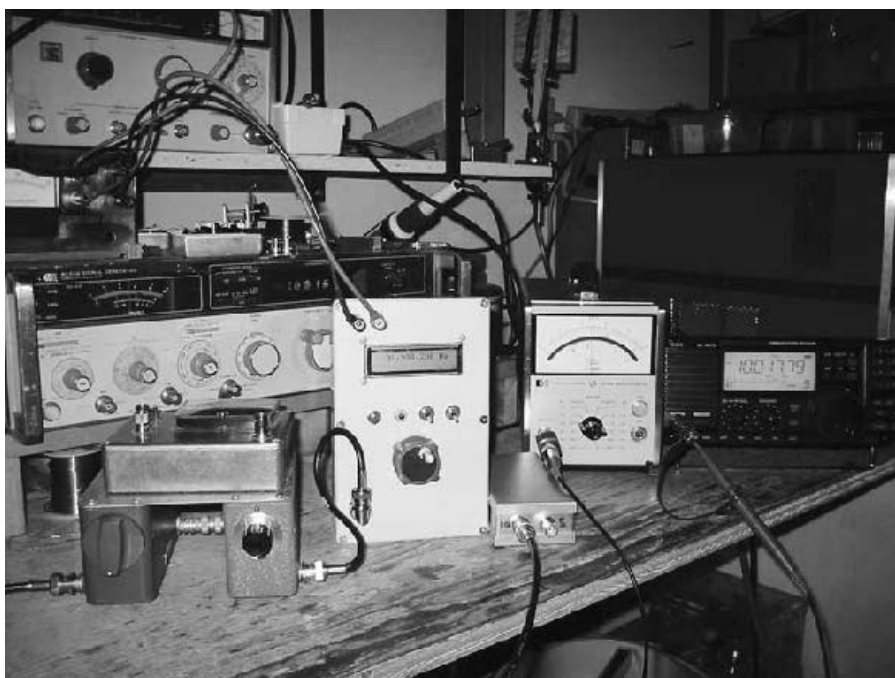


Figure 17 — Test setup during measurements with a receiver. In this case, the DDS was being measured at 10 MHz. It is useful to listen to the *oscillator under test* (OUT) if it is a DDS, for noise results are easily obscured by spurious responses.

As one might expect, numerous available oscillators have been measured. An especially interesting measurement was that of another Hartley LC JFET oscillator used in a home built signal source.¹³ The output from the source and a 6 dB pad was +3.6 dBm. The source was carefully tuned into the notch at 11.06 MHz. The receiver was then tuned 10 kHz above this attenuated carrier. The attenuator was set to 0 dB, and the 6 dB pad (see Figure 16) was removed from the receiver input. After noting the audio output level, which was still well above the system noise floor, the HP8640B was again used as an input signal to the receiver and audio meter. The substitution power was -116.5 dBm, so the CNR is 120.1 dBc. Again we add 10 Log(2200) to this to obtain CNR = 153.5 dBc/Hz at a 10 kHz spacing. This value is consistent with other measurements of this oscillator performed with simple reciprocal mixing, but this latest result tends to instill greater confidence, for the receiver is now far from an overload condition when the notch filter protects the front end. This is the example presented in Figure 1 in the introduction to this paper.

Conclusions and Additional Thoughts

A simple crystal notch filter can clearly allow oscillator noise measurements to be done with relative ease. The filters are very easy and inexpensive to build, making them practical, even for the relatively casual experimenter. There are still problems. The ideal test system would allow an oscillator to be tested over a wide frequency range. This is not possible with a single filter, although a family of filters could certainly be built from inexpensive microprocessor crystals to cover several discrete frequencies. Bandpass filters can also be used for oscillator evaluation, which was done long ago by K7HFD with the now well known low noise oscillator that he built.¹⁴

Virtually all quartz crystals exhibit spurious responses, usually related to resonances outside that part of the quartz disc that has metal plating. These spurs typically occur about 100 kHz above the main resonance. I looked for these resonances in my filters and was not disappointed. While several stray notches were found, for example, between 100 and 200 kHz above the 11 MHz notch, they were not deep. Most were only 1 or 2 dB with the worst being 6 dB. Similar results were seen above the other filter notches. While these spurious responses could complicate the search for DDS spurs, they are not a major deterrent.

Most of the incident power applied to a filter will be absorbed in the first crystal. It

is probably best to confine the available filter power to a few mW.

The reader may have noticed that I have not mentioned *phase noise*, but just *oscillator noise*. This is because there is no discrimination between phase and amplitude noise in the notch filter measurements. Both will contribute to measured noise output. A phase noise test set using a delay line discriminator can be set to differentiate between noise types, forcing the baseband noise to be either in phase with or in quadrature with the carrier.

Other workers have also used crystal notch filters for RF measurements. We found one Web reference to a crystal notch filter used for oscillator evaluation.¹⁵ In another, notch filters were used to enhance the measurement of intermodulation distortion.¹⁶

Acknowledgements

Several colleagues were very supportive in this investigation. Roger Hayward, KA7EXM, loaned me his HP8558B spectrum analyzer while Trevor Jacobs, K6ESE, contributed a DDS to my collection of test equipment. Rick Campbell, KK7B; Bill Carver, W7AAZ; Fred Telewski, WA7TZY; Bob Kopski, K3NHI; Bob Larkin, W7PUA; Steve Ratzlaff, AA7U; Linley Gumm, K7HFD; and Bob Culter, N7FKI, were all encouraging and served as a sounding board for the ideas. Harold Johnson, W4ZCB, and Paul Kiciak, N2PK, both built and tested notch filters, and then extended the ideas. Nic Hamilton, G4TXG, emphasized the need to consider crystal spurious responses. Many thanks to all of these experimenters.

Notes

¹See HP Application Note 207, Oct. 1976. Many HP and Agilent application notes are available on the Web. See www.home.agilent.com/agilent/editorial.jspx?cc=US&lc=eng&ckey=1127547&id=1127547 (Bravo to Agilent for this wonderful service!)

²Reciprocal mixing is described in numerous texts. See, for example, M Wilson, ed., *The ARRL Handbook*, 2008 Edition, p 10.7; Hayward, Campbell, and Larkin, *Experimental Methods in RF Design*, (EMRFD), ARRL, 2003, p 4.12 and p 6.28; Hayward, *Introduction to RF Design*, ARRL, 1995, p 300; Sabin and Schoenike, *Single Sideband Systems & Circuits*, Second Edition, pp 617-619.

³J. Makhinson, "Demphano — A device for Measuring Phase Noise," *Communications Quarterly*, Spring 1999, pp 9-17.

⁴This filter was simulated with GPLA, a General Purpose Ladder Analysis program included on the CD that accompanies EMRFD. See Note 2, ARRL, 2003. Other simulators can be used.

⁵Steven O. Smith, "Build a 1-dB Noise Figure

Amplifier for 50-Ohm Systems," *Electronic Design Magazine*, June 27, 1994 Analog Applications Issue. A simple two stage feed-back amplifier with higher NF would serve for most of these measurements.

⁶Our initial DDS CNR results were 37 dB worse than this. The noise was so robust that it was hard to even see the DDS spurs. The problem was traced to an Epson 120 MHz SG615 clock module that I believe is a phase locked RC ring oscillator. Replacing this clock with an ECS-3951M-1000-BN-TR immediately fixed the DDS noise problems. The DDS spurs are, of course, still present.

⁷See EMRFD, (Note 2), Figure 4.21, p 4.13.

⁸Hayward and Larkin, "Simple RF Power Measurement," *QST*, June, 2001, pp 38-43.

⁹The 7.373 MHz filter used five HC-49 case crystals from ECS in the circuit of Figure 7. The four inductors were 3.9 μH molded RF chokes, the three interior capacitors were 220 pF, while those at the ends were 100 pF. The transformers at the end were the same as used with the 10 MHz filter.

¹⁰The best measurements are done with receiver AGC off, which is possible with my ICOM R75. I tried the measurements with the AGC on and the scheme still worked, but with reduced resolution.

¹¹The voltmeter used was a true RMS reading HP-3400A. This true RMS function can also be realized with homebrew tools. See the classic paper by W. Sabin, "Measuring SSB/CW Receiver Sensitivity," *QST*, Oct 1992, pp 30-34. The homebrew solution would be preferred, because video filtering can easily be added to smooth the noise in time. Depending on the detector used to measure eventual power, a correction may be required to account for a difference between band limited white noise and a sine wave. Noise is lower than a sine wave amplitude by 1.05 dB. In addition, a logarithmic amplifier will read low by 1.45 dB when subjected to noise. Hence, the noise measurements should be increased by 2.5 dB when a spectrum analyzer is used. See M. Engelson, *Modern Spectrum Analyzer Theory and Applications*, Artech House, 1984, p 186. These corrections have not been applied to the data quoted in the text of this paper.

¹²See EMRFD, (Note 2), Figure 4.4, p 4.3.

¹³See EMRFD, (Note 2), Figure 7.27, p 7.15.

¹⁴The oscillator built by Linley Gumm, K7HFD, was tested for noise with a 3 kHz wide bandpass crystal filter at the frequency where noise was to be determined. See the details in Hayward and DeMaw, *Solid-State Design for the Radio Amateur*, ARRL, 1977, p 126.

¹⁵Jack Smith, K8ZOA. See his Web site at www.cliftonlaboratories.com/oscillator_noise_measurements.htm.

¹⁶Leif Åsbrink, SM5BSZ. See his Web site at www.nitehawk.com/sm5bsz/dynrange/dubus403/dubus403.htm.

Wes Hayward, W7ZOI, has been licensed for over 50 years and has contributed papers to QST, QEX, and ham radio during much of that interval. He has also written several books, the latest being a collaboration with KK7B and W7PUA: *the 2003 ARRL book Experimental Methods in RF Design*.



Ground System Configurations for Phased Vertical Arrays

What is the best ground system for a two-element vertical array or a four square array? The author presents extensive modeling data to help you decide.

The July/August 2005 issue of *QEX* includes an article I wrote, comparing the performance of single-element vertical-monopole antennas when they were mounted over a variety of ground systems.¹ Here, we examine ground systems for the two-element cardioid array, and for the widely used four square array. These ground systems all use buried wires, which are arranged in several different configurations. Computer analysis using *EZNEC4* indicates that, for a given total length of wire, some configurations perform much better than others.²

All simulations were performed on the 80-meter DX phone band at a frequency of 3.8 MHz. Average soil was used in the computer models, with a conductivity of 0.005 Siemens/meter and a dielectric constant of 13. In each case the radiator has a physical height of 0.25λ , or about 64.71 feet. All conductors are made of no. 12 AWG copper, and the wire segment-lengths are tapered in accordance with the most conservative NEC guidelines. The shortest segments, such as

the one containing the feed point at the base of the monopole, have a length of 6 inches. The ground wires all begin at the base of the vertical element (at zero height) and the inner segment of each wire slopes downward so that its outer end is at the “final” burial depth in the soil, which is 3 inches, on average.

Cardioid Arrays

The cardioid arrays consist of two 0.25λ vertical elements spaced 0.25λ apart and positioned along an east-west line, as shown in Figure 1. The bases of both elements are fed with equal-amplitude currents, at either 0° or -90° phase-angles, and the main lobe of radiation is in the direction of the element with the lagging current.

Cardioid Arrays with Symmetrical Radial Ground Screens

If radials are buried, it is difficult to make them overlap one another in a real-world scenario. But, if they are simply laid on the surface of the earth, the task becomes much easier. In *NEC*, it is not possible to place wires exactly at the earth-air boundary, as they would be if they were laid atop the ground. Therefore, the first fifteen simulated ground systems each incorporate symmetrically positioned equal-length (“SEL”) buried radials. The number of radials varies from 15 to 120 per element, and the length of the radials spans the range from 0.25 to 0.5λ . Figure 1 shows a typical cardioid array [model 1] using 30 buried $0.25\text{-}\lambda$ radials for each element. Throughout this article, “model numbers” represent the 62 *EZNEC4*

¹Notes appear on page 21.

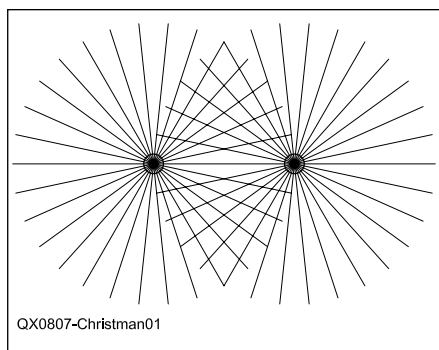


Figure 1 — EZNEC representation (plan view) of a two-element cardioid array using symmetrically placed equal-length (SEL) radials for the ground screen. Each element has 30 quarter-wave radials; those for the east monopole are buried 2 inches deep, while those for the west monopole are buried 4 inches deep.

Table 1
Performance data for cardioid arrays with ground systems composed of symmetrically disposed equal-length (SEL) radials. The ground screens are listed in order of increasing number and length of radials.

Model Number	Number of Radials per Element	Length (λ)	Gain (dBi)	Take-off Angle (Degrees)	Total Length of Buried Wire (λ)
1	30	0.25	3.37	25	15
2	60	0.25	3.675	24.5	30
3	90	0.25	3.775	25	45
4	120	0.25	3.81	24.5	60
5	20	0.375	3.22	24	15
6	40	0.375	3.785	24.5	30
7	60	0.375	3.96	25	45
8	80	0.375	4.125	25	60
9	100	0.375	4.155	25	75
10	15	0.5	3.03	24.5	15
11	30	0.5	3.695	24.5	30
12	45	0.5	3.99	25	45
13	60	0.5	4.165	25	60
14	75	0.5	4.305	26	75
15	90	0.5	4.36	25	90

Note:
Since the radials for the east element are buried more shallowly than those of the west element, the gain of the array tends to be slightly higher when beaming east. The gain values shown in the table represent the average of the “east” and “west” results.

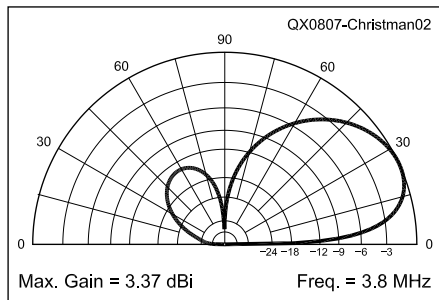


Figure 2 — Elevation-plane radiation pattern for the cardioid array shown in Figure 1. The peak gain is 3.37 dBi at 25° take-off angle and the front-to-back ratio is 13.6 dB.

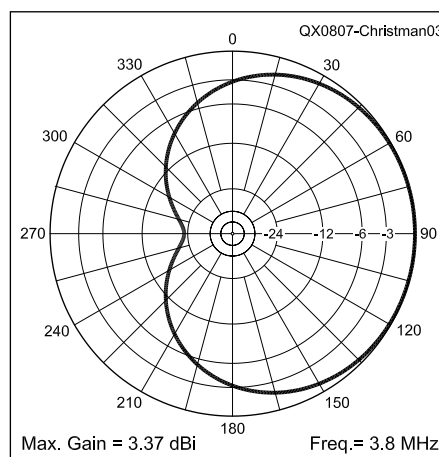


Figure 3 — Azimuthal-plane radiation pattern for the array shown in Figure 1. The front-to-back ratio is 22.79 dB at 25° take-off angle, and the half-power beamwidth is 177.4°. Note that the pattern is heart-shaped, or “cardioid.”

antenna models that I studied to collect the data presented here. The models with the longest radial wires are available for download from the QEX Web site. Interested readers can modify those models by shortening the radials to create other models for their own study.³

Figures 2 and 3 display the corresponding elevation and azimuthal-plane radiation patterns for this antenna. Notice that the azimuthal pattern is heart-shaped, which is why these arrays bear the name “cardioid.” In each case, the radials of the “east” element are buried to a depth of two inches, while those of the “west” monopole are buried four inches deep, in order to avoid computer crashes that would otherwise occur when two radials buried at the same depth intersected one another. Thus, none of the radials from the east element ever touch any of the radials of the west monopole.

Table 1 lists the number of radials per element and their length, the peak gain and corresponding take-off angle (TOA) at which maximum gain occurs, and the total length of buried wire required for each ground system. The antennas are listed in order of

increasing number and length of radials. For any particular radial length, adding more of them always boosts the gain, but eventually a point is reached at which the installation of more radials is hardly worth the effort. Since the radials for the east element are

buried more shallowly than those of the west monopole, the gain of the array tends to be slightly higher when beaming to the east. For this reason, the gain values shown in the table represent the average of the “east” and “west” results.

**Table 2
Performance data for cardioid arrays with ground systems composed of symmetrically disposed equal-length (SEL) radials. Here, the ground screens are listed in order of increasing gain.**

Model Number	Number and Length (λ) of Radials per Element	Gain (dBi)	Take-off Angle (Degrees)	Total Length of Buried Wire (λ)
10	15 0.5	3.03	24.5	15
5	20 0.375	3.22	24	15
1	30 0.25	3.37	25	15
2	60 0.25	3.675	24.5	30
11	30 0.5	3.695	24.5	30
3	90 0.25	3.775	25	45
6	40 0.375	3.785	24.5	30
4	120 0.25	3.81	24.5	60
7	60 0.375	3.96	25	45
12	45 0.5	3.99	25	45
8	80 0.375	4.125	25	60
9	100 0.375	4.155	25	75
13	60 0.5	4.165	25	60
14	75 0.5	4.305	26	75
15	90 0.5	4.36	25	90

Note:
Since the radials for the east element are buried more shallowly than those of the west element, the gain of the array tends to be slightly higher when beaming east. The gain values shown in the table represent the average of the “east” and “west” results.

**Table 3
Performance data for cardioid arrays with ground systems composed of symmetrically disposed equal-length (SEL) radials. Here, the ground screens are listed in order of increasing total length of buried wire.**

Model Number	Number and Length (λ) of Radials per Element	Gain (dBi)	Take-off Angle (Degrees)	Total Length of Buried Wire (λ)
10	15 0.5	3.03	24.5	15
5	20 0.375	3.22	24	15
1	30 0.25	3.37	25	15
2	60 0.25	3.675	24.5	30
11	30 0.5	3.695	24.5	30
6	40 0.375	3.785	24.5	30
3	90 0.25	3.775	25	45
7	60 0.375	3.96	25	45
12	45 0.5	3.99	25	45
4	120 0.25	3.81	24.5	60
8	80 0.375	4.125	25	60
13	60 0.5	4.165	25	60
9	100 0.375	4.155	25	75
14	75 0.5	4.305	26	75
15	90 0.5	4.36	25	90

Note:
Since the radials for the east element are buried more shallowly than those of the west element, the gain of the array tends to be slightly higher when beaming east. The gain values shown in the table represent the average of the “east” and “west” results.

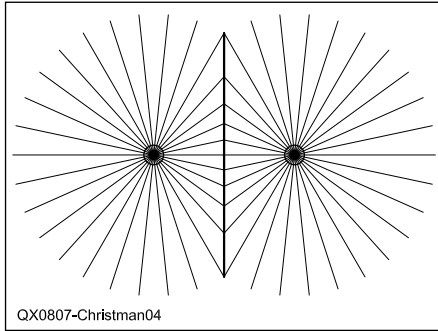


Figure 4 — EZNEC representation (plan view) of a two-element cardioid array using a broadcast-type (BCT) ground screen, in which some of the radials are truncated and bonded to a bus-wire. Each element has 30 radials whose maximum length is 0.25λ . All radials (and the bus wire) are buried 3 inches deep.

Table 2 contains the same information as Table 1, but the antennas are listed in order of increasing gain, without regard for the number or length of the radials. If at least 3.5 dBi of gain is desired, then roughly 30λ of wire needs to be installed in the ground screen. Notice that only those arrays using ground systems with “long” (0.375 or 0.5λ) radials are able to achieve a gain of more than 4 dBi. If one is limited to radials no longer than 0.25λ , then a very large number must be used in order to approach the 4 dB gain figure (a ground screen with 120 $0.25\text{-}\lambda$ radials per element yields a gain of 3.81 dBi).

Table 3 again repeats the data from Table 1, but now the order of entry has been changed so that the overall length of wire in the ground system takes priority. Whenever two or more ground systems use the same total length of buried wire, they are listed in order of increasing gain. Notice that, when the total amount of wire to be buried is fixed, some combinations of number and length of radials generate 0.2 to 0.3 dBi more gain than do others. Thus, if a maximum of 15λ of wire is available for the ground screen, then thirty $0.25\text{-}\lambda$ radials per element works best. For 30λ of wire, forty $0.375\text{-}\lambda$ radials (per monopole) are slightly better than either thirty $0.5\text{-}\lambda$ or sixty $0.25\text{-}\lambda$ radials. If you are willing to install 45λ of wire (or more), then $0.5\text{-}\lambda$ radials provide the most gain. Designs using radials whose length exceeds 0.5λ were not analyzed, because I thought that most hams would not be willing to build such large ground screens.

Cardioid Arrays with Broadcast-Type Radial Ground Screens

The radials are not allowed to cross or overlap in the ground screen of a typical AM-broadcast antenna. Instead, they are cut off (truncated) and bonded to a bus-wire, as shown in Figure 4. The ground screen for this array [model 16] is similar to that of Figure 1, but now all of the radials are buried to a depth of 3 inches (the average of the two different

burial depths used in Figure 1). Since many of these radials are cut short, the total length of buried wire is less than in Figure 1, although the maximum radial length is still 0.25λ .

The next fifteen antennas (models 16 through 30) which were modeled on the computer use broadcast-type (“BCT”) ground systems. Again, the number of radials varies from 15 to 120 per element, and the maximum length of the radials spans

the range from 0.25 to 0.5λ . Table 4 lists the number of radials per element and their maximum length, the peak gain and corresponding take-off angle (TOA) at which maximum gain occurs, and the total length of buried wire required for each ground screen. The antennas are listed in order of increasing number and length of radials. As expected, for any given length of radials, adding more of them produces more gain,

Table 4
Performance data for cardioid arrays with broadcast-type (BCT) radial ground systems. The ground screens are listed in order of increasing number and length of radials.

Model Number	Number and Maximum Length (λ) of Radials per Element	Gain (dBi)	Take-off Angle (Degrees)	Total Length of Buried Wire (λ)
16	30 0.25	3.33	24	13.61
17	60 0.25	3.63	24	26.72
18	90 0.25	3.73	25	39.89
19	120 0.25	3.77	25	53.03
20	20 0.375	3.10	25	12.37
21	40 0.375	3.60	25	24.44
22	60 0.375	3.80	25	36.44
23	80 0.375	3.90	25	48.29
24	100 0.375	3.96	25	60.36
25	15 0.5	2.86	24	11.94
26	30 0.5	3.48	25	22.92
27	45 0.5	3.75	25	34.24
28	60 0.5	3.90	25	45.65
29	75 0.5	4.01	25	56.62
30	90 0.5	4.07	25	67.88

Note:

Since the radials for both elements are buried to the same depth, the gain of the array is the same when beaming in either direction.

Table 5
Performance data for cardioid arrays with broadcast-type (BCT) radial ground systems. The ground screens are listed in order of increasing gain.

Model Number	Number and Maximum Length (λ) of Radials per Element	Gain (dBi)	Take-off Angle (Degrees)	Total Length of Buried Wire (λ)
25	15 0.5	2.86	24	11.94
20	20 0.375	3.10	25	12.37
16	30 0.25	3.33	24	13.61
26	30 0.5	3.48	25	22.92
21	40 0.375	3.60	25	24.44
17	60 0.25	3.63	24	26.72
18	90 0.25	3.73	25	39.89
27	45 0.5	3.75	25	34.24
19	120 0.25	3.77	25	53.03
22	60 0.375	3.80	25	36.44
23	80 0.375	3.90	25	48.29
28	60 0.5	3.90	25	45.65
24	100 0.375	3.96	25	60.36
29	75 0.5	4.01	25	56.62
30	90 0.5	4.07	25	67.88

Note:

Since the radials for both elements are buried to the same depth, the gain of the array is the same when beaming in either direction.

Table 6

Performance data for cardioid arrays with broadcast-type (BCT) radial ground systems. The ground screens are listed in order of increasing total length of buried wire.

Model Number	Number of Radials (λ) of Radials per Element	Maximum Length of Radial (λ)	Gain (dBi)	Take-off Angle (Degrees)	Total Length of Buried Wire (λ)
25	15	0.5	2.86	24	11.94
20	20	0.375	3.10	25	12.37
16	30	0.25	3.33	24	13.61
26	30	0.5	3.48	25	22.92
21	40	0.375	3.60	25	24.44
17	60	0.25	3.63	24	26.72
27	45	0.5	3.75	25	34.24
22	60	0.375	3.80	25	36.44
18	90	0.25	3.73	25	39.89
28	60	0.5	3.90	25	45.65
23	80	0.375	3.90	25	48.29
19	120	0.25	3.77	25	53.03
29	75	0.5	4.01	25	56.62
24	100	0.375	3.96	25	60.36
30	90	0.5	4.07	25	67.88

Note:

Since the radials for both elements are buried to the same depth, the gain of the array is the same when beaming in either direction.

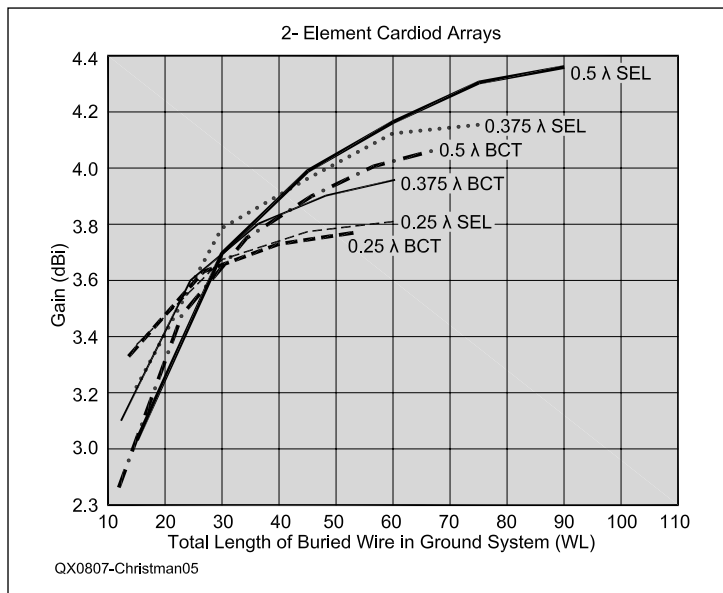


Figure 5 — A plot of antenna gain versus total length of buried wire, for all 30 of the cardioid arrays which use radial ground screens. SEL = symmetrically placed equal-length radials, BCT = broadcast-type radials

but eventually a point of diminishing returns is reached. A BCT ground screen uses the same burial depth for all radials, so the gain of these arrays is the same when firing either to the east or west. The total length of buried wire in a BCT ground system, however, is always less than that of the corresponding SEL antenna (with the same maximum radial length and number of radials).

Table 5 contains the same information as Table 4, but now the antennas are listed in order of increasing gain, without regard for the number or length of the radials. When two arrays have the same gain, they are listed in order of maximum radial length. If at least 3.5 dBi of gain is desired, then the ground screen needs to include about 24 λ of wire. With a BCT array, only those ground sys-

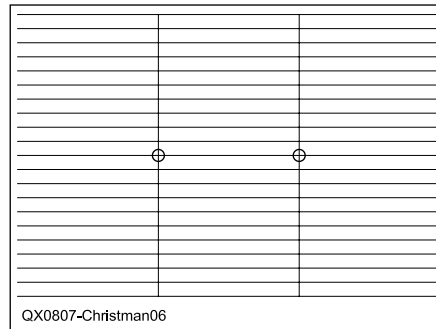


Figure 6 — EZNEC representation (plan view) of a two-element cardioid array whose ground screen employs 21 equally spaced parallel wires which are oriented along (parallel to) the direction of fire.

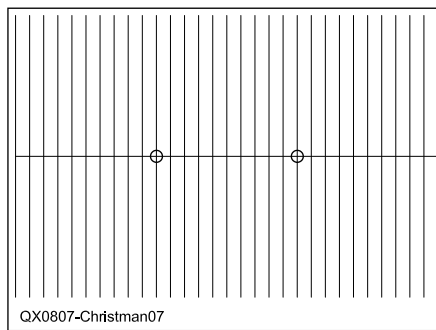


Figure 7 — EZNEC representation (plan view) of a two-element cardioid array whose ground screen employs 31 equally spaced parallel wires which are oriented perpendicular to the direction of fire.

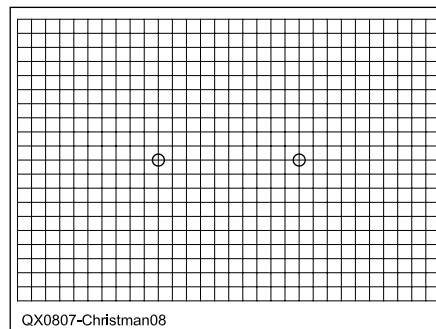


Figure 8 — EZNEC representation (plan view) of a two-element cardioid array whose ground screen employs a mesh (grid) of "squares" whose side length is 0.025 λ .

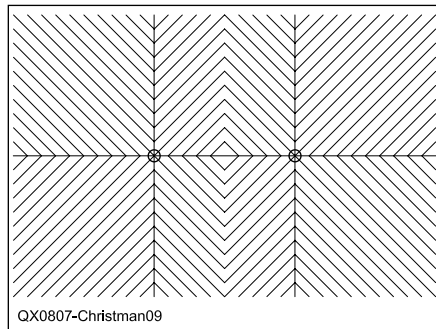


Figure 9 — EZNEC representation (plan view) of a two-element cardioid array whose ground screen employs "tree branches" composed of parallel wires which are spaced 0.025 λ apart.

tems with 0.5λ radials are able to achieve a gain of more than 4 dBi. As was true for the SEL antennas, if the maximum allowable radial length is 0.25λ , then a very large number must be used in order to approach 4 dB of gain. (A BCT ground screen with 120 radials per element yields a gain of 3.77 dBi.)

Table 6 repeats the data from Table 4 once more, but now the order of entry has been changed so that the overall length of wire in the ground system takes priority. Generally speaking, the gain of the antenna rises continually as more and more wire is buried in the ground. Notice that exactly 3.90 dBi of gain is available when each element has either 60 radials (whose maximum length is 0.5λ) or 80 radials (whose maximum length is 0.375λ). The ground-screen with half-wave radials uses somewhat less wire, but takes up more acreage.

Figure 5 is a plot of antenna gain versus the total length of buried wire in the ground system, for all 30 of the cardioid arrays discussed thus far. This drawing provides a quick visual summary of the relative performance of the various BCT and SEL radial ground screens. Notice that if the total length of wire in the ground screen exceeds about 25λ , then an SEL-type ground screen (with 0.375 or 0.5λ radials) always provides the most gain.

Cardioid Arrays with Non-Radial Ground Screens

Thus far, we have only looked at ground systems in which the buried wires were actually “radial,” that is, extending outward from the base of the elements like spokes from the hub of a wheel. It is certainly possible to orient the ground wires differently, however. Other configurations that were simulated include parallel wires placed along the direction of fire (see Figure 6), parallel wires placed perpendicular to the direction of fire (Figure 7), meshes or grids of wires (Figure 8), and tree-branch-style systems (Figure 9). In each case, the overall dimensions of the ground screen are 0.75λ (east-west) by 0.5λ (north-south). The performance of these alternative ground screens is listed in Table 7. A comparison of these results with those shown in Figure 5 reveals that none of these “exotic” configurations [models 31 through 34] are competitive with any of the more-conventional (SEL or BCT) radial ground systems.

Cardioid Arrays with Partial Ground Screens

For some applications, a ham might wish to build a two-element cardioid array with the intention of using it to fire in only one direction. In such a case, is a “complete” (symmetrical) ground system really necessary, or can you omit those radials that “point” in the opposite direction? To answer this question,

I modified the antennas with SEL and BCT ground screens (models 1 through 30), and then simulated these antennas.

For the 15 arrays with SEL ground systems, I removed all of the radials that point toward the west from each element, and kept only those that were oriented toward the east. Figure 10 [model 1-p, where the letter “p” stands for “partial ground screen”] displays the same antenna that was originally shown in Figure 1 [model 1], but now I have removed the “west” radials from both mono-

poles to create a new array with an “incomplete” ground screen. Table 8 lists the results for these modified antennas, including the gain when firing to the east (preferred) as well as the gain when firing west (undesired). Notice that removing only the west radials actually reduces the gain in *both* directions of fire (compare Table 1 with Table 8), but the gain toward the east falls only slightly.

Some of the results in this table appear to be a bit odd. Consider model 9-p, which has less “eastward-firing” gain than model 8-p,

Table 7
Performance data for cardioid arrays with non-radial ground systems. The ground screens are listed in accordance with their description.

Model Number	Description of Ground Screen	Gain (dBi)	Take-off Angle (Degrees)	Total Length of Buried Wire (λ)
31	21 parallel wires, length = 0.75λ , oriented along the direction of fire (Figure 6)	2.46	25	16.75
32	31 parallel wires, length = 0.5λ , placed perpendicular to the direction of fire (Figure 7)	1.88	24	16.25
33	Mesh using “squares” whose side-length = 0.025λ (Figure 8)	3.23	25	31.25
34	“Tree-branches” using wires spaced 0.025λ apart (Figure 9)	3.18	24	22.96

Table 8
Performance data for cardioid arrays with partial SEL ground screens. The antennas listed here are similar to those shown in Table 1, but now all of the “west” radials have been removed from each element.

Model Number	Firing East		Firing West		Total Length of Buried Wire (λ)
	Gain (dBi)	Take-off Angle (Degrees)	Gain (dBi)	Take-off Angle (Degrees)	
1-p	2.94	25	1.85	24	7.75
2-p	3.33	25	2.11	23	15.5
3-p	3.42	25	2.14	23	22.75
4-p	3.51	25	2.23	23	30.5
5-p	2.68	25	1.56	24	7.5
6-p	3.36	25	2.08	24	15
7-p	3.54	26	2.18	24	22.5
8-p	3.77	26	2.37	24	30
9-p	*3.73	26	2.27	23	37.5
10-p	2.41	25	1.38	24	7
11-p	3.26	25	1.96	24	16
12-p	3.52	25	2.02	24	22
13-p	3.73	26	2.19	24	30
14-p	3.95	26	2.39	24	38
15-p	*3.95	26	2.31	23	46

*These odd values of gain are discussed in the text.

even though its ground screen has more radials. Also, models 14-p and 15-p both have exactly the same “eastward” gain, despite the fact that 15-p has more radials than 14-p. This anomalous behavior will be explained later, and highlights an interesting aspect of ground-screen construction.

It is also feasible to omit radials from the cardioid arrays using BCT ground systems, but here the radials will be removed only from the “west” monopole, since the ground wires do not overlap in the area between the two elements. Figure 11 [model 16-p] shows what remains after all of the “west” radials are removed from the “west” monopole of the antenna shown earlier in Figure 4 [model 16]. The results for the 15 modified arrays [models 16-p through 30-p] with BCT ground screens are displayed in Table 9. Comparing this table with Table 4, again we see that removing the west radials leads to a significant reduction in array gain when firing west, but only a slight diminution when the antenna is beaming eastward.

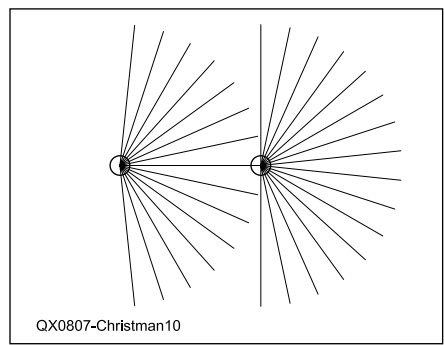


Figure 10 — EZNEC representation (plan view) of a two-element cardioid array which originally used a full SEL radial ground screen, as in Figure 1. Here, all of the “west” radials have been removed from each monopole. Those for the east element are buried 2 inches deep, while those for the west monopole are buried to a depth of 4 inches.

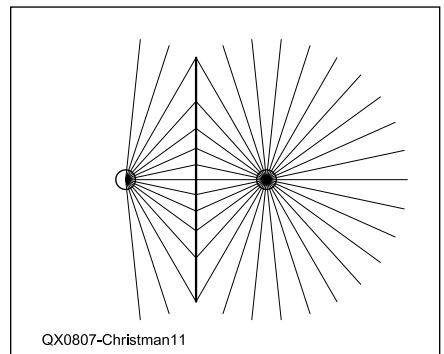


Figure 11 — EZNEC representation (plan view) of a two-element cardioid array which originally used a full BCT radial ground screen, as in Figure 4. Now, all of the “west” radials have been removed from the west monopole. All radials are buried 3 inches deep.

Four-Square Arrays

The four-square arrays are traditional in design, consisting of four 0.25-λ vertical elements placed at the corners of a square whose side length is 0.25 λ. The sides of the square are oriented north-south and east-west, so the vertical monopoles are positioned at the northeast, northwest, southwest, and southeast corners respectively. The bases of all four elements are fed with equal-amplitude currents, at phase angles of -180° for the front element, -90° for the two side elements,

and 0° for the rear element.

Four-Square Arrays with Symmetrical Radial Ground Screens

The first twelve ground systems for four-square arrays [models 35 through 46] all use symmetrically positioned equal-length (SEL) buried radials. The number of radials varies from 15 to 120 per element, and the length of the radials spans the range from 0.25 to 0.5 λ. Figure 12 illustrates a typical four square array [model 35] with 30 buried 0.25-λ radials for each element. To prevent

Table 9
Performance data for cardioid arrays with partial BCT ground screens. The antennas listed here are similar to those shown in Table 4, but now all of the “west” radials have been removed from the “west” element.

Model Number	Gain (dBi)	Take-off Angle (Degrees)	Gain (dBi)	Take-off Angle (Degrees)	Total Length of Buried Wire (λ)
	Firing East		Firing West		
16-p	3.06	25	2.39	24	9.86
17-p	3.40	24	2.65	24	19.47
18-p	3.49	25	2.69	24	28.64
19-p	3.55	25	2.74	24	38.28
20-p	2.80	24	2.16	24	8.62
21-p	3.31	25	2.50	24	16.94
22-p	3.51	25	2.62	24	25.19
23-p	3.63	25	2.70	23	33.67
24-p	3.68	26	2.71	23	41.61
25-p	2.52	25	1.89	24	7.94
26-p	3.23	25	2.43	24	15.92
27-p	3.48	25	2.54	24	23.24
28-p	3.63	25	2.60	24	30.65
29-p	3.72	26	2.64	24	37.62
30-p	3.80	26	2.70	24	45.88

Table 10
Performance data for four-square arrays with ground systems composed of symmetrically disposed equal-length (SEL) radials. The ground screens are listed in order of increasing number and length of radials.

Model Number	Number and Length (λ) of Radials per Element		Gain (dBi)	Take-off Angle (Degrees)	Total Length of Buried Wire (λ)
35	30	0.25	5.84	23	30
36	60	0.25	6.13	23	60
37	90	0.25	6.45	23	90
38	120	0.25	*6.22	23	120
39	20	0.375	5.74	23	30
40	40	0.375	6.39	24	60
41	60	0.375	6.45	24	90
42	80	0.375	*6.01	24	120
43	15	0.5	5.61	23	30
44	30	0.5	6.31	24	60
45	45	0.5	6.56	24	90
46	60	0.5	6.70	24	120

Notes:
Since the radials for each element are buried at a slightly different depth, the gain of the array tends to vary from one direction of fire to another. The gain values shown in the table are the average of the results from all four directions.
*These surprisingly low values of gain are discussed in the text.

computer crashes, the radials for each monopole were buried at slightly different depths: 1.5 inches for the NE element, 2.5 inches for the NW element, 4.5 inches for the SW element, and 3.5 inches for the SE element. The

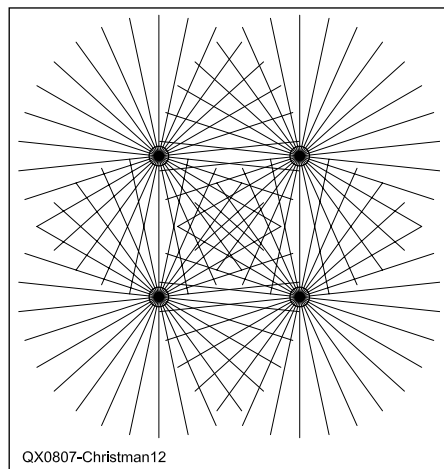


Figure 12 — EZNEC representation (plan view) of a four-square array using symmetrically placed equal-length (SEL) radials for the ground screen. Each element has 30 quarter-wave radials, which are buried at depths ranging from 1.5 to 4.5 inches.

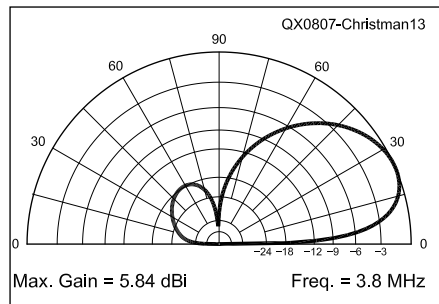


Figure 13 — Elevation-plane radiation pattern for the four-square array shown in Figure 10. The peak gain is 5.84 dBi at 23° take-off angle and the front-to-back ratio is 17.91 dB.

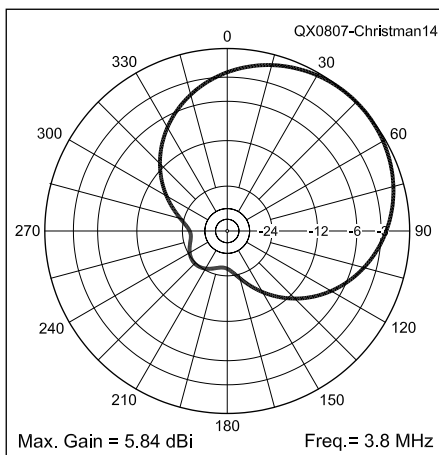


Figure 14 — Azimuthal-plane radiation pattern for the four-square array shown in Figure 10. The front-to-back ratio is 23.69 dB at 23° take-off angle, and the half-power beamwidth is 100.6°.

average burial depth is 3 inches. Figures 13 and 14 display the elevation and azimuthal-plane radiation patterns for this antenna.

Table 10 lists the number of radials per element and their length, the peak gain and corresponding take-off angle (TOA) at which maximum gain occurs, and the total length of buried wire required for each ground system. The antennas are listed in order of increasing number and length of radials. One would expect that the gain might vary a bit as the direction of fire was changed, because the radials for each element are buried at a dif-

ferent depth, and this is indeed the case; the numbers shown in the table represent the average for all four directions of fire.

Reviewing the table, we can see that, for any specific radial-length, adding more radials increases the gain, with two notable exceptions (indicated by asterisks). It seems reasonable to assume that a “better” ground screen (more and/or longer radials) would generate more gain, but this rule is violated in two of the computer models (models 38 and 42). I described this unusual behavior to Roy Lewallen, W7EL, the author of EZNEC, and here is part of his reply:

Table 11 Performance data for four-square arrays with ground systems composed of symmetrically disposed equal length (SEL) radials. The ground screens are listed in order of increasing gain.

Model Number	Number of Radials per Element	Length (λ)	Gain (dBi)	Take-off Angle (Degrees)	Total Length of Buried Wire (λ)
43	15	0.5	5.61	23	30
39	20	0.375	5.74	23	30
35	30	0.25	5.84	23	30
36	60	0.25	6.13	23	60
44	30	0.5	6.31	24	60
40	40	0.375	6.39	24	60
37	90	0.25	6.45	23	90
41	60	0.375	6.45	24	90
45	45	0.5	6.56	24	90
46	60	0.5	6.70	24	120

Notes:

Since the radials for each element are buried at a slightly different depth, the gain of the array tends to vary from one direction of fire to another. The gain values shown in the table are the average of the results from all four directions. The two “odd” entries (models 38 and 42), which are listed in Table 8 and discussed in the text, have been omitted here.

Table 12 Performance data for four-square arrays with broadcast-type (BCT) radial ground systems. The ground screens are listed in order of increasing number and length of radials.

Model Number	Number and Maximum Length (λ) of Radials per Element	Gain (dBi)	Take-off Angle (Degrees)	Total Length of Buried Wire (λ)
47	30 0.25	5.74	23	24.16
48	60 0.25	6.04	23	47.32
49	90 0.25	6.13	24	70.41
50	120 0.25	6.16	23	93.49
51	20 0.375	5.53	23	20.6
52	40 0.375	6.04	23	39.89
53	60 0.375	6.24	24	59.35
54	80 0.375	6.33	24	78.43
55	100 0.375	6.39	23	97.83
56	15 0.5	5.32	23	19.74
57	30 0.5	5.95	23	36.48
58	45 0.5	6.23	23	53.36
59	60 0.5	6.40	24	70.28
60	75 0.5	6.50	24	87.18
61	90 0.5	6.57	24	104.15

Note:

Since the radials for all of the elements are buried to the same depth, the gain of the array is identical in all four directions of fire.

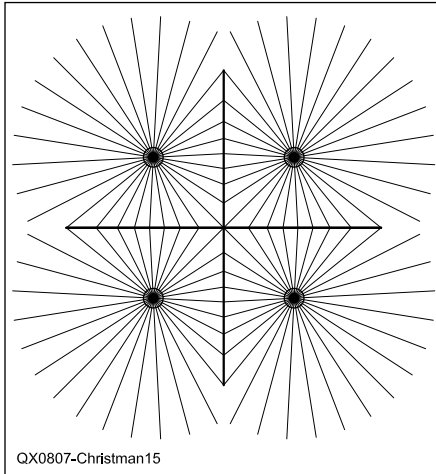


Figure 15 — EZNEC representation (plan view) of a four-square array using a broadcast-type (BCT) ground screen, in which some of the radials are truncated and bonded to a bus wire. Each element has 30 radials whose maximum length is 0.25 λ . All radials (and the bus wires) are buried to a depth of 3 inches.

“I wouldn’t be surprised if it is ground loss, for the following reason. In a system consisting of a single vertical, the currents returning to the element are all radial, in the same directions as the ground wires, so the analysis is simple. In an array, you’ve got substantial currents from one element to another via mutual coupling, and an equal amount has to flow between elements via the ground wires. For those cases, the currents have to couple from one element’s radial wires to crossing ones from the other element. For some element combinations in your system, a current trying to get from one element’s ground system to another has to traverse the ground system of one or two other elements. The more dense the radials from those other elements, the more difficulty the current will have getting between the original two. In other words, the ground systems of some elements would act as a shield to the currents between other elements, and the effectiveness of the shield increases with the number of radials. I’d think that in a real system you’d want to put all the radials at the same depth and bond them with a good connection where they cross.”⁴

Roy’s analysis makes sense to me, and his conclusion is very important: whenever one radial crosses another in the ground system of a multi-element array, the wires should be connected together electrically. This is especially important if the number and/or length of the radials is large. It is entirely possible that the actual gain of the arrays with SEL ground screens would be even higher than what was reported by EZNEC, if all the radials had been installed at the same depth and connected together at their crossing points.

The two instances of anomalous behav-

ior noted earlier in Table 8 (for the cardioid arrays with partial SEL ground systems) can also be explained by the same mechanism. When the radials are long enough to achieve significant overlap, then the displacement current from one monopole to its own set of radials can be partially obstructed by the radi-

als of the other element. To be safe, it is probably a good idea to solder all radial crossing points in any SEL ground system, no matter how many elements.

Table 11 contains the same information as Table 10, but here the antennas are listed in order of increasing gain, without concern

Table 13
Performance data for four-square arrays with broadcast-type (BCT) radial ground systems. The ground screens are listed in order of increasing gain.

Model Number	Number and Maximum Length (λ) of Radials per Element	Gain (dBi)	Take-off Angle (Degrees)	Total Length of Buried Wire (λ)
56	15 0.5	5.32	23	19.74
51	20 0.375	5.53	23	20.6
47	30 0.25	5.74	23	24.16
57	30 0.5	5.95	23	36.48
48	60 0.25	6.04	23	47.32
52	40 0.375	6.04	23	39.89
49	90 0.25	6.13	24	70.41
50	120 0.25	6.16	23	93.49
58	45 0.5	6.23	23	53.36
53	60 0.375	6.24	24	59.35
54	80 0.375	6.33	24	78.43
55	100 0.375	6.39	23	97.83
59	60 0.5	6.40	24	70.28
60	75 0.5	6.50	24	87.18
61	90 0.5	6.57	24	104.15

Note:

Since the radials for all of the elements are buried to the same depth, the gain of the array is identical in all four directions of fire.

Table 14
Performance data for four-square arrays with broadcast-type (BCT) radial ground systems. The ground screens are listed in order of increasing total length of buried wire.

Model Number	Number and Maximum Length (λ) of Radials per Element	Gain (dBi)	Take-off Angle (Degrees)	Total Length of Buried Wire (λ)
56	15 0.5	5.32	23	19.74
51	20 0.375	5.53	23	20.6
47	30 0.25	5.74	23	24.16
57	30 0.5	5.95	23	36.48
52	40 0.375	6.04	23	39.89
48	60 0.25	6.04	23	47.32
58	45 0.5	6.23	23	53.36
53	60 0.375	6.24	24	59.35
59	60 0.5	6.40	24	70.28
49	90 0.25	6.13	24	70.41
54	80 0.375	6.33	24	78.43
60	75 0.5	6.50	24	87.18
50	120 0.25	6.16	23	93.49
55	100 0.375	6.39	23	97.83
61	90 0.5	6.57	24	104.15

Note:

Since the radials for all of the elements are buried to the same depth, the gain of the array is identical in all four directions of fire.

for the number or length of the radials. When two antennas have the same gain, they are listed in order of increasing radial length. If at least 6 dBi of gain is desired, then about 60λ of wire needs to be used in the ground screen. Notice that only those arrays using ground systems with 0.5λ radials are able to achieve a gain of more than 6.5 dBi. If one can install radials no longer than 0.25λ , then at least 90 (per element) must be used in order to approach the 6.5 dBi gain figure. Models 37 and 41 are interesting because they use different lengths and numbers of radials, yet both achieve the same forward gain, and both employ the same total length of buried wire.

Four Square Arrays with Broadcast-Type Radial Ground Screens

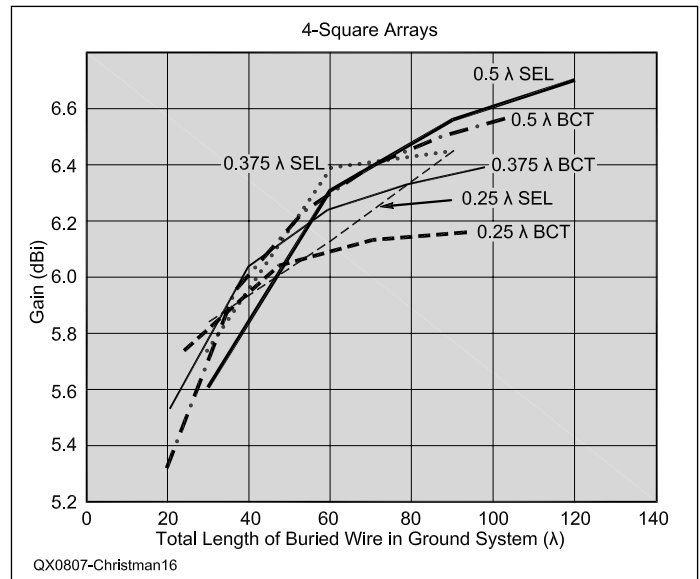
Figure 15 shows a four square array [model 47] which is similar to that of Figure 12, but this antenna employs a BCT ground-screen rather than the SEL type. All of the radials are buried to a depth of 3 inches; wherever they touch one another, they are truncated and bonded to a bus-wire. There are 30 radials per element, and their maximum length is 0.25λ .

The final group of four square arrays that were simulated on the computer [models 47 through 61] use a broadcast-type (BCT) ground system. Again the number of radials varies from 15 to 120 per element, and the maximum length of the radials spans the range from 0.25 to 0.5λ . Table 12 lists the number of radials per element, along with their maximum length, the peak gain and corresponding take-off angle (TOA) at which maximum gain occurs, and the total length of buried wire required for each ground screen.

The antennas are listed in order of increasing number and length of radials. As usual, for any given length, the addition of more radials always produces more gain, although the incremental improvement decreases as the number of radials becomes very large. A BCT-style ground screen uses the same burial depth for all radials, so the gain of these arrays is identical in all four directions of fire. The total length of buried wire in a BCT ground system, however, is always less than that of the corresponding SEL screen (with the same number of radials and maximum radial length).

Table 13 contains the same information as Table 12, but now the arrays are listed in order of increasing gain, irrespective of the number and/or length of the radials. When two antennas have the same gain, they are listed in order of maximum radial length. If at least 6 dBi of gain is desired, then a minimum of about 40λ of wire needs to be installed in the ground screen (model 52). If the maximum allowable radial length is 0.25λ , then at least 60 must be used (per element) in order

Figure 16 — A plot of antenna gain versus total length of buried wire, for all of the four-square arrays, using both styles of radial ground screen (SEL and BCT).



to achieve 6 dBi of forward gain. As was true with the SEL arrays, only those BCT ground systems with 0.5λ -radials are able to achieve a gain of 6.5 dBi or more.

Table 14 repeats the data from Table 12 once more, but now the order of entry has been changed so that the overall length of wire in the ground system has precedence. Generally speaking, the gain of the antenna increases as more wire is buried in the soil, although there are a few exceptions. Notice that 6.04 dBi of gain is achievable by using either 60 radials whose maximum length is 0.25λ , or 40 radials whose maximum length is 0.375λ . The ground-screen with 0.375λ -radials uses less buried wire, but requires a lot of extra space.

Figure 16 plots antenna gain versus the total length of buried wire in the ground system, for all of the four square arrays discussed in this section, including both SEL and BCT types. The chart provides a concise overview of the relative performance of the various radial ground screens. If the total length of wire in the ground screen is on the order of 35 to 45λ , then a BCT-type system (with 0.375 or 0.5λ -radials) works best; if 50λ or more of wire is employed, then an SEL-type screen (again with 0.375 or 0.5λ -radials) is superior. Other configurations of buried wires were not examined for use with four-squares, because they had proven to be inferior to radial ground systems when examined earlier in this study.

Limitations

I must emphasize that these computer simulations are imperfect representations of the real world, and cannot include all of the features that are actually present, such as buildings, vegetation, other conductive

objects, irregularities in the terrain, non-uniform ground constants, and so on.

Conclusions

For a multi-element phased-vertical array, it appears that a ground system composed of symmetrically placed equal-length (SEL) radials can provide the highest gain for a given total length of wire, in most situations. Computer simulation suggests, however, that it is important to bond the various radials together wherever they cross one another. If non-overlapping radials are desired, then a broadcast-type (BCT) ground screen is a practical alternative to the SEL arrangement, although it usually generates somewhat less gain. None of the more “exotic” ground-screen configurations that were examined in this study proved to be competitive.

Notes

¹Al Christman, K3LC, “Ground System Configurations for Vertical Antennas,” *QEX*, Jul/Aug 2005, pp. 28-37.

²Several versions of the *EZNEC* antenna-modeling software are available from Roy Lewallen, W7EL, PO Box 6658, Beaverton, OR 97007.

³*EZNEC4* models for several of the arrays described in this article are available for download from the *QEX* Web site. Go to www.arrl.org/qexfiles and look for the file **07x08_Christman.zip**.

⁴Private communication with Roy Lewallen, W7EL, June 2005.

Al Christman, K3LC, is a Vietnam-era veteran of the US Army, and is currently a professor of electrical engineering at Grove City College, Grove City, PA. First licensed as WA3WZD in 1974, Al is an active DXer with honor roll status on 20 m SSB.



Observations on Ferrite Rod Antennas

Here are the results of the author's extensive research into winding ferrite rod antennas

Although the air-core loop antenna was known from the earliest days of radio, its modern variant, the ferrite loopstick, was made possible by the development of ferrite materials in the mid 1940s.¹ Coupled with the introduction of transistors, the loopstick made it possible to produce compact, truly portable AM broadcast band receivers.

Although the Amateur Radio literature contains ferrite loop antenna design articles, their focus is upon replication of the presented designs.² Two notable exceptions aside, many of the peculiarities of working with ferrite loop antennas are not well covered in the amateur literature.³ Even the readily available engineering literature gives short shrift to ferrite loops.⁴

In working with ferrite loops while building receiving antennas for the frequency range of 10 kHz to 2 MHz, I found considerable divergence between practice and theory. This article attempts to capture my experiences in building and testing more than 50 ferrite rod antenna configurations.

These results are not oriented to designs that may be copied and replicated, but rather serve as a guide for those wishing to experiment with this small corner of antenna development. Nevertheless, sufficient detail is provided to permit replication of the more successful configurations.

Theoretical Considerations

By Faraday's law, we know the voltage induced into a loop of wire is equal to the rate of change of the magnetic flux through the loop. If the loop contains more than one turn, and is physically small, each turn's induced voltage, in essence, is in series with all other turns. Ignoring signs, since the amplitude of the received signal is our interest,

¹Notes appear on page 34.

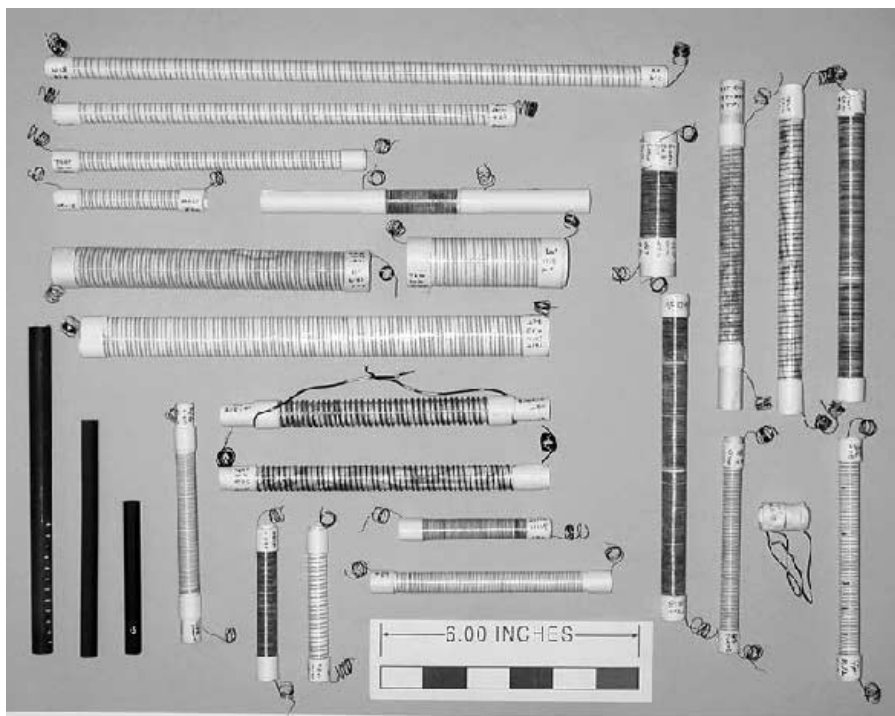


Figure 1 — Selection of test coils and rods.

we have, by Faraday's Law:⁵

$$V_{oc} = N \frac{d\Phi}{dt} \quad [\text{Eq 1}]$$

where:

V_{oc} = Open circuit voltage (volts)

N = number of turns

Φ = magnetic flux (webers)

with $\frac{d\Phi}{dt}$

representing the rate of change of the flux with time.

If the loop is small compared with a

wavelength, Φ may be assumed to be constant throughout the loop area at any instant of time. If so, the total flux, Φ , and the flux density, B , have a simple relationship:⁶

$$\Phi = BA \cos \phi \quad [\text{Eq 2}]$$

where:

B = flux density (webers / square meter)

A = loop area (square meters)

ϕ = angle between the plane of the loop axis and the incoming flux

A radiated electromagnetic field, such as a radio wave, contains both electric and magnetic field components, related as follows:⁷

$$E = cB \quad [\text{Eq 3}]$$

where:

E = electric field (volts / meter)

c = the speed of light, approximately 300×10^6 meters / second in a vacuum

B = flux density (webers / square meter)

Solving Equation 3 for B and substituting it into Equation 2 allows us to express the open circuit voltage induced in a loop as a function of the electric field strength of the incoming electromagnetic signal.

$$V_{oc} = \frac{NA}{c} \frac{dE}{dt} \cos \phi \quad [\text{Eq 4}]$$

For radio waves of the type we are interested in receiving, both the electric and magnetic field strength varies with time in a sinusoidal fashion, such that:

$$E = E' \sin(2\pi ft) \quad [\text{Eq 5}]$$

where:

E = instantaneous value of electric field

E' = peak electric field

f = frequency in Hz

t = time

$\frac{dE}{dt}$ is thus simply

$$E' 2\pi f \cos(2\pi ft)$$

Since we are interested only in the peak magnitude of V_{oc} , we may further simplify ($\cos(2\pi ft) = 1$, $E = E'$) with the result that

$$\frac{dE}{dt} = E' 2\pi f$$

We have now arrived at the relationship between the incident electric field signal

strength and the induced loop voltage:

$$V_{oc} = \frac{NAE' 2\pi f}{c} \cos \phi \quad [\text{Eq 6}]$$

Since f/c is simply the reciprocal of wavelength, λ , we can further simplify and recast Equation 6 into its familiar form:

$$V_{oc} = \frac{2\pi ENA}{\lambda} \cos \phi \quad [\text{Eq 7}]$$

where:

λ = wavelength in meters

A loop antenna is also, of course, an inductor. If the loop is resonated, the induced voltage will be increased. Recalling from basic circuit theory that Q is also the voltage magnification factor, Equation 7 can be modified to reflect the tuned case:

$$V_{oc} = \frac{2\pi ENAQ}{\lambda} \cos \phi \quad [\text{Eq 8}]$$

where:

Q = the loaded Q of the tuned circuit

Adding a ferrite rod core to the receiving loop increases V_{oc} . Theory provides that the ferrite core, having a large relative permeability, collects and concentrates the incident magnetic flux, thereby increasing dB/dt , and consequently V_{oc} . The literature shows V_{oc} increasing directly with the effective relative permeability, μ_{eff} , of the core:⁸

$$V_{oc} = \frac{2\pi ENAQ\mu_{eff}}{\lambda} \cos \phi \quad [\text{Eq 9}]$$

where:

μ_{eff} = effective permeability of the rod/coil combination

The $\cos \phi$ factor is responsible for the

familiar null as the loop is rotated in azimuth. When the loop plane is 90° to the magnetic field, $\cos(\phi) = 0$ and hence V_{oc} is also zero.

Equation 9 is deceptively simple — for a given frequency and incident field strength, the received signal level is directly proportional to the loop area, the number of turns, the Q , and the effective permeability of the core.

Air cored loops are well behaved and Equation 8 describes their behavior with remarkable accuracy, as $\mu_{eff} = 1.0$ regardless of the loop geometry. However, as the remainder of this article demonstrates, the behavior of practical ferrite rod antennas is anything but simple! We will discover, for example, that μ_{eff} is not a constant, but rather depends upon:

- The type of material used in the core;
- The length of the winding in proportion to the length of the core;
- The ratio of the length of the core to its diameter;
- The position of the windings along the core;
- The ratio of wire diameter to wire spacing; and
- The frequency

The effect of these factors, and others, are presented in the remainder of this article.

Terminology

A number of terms are used through the text, and are defined below for convenience.

- L_0 — the inductance of a test coil without a ferrite rod inserted (with an air core).
- L — the inductance with a ferrite rod inserted.
- μ_{eff} — the ratio L/L_0 , or the ratio of increase in inductance when a ferrite rod is inserted into a coil with a specific geometry.

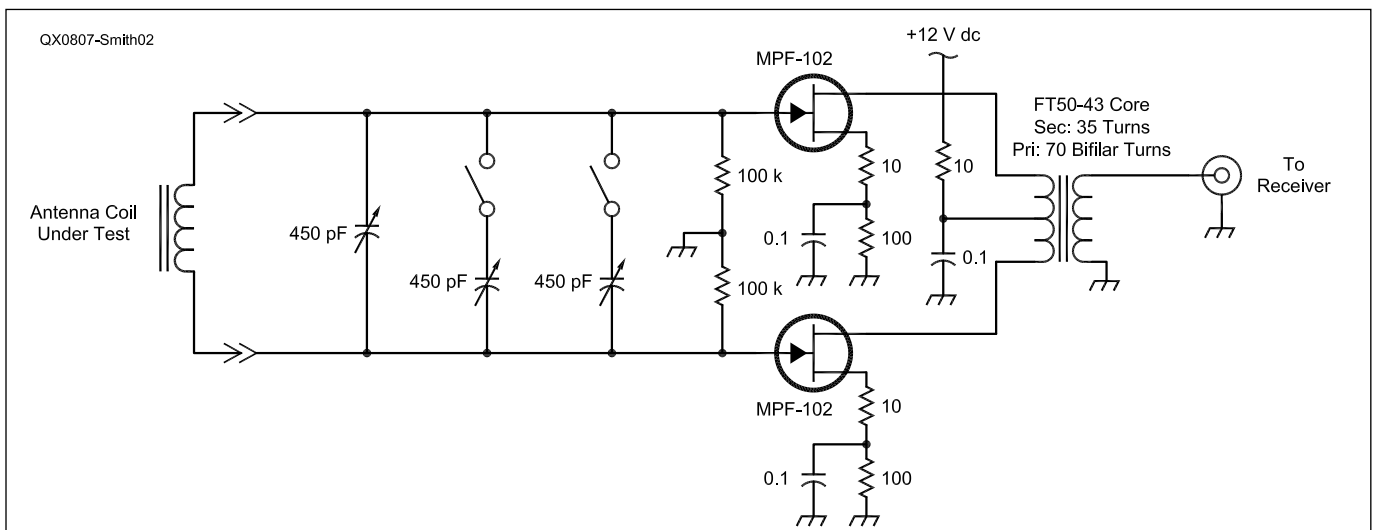


Figure 2 — Test amplifier.

- μ_0 — the permeability of free space; numerically $4\pi \times 10^{-7}$ henry/meter in SI units.
- μ_i — initial relative permeability of the material comprising the core, usually measured in a toroidal configuration.
- μ_{rod} — relative permeability of a ferrite rod of a specific geometry, determined using the theoretical demagnetization factor. Adjustments must be made to μ_{rod} to yield μ_{eff} .

Coil Construction

The data presented is based on more than 50 test coils I constructed and evaluated during June and July 2000. Each coil was wound over a paper core, with wire sizes from AWG no. 34 through AWG no. 16, as required for the purpose, and was given a unique number for identification. A sampling of the test coils is shown in Figure 1. Most coils were tested with at least two rod types, with varying positions, frequencies, and so on, so that several thousand individual measurements were taken.

The paper core consisted of approximately four wraps of standard copy paper, secured with household glue, wound over a steel mandrel. The mandrel was turned in a Myford Super-7 lathe to the appropriate size to permit the different ferrite cores to be snugly slid inside the core, 0.500-inch diameter for the Type 33 and Type 61 cores, and approximately 0.390-inch diameter for the surplus cores. Where multiple cores were used, such as the test of six surplus cores, arranged in a 3-long by 2-wide configuration, separate paper cores were used, which were then, in turn, wrapped with an outer paper core, upon which the windings were wrapped. After winding, the coil was coated with GC "Coil Dope" to secure the windings. The coil ends were additionally secured with several turns of 0.5-inch adhesive tape. Generous leads were allowed.

Standard paper is usually considered as an undesirable material for coil formers, as it is hygroscopic. However, for short-term test purposes, in a controlled environment, the cost and ease of working outweigh the long-term problems of the paper.

The coils were wound using a home-made wire feed installed on a Myford Super 7 lathe, equipped with a gearbox offering a range of pitch options from 8 through 56 TPI. Finer increments were available, but were not used during these tests.

Test Procedures

Inductance, Q and μ_{eff} — Inductance (both L_0 and L) and Q were measured using a Boonton Model 260A Q-meter. The rated accuracy in the frequency ranges used is $\pm 5\%$

for Q and $\pm 3\%$ for inductance. Checks using a selection of Boonton Model 103 inductance standards indicate that the Q-meter meets these performance specifications. L_0 measurements were in most cases taken at 7.9 MHz, while L measurements were at 790 kHz. These are "standard" test frequencies for Boonton/HP Q meters, at which the instrument's inductance scales may be directly read. Inductances outside the range permitted at these two test frequencies used a different frequency, based on the instrument's recommended test frequency for the inductance being measured. Since μ_{eff} is defined as L/L_0 , it was calculated based upon these two measured inductances, not directly measured. Ideally, L and L_0 would both be measured at the same frequency, but practical limitations make this difficult at best.

Signal Level — To measure the receiving effectiveness of various configurations, a simple balanced input resonator/amplifier, based upon a published design by DeMaw was used.⁹ See Figure 2. The amplifier output was fed into a Racal RA6790/GM receiver, as illustrated in Figure 3. The receiver was operated with AGC off and the IF-gain manually adjusted to be in the linear mode. Under these conditions, the 455 kHz IF output of the receiver is proportional to the received signal level. This level was read with a Hewlett Packard 3400A true RMS analog voltmeter, with an upper frequency limit of 10 MHz.

A local standard AM broadcast station, WMAL, 630 kHz, was used for medium wave signal comparisons. Some long wave comparisons were made using non-directional beacons, DC, at 332 kHz and IA at 346 kHz. Limited measurements were also made with WWVB, 60 kHz.

Each test antenna was connected to the amplifier and the resonating capacitor adjusted for peak signal. Additional sections of the tuning capacitor were selected, as necessary for resonance. The 3400A voltmeter reading was recorded, with care taken to read the meter during speech pauses or quiet carrier times for the non-directional beacons. WWVB was read at modulation peaks. At the outset of any test run, the antenna fixture was adjusted to peak the received signal with

initial antenna tested. The orientation was not moved for subsequent tests of different antennas.

The signal readings are *relative* and thus indicate only the performance of one antenna against another. In most cases, comparison readings were taken at one sitting. However, some later measurements were made as new configurations were developed. In these cases readings were also taken with a reference antenna, thereby enabling later measurements to be correlated with earlier measurements.

Out-Of-Range Tests — A final series of tests were run on several coils to determine their performance as inductors at frequencies between 4 and 50 MHz using a HP 8754 network analyzer with the configuration shown at Figure 4. The inductor under test is placed in series with the swept output of the network analyzer using a homemade test fixture. A Tektronix TDS430 digital oscilloscope was used to capture the network analyzer output in a convenient digital form.

Unloaded or Loaded Q?

Unless explicitly stated to the contrary, references to the coil quality factor, Q , in this article are to the values measured using the 260A Q-meter. For practical purposes, the 260A measures "unloaded" Q .¹⁰ When a coil is used as an antenna in the test circuit of Figure 2, it is shunted by the 100 k Ω gate resistors. Since the gate resistors are effectively in series, 200 k Ω is imposed across the tuned circuit, thereby lowering the Q , and the resultant voltage magnification of the signal level.

For a 200 μ H antenna coil — a value typical of those measured—the effect of the gate resistor shunt can be significant. For example, at 1 MHz, an unloaded Q of 200 is reduced to 88.6 by the effect of the 200 k Ω shunt impedance.

The following approach may be used to calculate Q_{loaded} .

Q is defined, for the parallel model, as:

$$Q_{unloaded} = \frac{R_p}{2\pi fL} \quad [\text{Eq 10}]$$

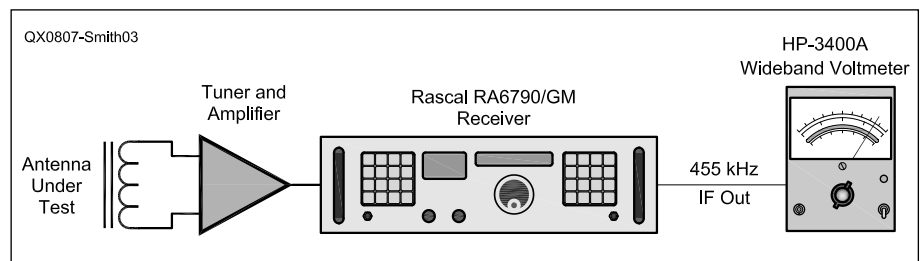


Figure 3 — Signal measurement setup.

Or, rearranging:

$$R_p = 2\pi fLQ_{\text{unloaded}}$$

where:

R_p = equivalent parallel resistance of the internal coil losses

f = frequency

L = inductance

Using the unloaded Q , calculate R_p

Determine the effective shunt resistance,

$$R_p' = \frac{R_p R_G}{R_p + R_G}$$

R_G = the gate resistance shunting the coil
The loaded Q is then:

$$Q_{\text{loaded}} = \frac{R_p'}{2\pi fL}$$

The most significant effect of using 100 k Ω gate resistors in the test amplifier is to diminish the benefit of using the higher Q , Type 61 core material. Thus, the relative benefits of the Type 61 material are understated in this article's signal level comparisons. However, in practice, a relatively low value of R_G may be desirable to intentionally reduce the loaded Q . At 1000 kHz, for example, a Q of 300 — a value easily achievable with Type 61 material — yields a 3 dB bandwidth of 3.3 kHz. This narrow bandwidth imposes tuning difficulties, may give rise to temperature stability concerns and will muffle the audio of AM broadcast radio signals. These concerns are ameliorated if the Q is reduced through parallel resistance. In this example, the 100 k Ω gate resistors reduce the loaded Q to 104, assuming $L = 200 \mu\text{H}$. The 3 dB bandwidth is correspondingly increased to about 10 kHz, and tuning is much easier. Of course, the price paid for the lower Q is the received signal voltage is reduced to about one-third the $Q = 300$ case. The gate resistors in Figure 2 could be increased to several megohms, if desired, to improve loaded Q .

Length/Diameter Ratio Effect on Rod Permeability

If a test coil is wound over the full length of a ferrite core and the inductance of the test coil is measured with and without the rod in place, μ_{eff} will be found to be, for reasonable rod dimensions, much less than the permeability of material from which the rod is constructed, μ_i . (The permeability value based upon theoretical considerations for a coil wound over 100% of the rod length is commonly referred to as the "rod permeability," or μ_{rod} . However, the actual measured permeability μ_{eff} is almost always less than μ_{rod} , and if the coil occupies less than the full length of the rod, μ_{eff} will be even lower.)

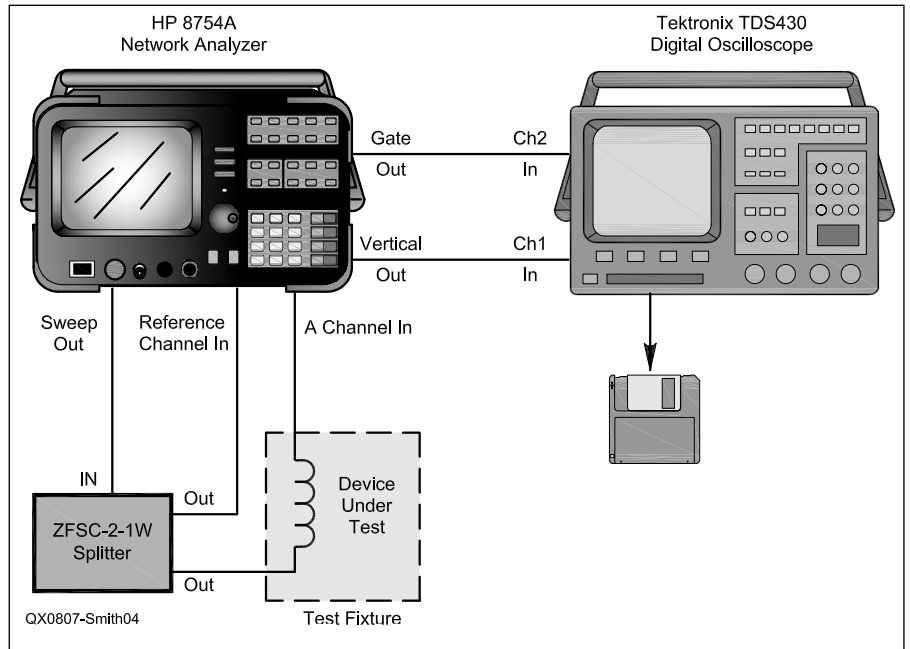


Figure 4 — Out-of-band sweep configuration.

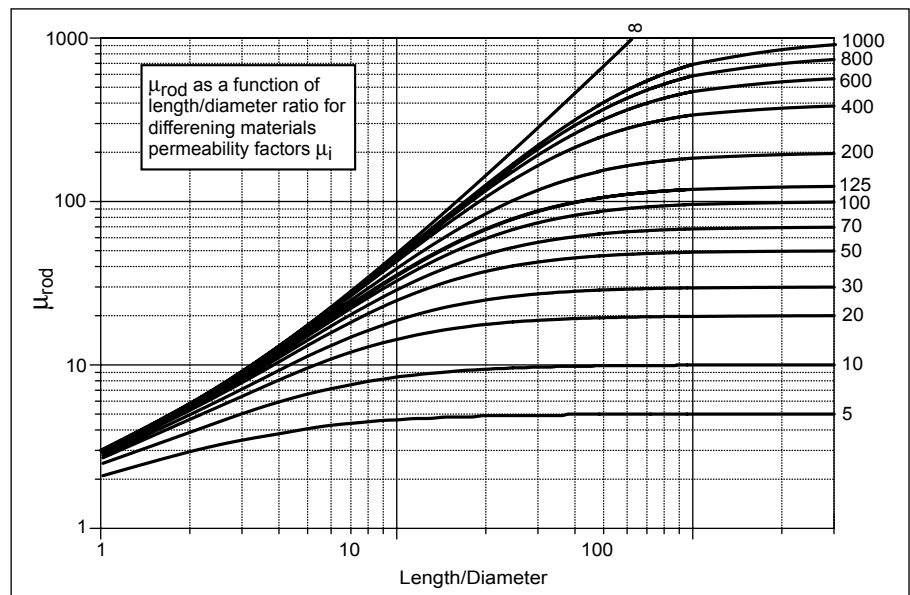


Figure 5 — Effect of rod length / rod diameter of rod permeability.

The theoretical relationship between μ_{rod} and μ_i is:^{11, 12}

$$\mu_{\text{rod}} = \frac{\mu_i}{1 + D(\mu_i - 1)} \quad [\text{Eq 11}]$$

where:

D = demagnetization factor

As Lenz's law provides, an induced current generates a magnetic field in the surroundings, including the core, in a direction opposing the inducing current's magnetic field. The demagnetizing factor, D , is a measure of effectiveness of the opposing field.

Computing D for an arbitrary core shape is difficult or impossible. Fortunately, D can be determined for a simple cylindrical rod-shaped core. In this case, D is a function of the ratio of the rod length, l , to the rod diameter, d . For an infinitely long cylindrical rod, $D=0$ and $\mu_{\text{rod}} = \mu_i$, while for a rod with a length/diameter ratio = 1.00, $D = 0.27$, and $\mu_{\text{rod}} = 3.6$ if $\mu_i = 125$.

Based upon Equation 11 and published D values, I calculated the relationship between μ_{rod} and μ_i and Figures 5 and 6 show my results.¹³ For l/d ratios below 10, both figures shows slightly lower μ_{rod} values than

provided in other published curves.¹⁴ Figure 5 presents the μ_{rod} versus l/d in the conventional fashion, while Figure 6 recasts the data to better illustrate the effect of l/d on μ_{rod} by parameterizing l/d .

Figure 7 plots D as a function of l/d to aid in making the calculations called for by Equation 11. Likewise, it is possible to work backwards and estimate μ_i from μ_{rod} measurements. Solving Equation 11 for μ_i yields:

$$\mu_i = \frac{\mu_{rod}(1-D)}{1-D\mu_{rod}} \quad [\text{Eq 12}]$$

In my experience, however, measured μ_{rod} values will almost never match the theoretical μ_{rod} numbers for commonly available rod materials and dimensions, although making the adjustments described below reduces divergence between measured and theoretical data.

Effect of Winding Over Less than the Full Length of the Rod

If the winding occupies less than the full rod length, μ_{eff} decreases. Q , however, in my measurements, is maximized for short centered windings and decreases as the winding extends over a greater proportion of the rod length. This is contrary to *The ARRL Antenna Book* statement that maximum Q is found when the winding occupies the full coil length.¹⁵ Figure 8 plots Q measured with air core, Type 33 core and Type 61 core for 28 coils versus core length to rod length ratio. The data is greatly scattered because the test coils have a variety of turns, wire diameters and pitch, but it shows an unmistakable trend to lower Q as the winding occupies a greater proportion of the core length. ($R = -0.42$ for Type 33 material and $R = -0.47$ for Type 61 material. No statistically valid similar trend can be seen for the air core Q data ($R = -0.06$) This data represents a limited range of coil geometry (0.5 inch diameter, 7.5 inch long rod) and hence may require caution in applying to the general case.

Since Equation 9 shows the received signal level in a tuned loop is proportional to product of μ_{eff} (increases with winding length) and Q (decreases with winding length), the length of winding providing maximum sensitivity requires further examination. We first turn to the relationship between V_{oc} , μ_{eff} , μ_{rod} and the ratio of winding length to rod length. We introduce an adjustment factor — the “Free End Factor” as it is known — relating μ_{eff} to μ_{rod} as a function of the length of the coil relative to the rod:

$$\mu_{eff} = \mu_{rod} \times f(l_c/l_r) \quad [\text{Eq 13}]$$

where:

- l_c is the length of the coil
- l_r is the length of the rod

$f(l_c/l_r)$ is a function providing an adjustment factor to relate the measured μ_{eff} to the theoretically predicted value, based on the ratio of winding length to total rod length.

I've found two versions of $f(l_c/l_r)$ in the literature, one presented in recent editions of *The ARRL Antenna Book* and the second in Johnson and Jasik's *Antenna Engineering Handbook*, 2nd Edition.

The ARRL Antenna Book version is:¹⁶

$$\mu' = \mu_{rod} \sqrt[3]{\frac{a}{b}} \quad [\text{Eq 14}]$$

where:

- μ' is μ_{eff} in the terminology of this article
- a is the length of the core (rod) (l_r)
- b is the length of the winding (coil) (l_c)

At a minimum, Equation 14 seems to incorrectly exchange a and b , as it has μ'

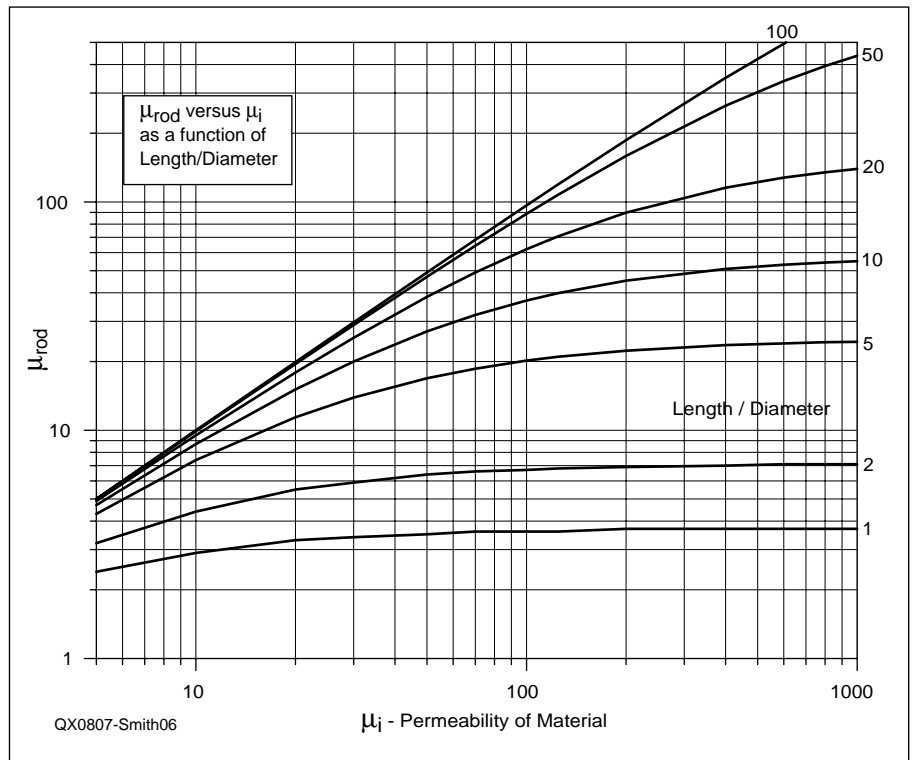


Figure 6 — μ_{rod} as a function of rod length/diameter.

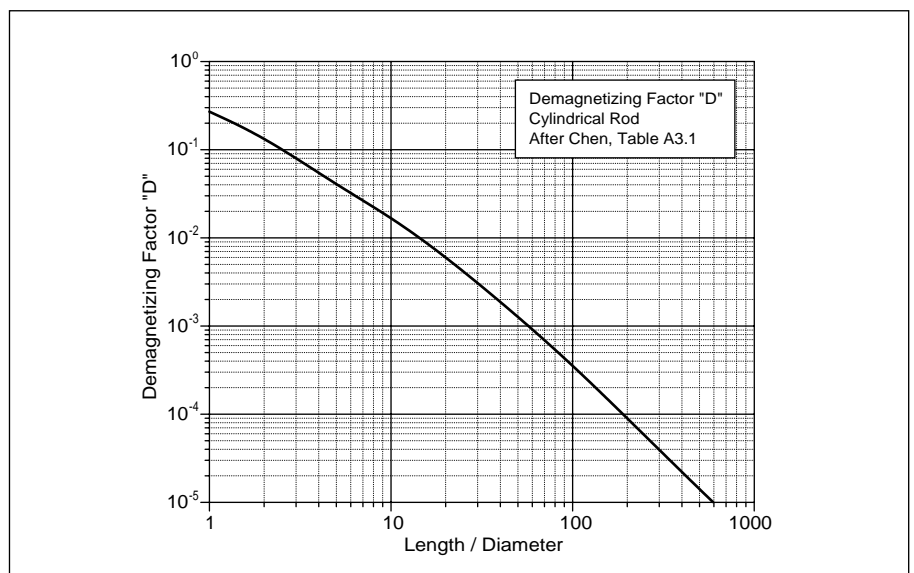


Figure 7 — Demagnetizing factor D versus l/d for cylindrical rod.

increasing without bounds as the winding length decreases as a proportion of core length. This is contrary to Johnson and Jasik, as well as other references and my measurements, in addition to being physically implausible. Since *The ARRL Antenna Book* provides the equation without source reference, it is not possible to determine if the error is a simple transcription error, inadvertently exchanging terms *a* and *b*, or if there are other problems with it. Assuming that, *arguendo*, parameters *a* and *b* were inadvertently reversed without other errors introduced, the corrected form of Equation 14 (with modified terminology consistent with this article) is:

$$\mu_{\text{eff}} = \mu_{\text{rod}} \sqrt[3]{\frac{l_c}{l_r}} \quad [\text{Eq 15}]$$

Johnson and Jasik provide only a graphical representation of the relationship between μ_{eff} and l_c/l_r , (which they call correction factor F_L) but I've extracted the data points and fitted a cubic equation to their data. Figure 9 shows excellent agreement between the curve fit and the underlying data (R = 0.99).

$$\mu_{\text{eff}} = \mu_{\text{rod}} (0.0699 + 1.547x - 1.109x^2 + 0.208x^3) \quad [\text{Eq 16}]$$

where *x* is the ratio l_c/l_r .

To determine the effect of varying the winding length as a proportion of the rod length, and to assess whether these various adjustment factors were accurate, I wound coils occupying 20%, 40%, 60%, 80% and 100% of the rod length over mandrels for cores of Type 61 and Type 33. The target inductance of the test coils for Type 33 cores was 200 μH . This was achieved within $\pm 10\%$. The coils wound for the Type 33 rod were also used with the Type 61 core, accepting the lesser inductance.

As the coil length was increased to cover a greater percentage of the core length, the winding pitch (turns per inch) was necessarily reduced to maintain the target inductance value, reducing from 24 TPI for 20% coverage to 8 TPI for 100%. This decision to reduce the winding pitch to maintain (approximately) the same inductance complicates an already difficult analysis. As discussed below, μ_{eff} is also affected by the "winding fill ratio," in other words, as the ratio of copper to open space increases, so does μ_{eff} . Thus, the choice to maintain constant inductance with varying length potentially changes two variables at once.

Figure 10 compares the free end adjustment factors predicted by Equation 5-8 in *The ARRL Antenna Book*, as corrected above, Johnson and Jasik's F_L factor, and the free end factor I measured for both Type

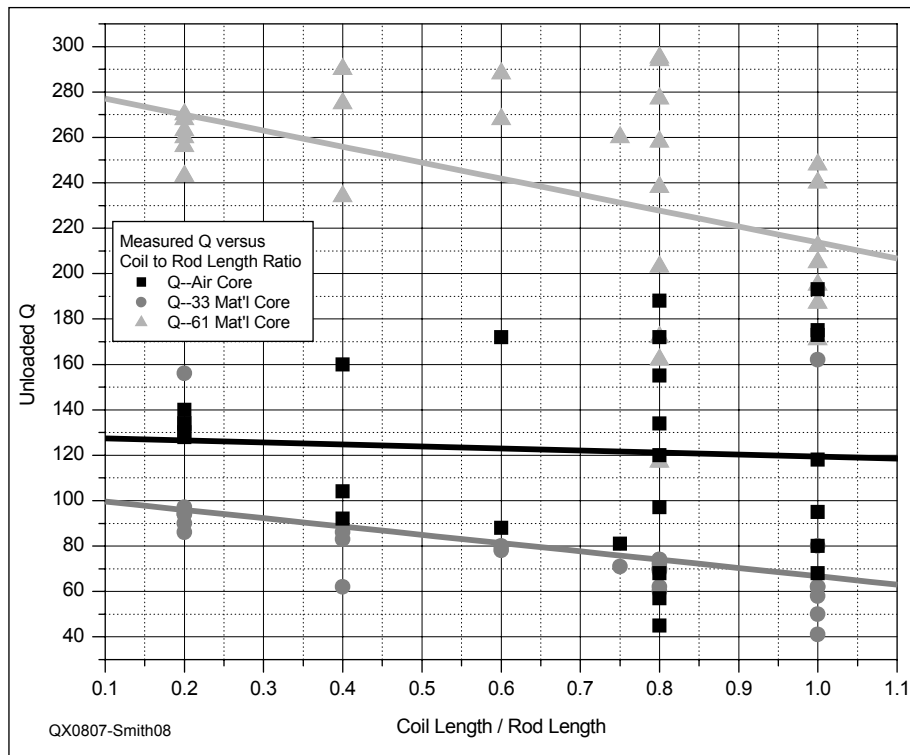


Figure 8 — Measured Q versus coil length to rod length ratio.

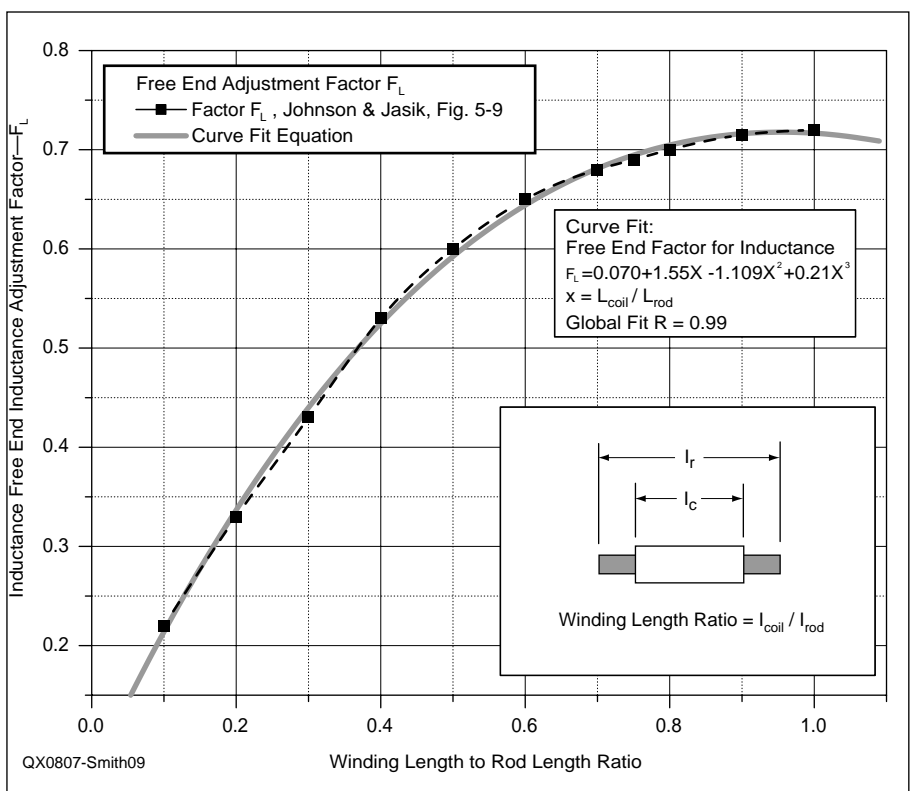


Figure 9 — Free end adjustment factor (μ_{eff}) (Johnson and Jasik).

33 and Type 61 material rods. The vertical bars in the measured data show the range of measured free end factor for different winding pitches and inductance values of my test coils. The figure shows significant divergence amongst the two prediction methods and my measured data. The reasons for the discrepancy remain unknown to me.

Further complicating an already complex matter, Johnson and Jasik note a different factor, F_v , relates the induced open circuit voltage to that computed with μ_{rod} :

$$V_{OC} = j\omega\mu_{rod}F_vNAB_z^i \quad [Eq 17]$$

where:
 V_{oc} is open circuit voltage induced in the loop
 $j\omega$ is the angular frequency, $2\pi f$ where f is frequency.

N is number of turns

A is the loop area

B_z^i is the component of the incident magnetic flux density normal to the plane of the loop.

Except for the factor F_v , Equation 17 is identical to Equation 7 when the simplifications introduced in this article are considered. F_v , like F_L , is provided in Johnson and Jasik only as a graphical factor, derived from experimental data. I've extracted data points for F_v and fitted a quadratic equation to it, as illustrated at Figure 11.

$$F_v = 0.998 + 0.0181x - 0.235x^2 \quad [Eq 18]$$

where x is the ratio l_c/l_r .

I have not, however, attempted to relate F_v to measured signal strength data.

Off-Center Windings

Where the coil winding occupies less than the entire length of the rod, it is possible to offset the winding so that it is no longer centered on the rod. To test this effect, I made a test coil of 20 turns close-wound, AWG no. 20 enamel magnet wire on a paper form. The length of the test coil was 0.62 inches and its measured inductance without a ferrite core was 3.2 μ H at 7.9 MHz, with a Q of 154. Measurements of Q , inductance, μ_{eff} and received signal voltage were taken as the test coil was moved in 0.25-inch increments from the center position, with rods of both Type 33 and Type 61 material.

Figure 12 shows that as the winding is displaced from center, Q and inductance decrease. (I observed a slight Q peak at an offset ratio around 0.6 for Type 33 material.) Q is little changed with moderate displacements, remaining within a few percent of the maximum value up to 40% off-center for Type 61 and up to 60% off-center for Type

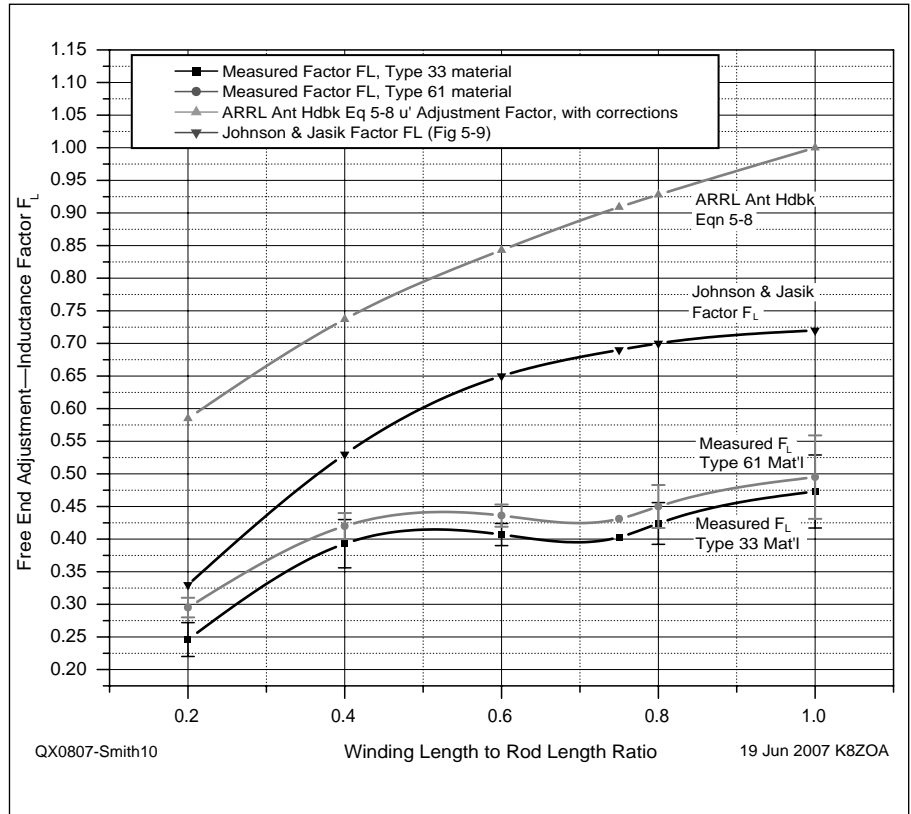


Figure 10 — Free end adjustment factors (μ_{eff}) compared with measured data.

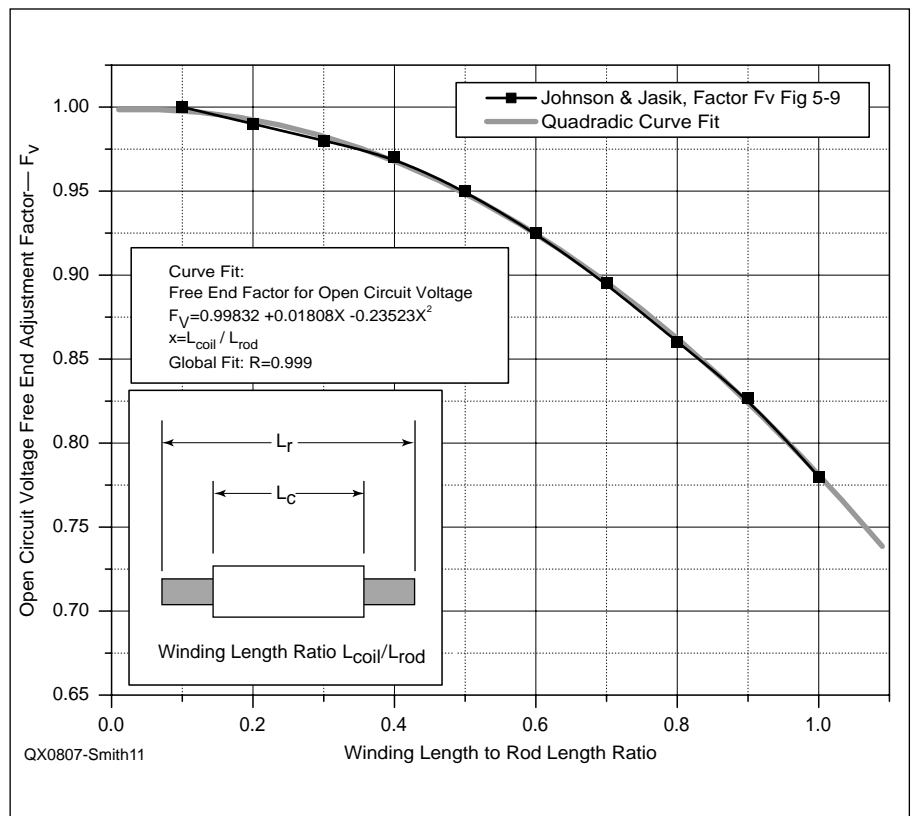


Figure 11 — Free end adjustment factor for open circuit voltage.

33 material. Inductance changes more with position, particularly with the higher μ Type 33 rod. Even here, however, 40% off-center placement reduces inductance by less than 10%. Both inductance and Q peak with the windings centered, consistent with statements in *The ARRL Antenna Book*. (One reason to offset the winding is to trim to a precise inductance value without materially affecting Q .)

Since μ_{eff} is defined as the observed inductance divided by the air-core inductance, the change in μ_{eff} with core offset the shape of inductance curve in Figure 12.

Equation 9 predicts that received signal voltage is proportional to $QN\mu_{\text{eff}}$. In this case, N is constant at 20 turns, while Q and μ_{eff} vary with the offset. Equation 9 therefore predicts the received signal voltage to be linearly proportional to the product $Q\mu_{\text{eff}}$. To test this, I collected relative signal strength data as the test coil was moved to different offsets and plotted the signal strength versus the product of the Q and μ_{eff} earlier measured for the same offset value. Figure 13 shows an excellent linear fit to the product of Q and μ_{eff} ($R = 0.997$) for the Type 61 rod, and almost as good fit for the Type 33 rod ($R = 0.985$). This analysis uses loaded Q values, and I have adjusted the measured Q to reflect the amplifier's input loading, although the amplifier results in less than a 10% reduction in Q for the test coil used. The signal readings in Figure 13 are relative, with the maximum observed signal level (Type 33 rod, coil centered) set to 1.00.

Figure 14 illustrates the variation in received voltage as the winding is offset from center. A twenty percent offset reduces the received signal only slightly.

Winding Fill Ratio

In addition to changes caused by core occupancy and off-center windings, μ_{eff} is a function of winding fill ratio. The winding fill ratio equals the conductor diameter divided by the winding pitch, as illustrated in Figure 15. The winding fill ratio is thus a measure of the "density" of the copper over the ferrite core. As the winding fill ratio approaches 1.00, the surface of the ferrite rod is nearly completely covered by the copper winding. (Of course, 1.00 is achievable only for one turn, as there must be some turn-to-turn gap.)

To study the effect of winding fill ratio, a series of 48-turn test windings were made, each 6.0 inches long, wound at 8 turns per inch on a paper core. To vary winding fill ratio, wire sizes from AWG no. 16 down to AWG no. 34 were used. Measurements were taken with both Type 33 and Type 61 cores.

Before discussing the results of varying the winding fill ratio on μ_{eff} , it is instructive

to consider its effect upon L_0 , the inductance without a ferrite core. Even though the number of turns and the coil length were held constant, L_0 , the coil inductance without a core, still varied. Two countervailing physical effects are responsible for most of the variation:

- Since the coils must be wound with a fixed inside diameter of 0.50 inches — so as to accommodate the ferrite core — as the wire diameter increases, the mean diameter of the coil necessarily increases. As the inductance of a solenoid is proportional to the square of its diameter, this factor alone accounts for an

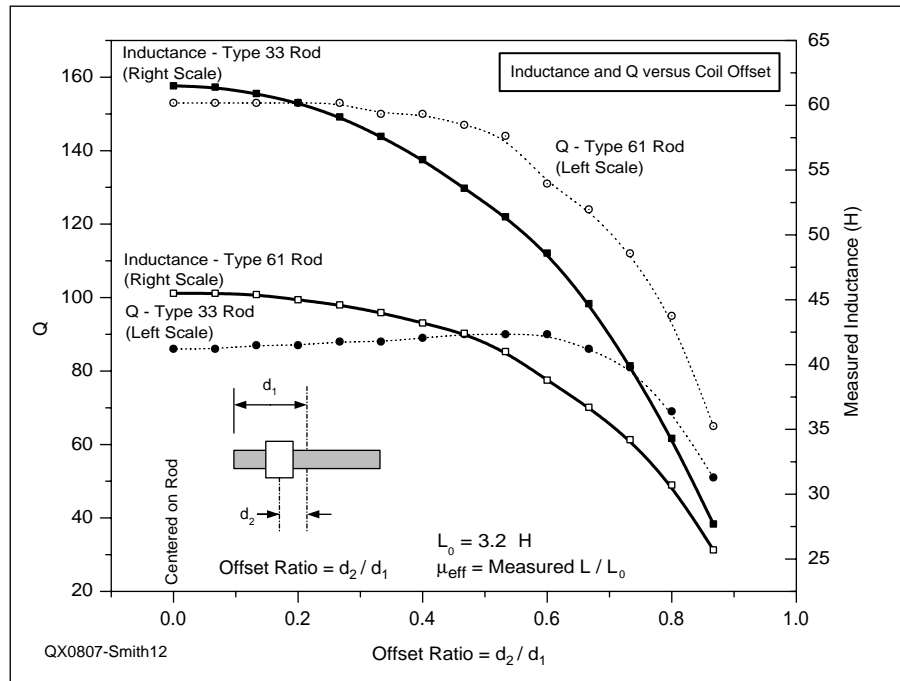


Figure 12 — Variation in L and Q with coil offset.

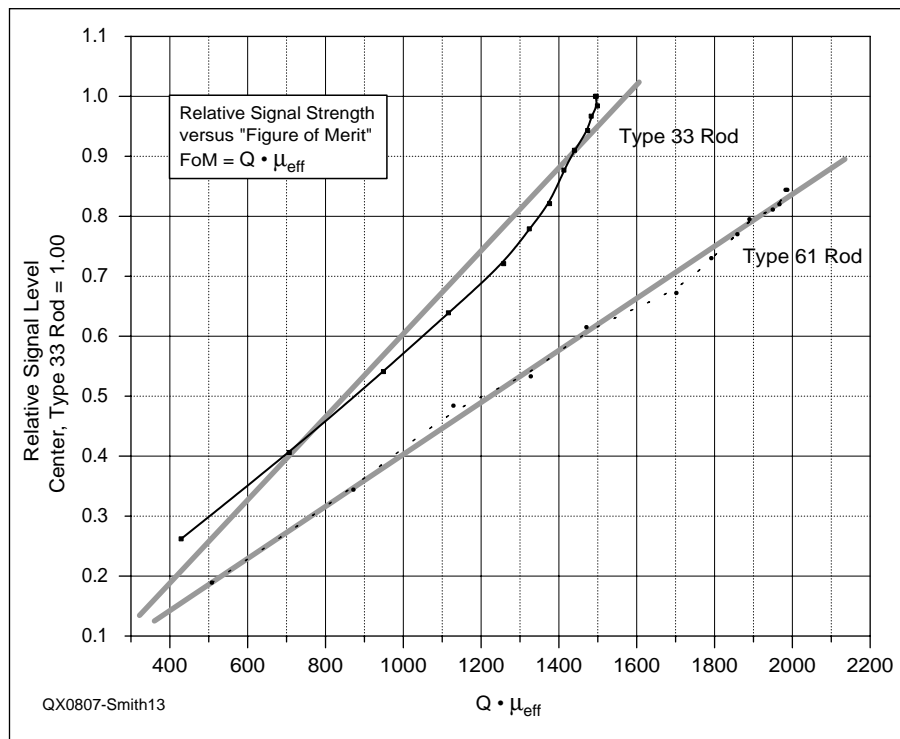


Figure 13 — Relative signal versus $Q\mu_{\text{eff}}$.

increase of 17% in the calculated inductance of the coil wound with 16 AWG wire over that of its 34 AWG counterpart.

• Commonly used inductance formulas — such as the classic Wheeler equation — are accurate only for current sheets, that is, where the current flows in an infinitesimally thin perfectly conducting tape with negligible gap between adjacent turns. A fixed pitch wound inductor looks less and less like a perfect current sheet as the wire diameter decreases and an appropriate correction must be applied if the coil is not close wound.¹⁷ Because the space-wound correction factor is not easily located, Appendix 1 reproduces the key equations, including Wheeler's basic single winding solenoid inductance equation.

After calculating the current sheet inductance using Wheeler's equation, the wire spacing adjustment outweighed the increase in inductance with larger wire diameter, with the coil wound with 34 AWG having a calculated inductance some 15% above that of its 16 AWG counterpart.

Returning to the effect of the winding fill factor upon μ_{eff} , Figure 16 illustrates that as the ratio of copper to open space increases, so does μ_{eff} .

Choice of Core Type

Two rod-type core materials are readily available from suppliers:

- Type 33 material; $\mu_i = 600$ to 800, optimum frequency 10 kHz to 1 MHz.¹⁸
- Type 61 material; $\mu_i = 125$, optimum frequency 0.2 MHz to 10 MHz.

These cores are commonly available in two sizes, both 0.5 inch diameter, with lengths of 4 inches and 7.5 inches. Some suppliers also stock other diameters and lengths.

When used as an antenna, our interest in ferrite rods is to maximize received signal strength at the frequency of interest, or, perhaps more correctly, to maximize the signal to noise ratio of the received signal. Of

interest in the mass production environment is selecting a core that permits a reasonably sized tuning capacitor and meets the cost targets. In the one-off amateur environment, these latter considerations are of less importance and will not be further considered in this article.

Based upon the material specifications, it might be assumed that Type 33 material would be preferred for up to 1 MHz, including the new sub-200 kHz amateur bands available in some countries, while Type 61 material would be better for general broadcast band listening up through the 160 meter band.

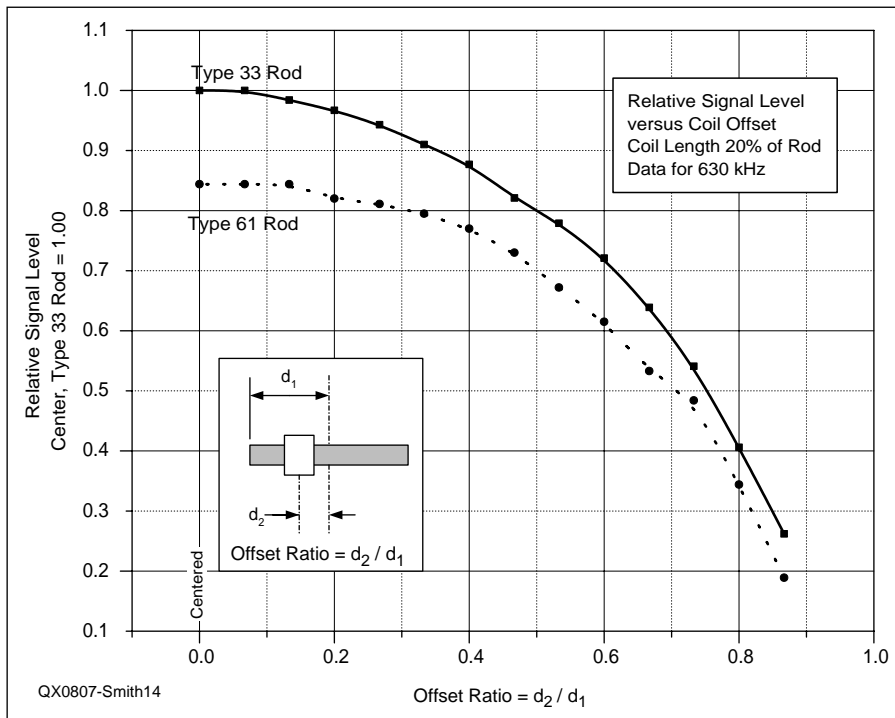


Figure 14 — Variation in received signal with coil offset.

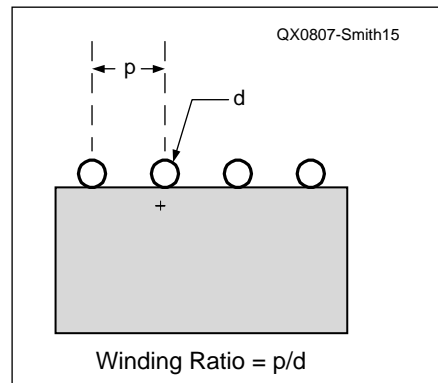


Figure 15 — Winding ratio.

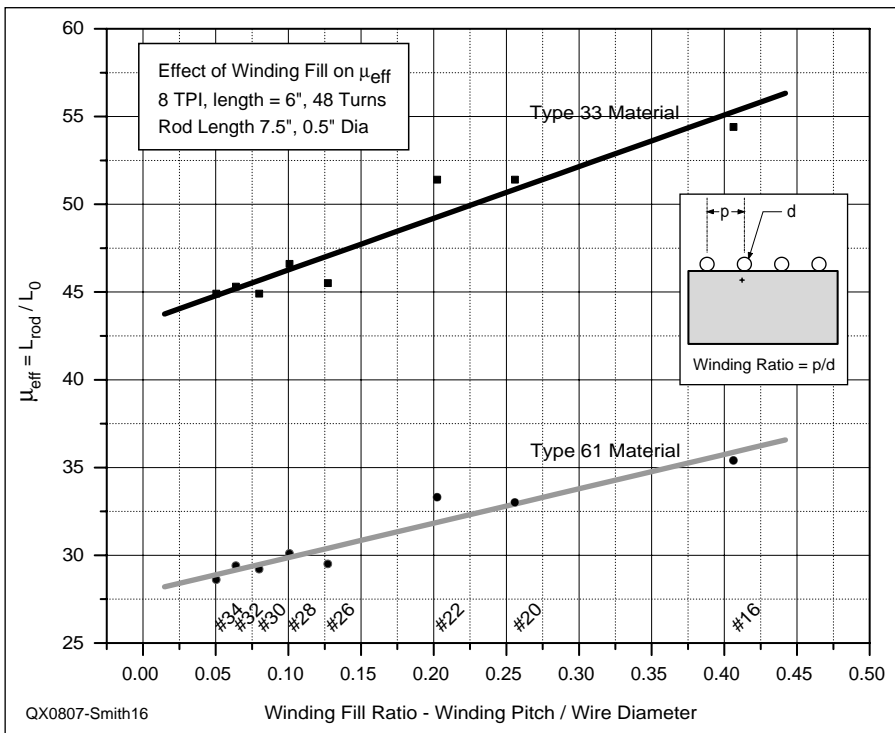


Figure 16 — μ_{eff} increases with increasing winding fill ratio.

This is not the case, however. My measurements demonstrate that Type 61 material is to be preferred for all frequencies between 60 kHz and 2 MHz.

Figure 17 illustrates the relative performance of three key parameters for Type 33 and Type 61 cores; received signal level, Q and μ_{eff} . The data is for a 6-inch long coil, 48 turns of AWG no. 22, wound at 8 turns/inch, and sets the performance of the Type 33 material version at 1.00. Ratios > 1 indicate Type 61 material is superior. Alternating measurements were made with a Type 33 rod and Type 61 rod cores, re-resonating the antenna after each core change. For almost all frequencies studied, from 60 kHz through 1600 kHz, the Type 61 rod provided more signal level than the same coil with a Type 33 core. Even at the lowest frequency measured, 60 kHz, well below the recommended minimum frequency for Type 61 material, the received signal level was essentially identical with Type 33 and Type 61 rods.

Also plotted in Figure 17 is the relative effect of the two rod materials upon measured Q and μ_{eff} . If variations in the received signal level were explained solely by differences in μ_{eff} , then we should have seen reverse performance, with Type 33 material core outperforming Type 61 material. The data shows a broadly parallel trend between Q and received signal level, although the sharp up-tick in received signal performance around 1300 kHz is not mirrored by a similar change in the ratio of $Q_{\text{rod61}}/Q_{\text{rod33}}$.

As may be apparent by now, when dealing with ferrite rod antennas changing any parameter has a knock-on effect upon others. However, the Type 61 rod retained its superiority for six winding configurations tested, albeit with varying margins.

Surplus Rods?

Purchasing new ferrite rods can be expensive, with the larger rods costing \$20 or more. Can surplus AM broadcast band ferrite rods be used outside of the broadcast band? How do small surplus rods compare with large Type 61 cores?

I ran tests with two groups of surplus AM broadcast band ferrite cores:

- Type "X" rods, diameter cylindrical with two flats, measuring approximately 0.388 inches (9.85 mm) across the round and approximately 0.340 inches (8.64 mm) across the flats, 3.55 inches (90.5 mm) long. These rods are of crude finish, compared with the other rods available, having notable bumps, blemishes and imperfections. The quoted dimensions vary by 0.040 inches (1.0 mm) or more for the same rod and between samples. Six of these rods were recently (as of summer, 2000) procured from a mail order

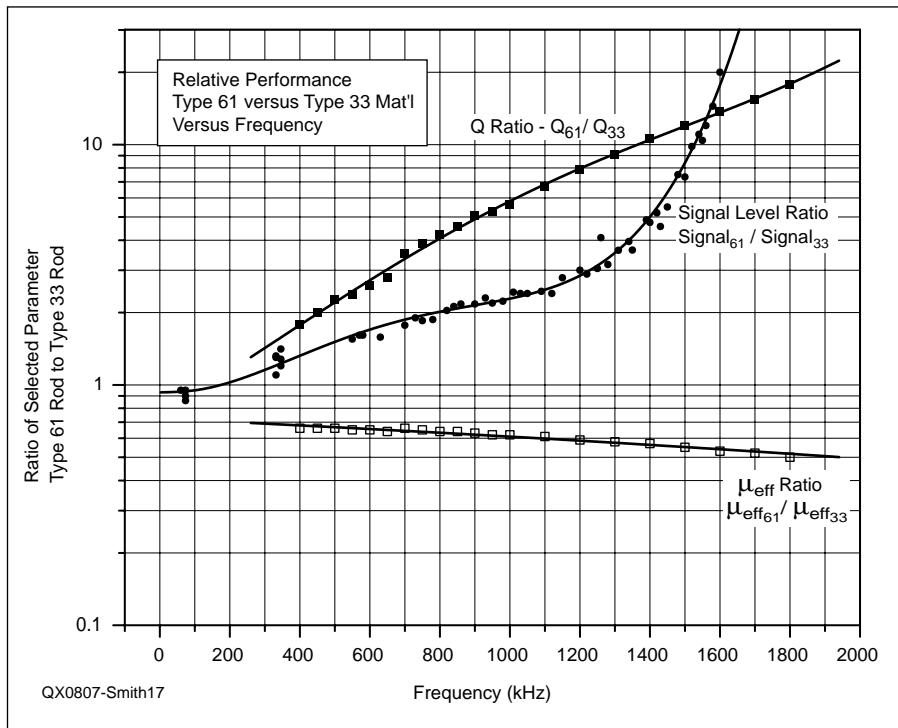


Figure 17 — Relative performance of Type 33 and Type 61 rods.

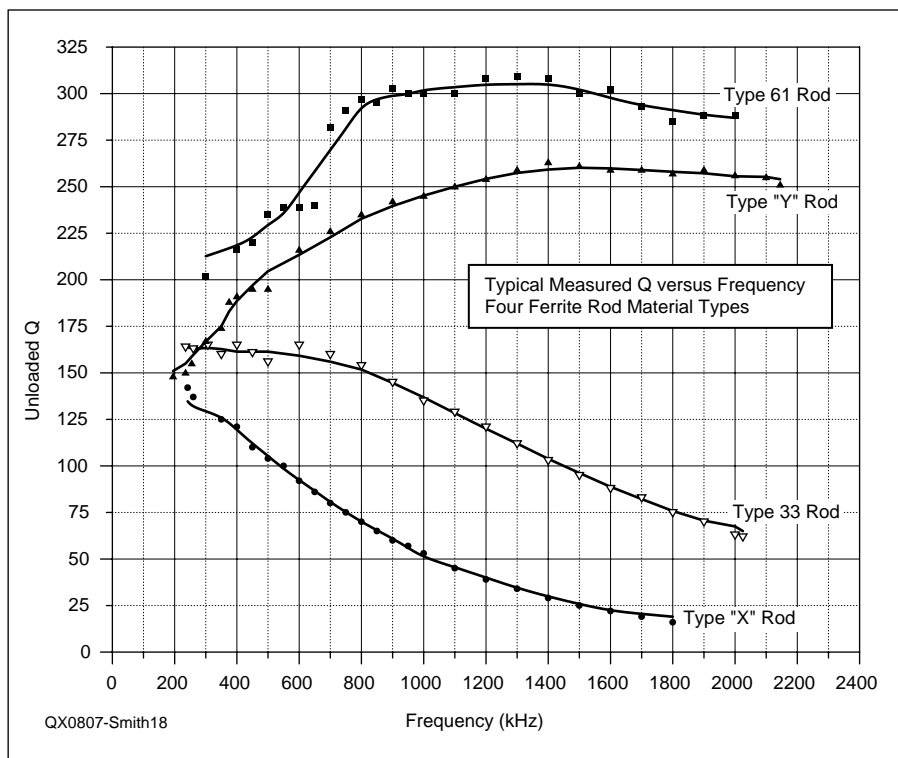


Figure 18 — Change in Q with frequency.

supplier for \$2.25 each.¹⁹

• Type “Y” rods, same shape and diameter as the Type X rods, but 5.51 inches (140 mm) long. These rods have a superior finish and are dimensionally identical within 0.002 inches (0.05 mm). Three of these rods were acquired several years ago from a surplus house and have resided in my junk box since. These rods are obviously unlikely to be found by anyone else, but are included as a point of reference.

To compare the Q possible with Type X and Y cores, I wound a test coil for each, with approximately equal inductance (180 μ H at 790 kHz with the rod inserted) and measured the Q between 200 kHz and 2000 kHz. For comparison, similar measurements were taken for test coils with Type 33 and Type 61 material. Figure 18 shows that the Type 61 and Type Y rods are similar, as are the Type 33 and Type X rods.

Although the Type X rod is a poor Q performer at most frequencies, its relative cheapness and availability leads to the question: “is it possible to use several relatively poor — but cheap — cores to match the performance of the expensive Type 61 rod?” The answer is yes, at least in the AM radio band. Figure 19 illustrates the relative signal level performance, measured at 630 kHz, for the test configurations described in Table 1. The relative comparison reference point is Test Configuration 21A, 48 turns at 8 TPI on a Type 61 core. Signal levels > 1.0 are better than the Type 61 core reference configuration.

Configurations 31, 32, 34 and 35, perform at least as well as the Type 61 rod reference. Reference coil 21A was the best performing Type 61 core configuration observed, so it is possible to duplicate the best Type 61 performance with less than one half the investment in ferrite. However these Type X rod configurations were not evaluated for signal reception outside of 630 kHz. The Q versus frequency data of Figure 18 strongly suggests, however, that Type X rods will deteriorate sharply at higher frequencies, and will likely be unsatisfactory above 1 MHz. However, Type X material may have merit below 500 kHz.²⁰

Distributed Capacitance

Terman succinctly stated the cause of distributed capacitance in coils:

“In a coil there are small capacitances between adjacent turns, between turns that are not adjacent, between terminal leads, between turns and ground, etc. ... The total effect that the numerous small capacitances have can be represented to a high degree of accuracy by assuming that they can be replaced by a single capacitor of appropriate

size shunted across the coil terminals.”²¹

Distributed capacitance sets a limit on the highest frequency at which a coil may be resonated; with no additional capacitance the inductance and C_{dist} parallel resonate at some frequency, referred to as the “self-resonant

frequency,” or f_{self} . In addition, self-capacitance causes a discrepancy between measured and true Q and inductance.²²

In addition to increasing the inductance, adding a ferrite core to a coil increases the distributed capacitance. This is because some

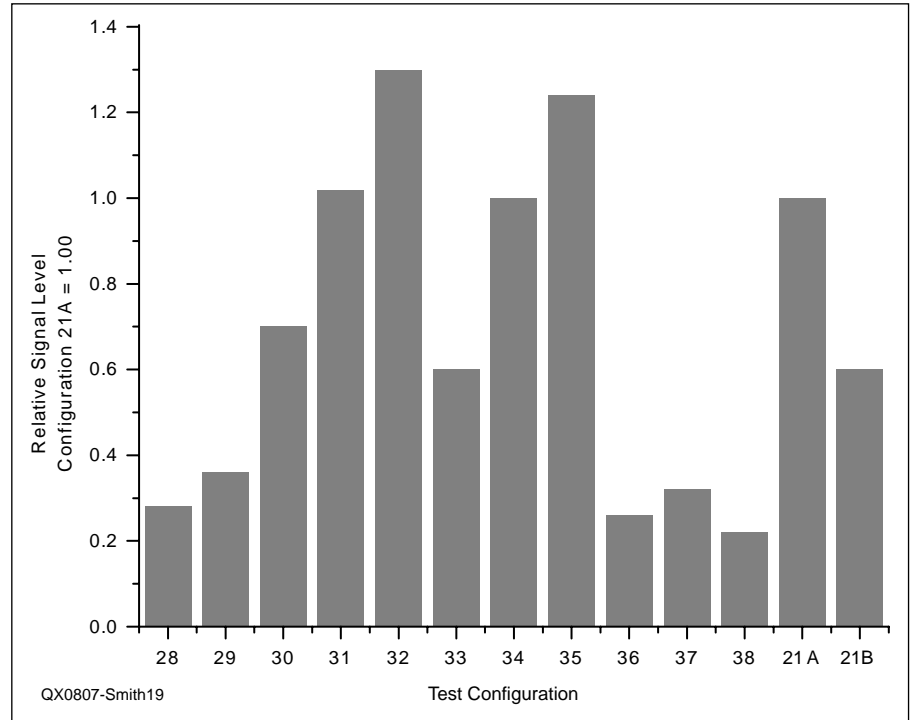


Figure 19 — Received signal level — Type X rod configuration.

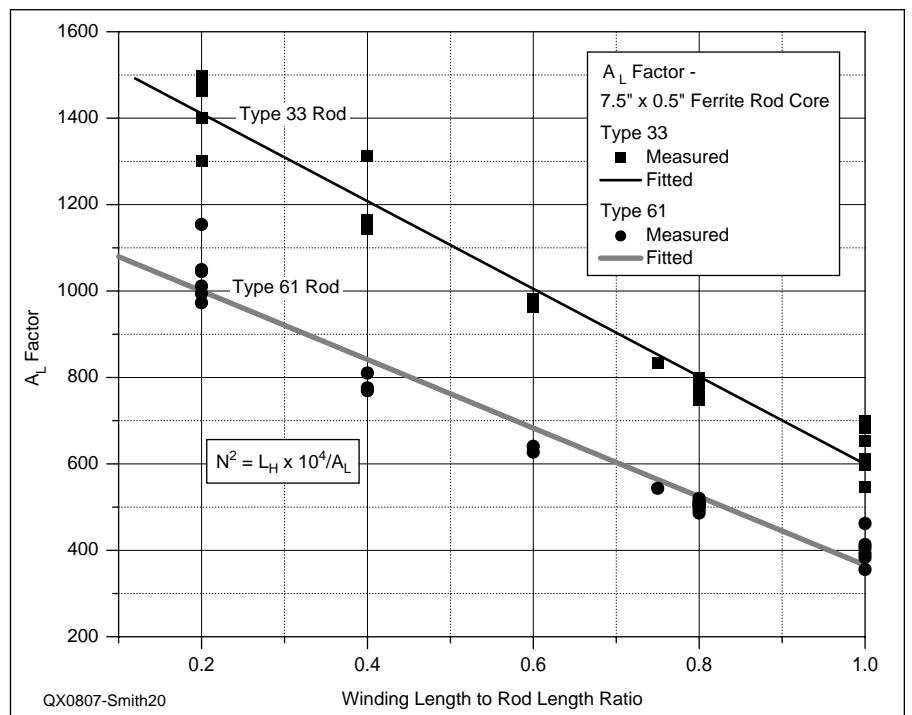


Figure 20 — A_L factor for Type 33 and Type 61 Material, 7.5 inch \times 0.5 inch rods.

of the electric field lines that give rise to C_{dist} are contained within the ferrite. Typical ferrites have a relative permittivity (dielectric constant) of 10 to 11.²³ Thus, C_{dist} will increase. Since only part of the electric field lines are within the ferrite, the total increase in C_{dist} will be less than indicated by the relative permittivity of the ferrite rod.

As the ferrite core increases both inductance and distributed capacitance, F_{self} will be significantly lower than for the same coil without the rod inserted.

To evaluate the reduction in F_{self} , measurements were made on a typical antenna coil with and without the ferrite rod. The coil measured is the one identified as Configuration number 38 in Table 1. The radius of the coil is approximately 0.2 inches and the winding length is approximately 3.5 inches.

Without a core inserted, I measured C_{dist} as 1.9 pF, using the auxiliary work coil method described in the Model 260-A Q meter instruction manual. Since L_0 was measured as 18.3 μ H, the f_{self} can be computed as 27 MHz.

With the Type X core inserted, C_{dist} increased to 8.5 pF. L increases to 1,100 μ H (measured at 250 kHz), resulting in an approximate f_{self} of 1.6 MHz. (L is, in fact, a function of frequency since μ_{eff} varies with frequency. An exact f_{self} would require adjustment of L to match that at the self-resonant frequency. Alternatively, F_{self} can be measured directly.)

In this example, C_{dist} increased by a factor of 4.5 and f_{self} decreased by approximately 17:1.

It is also interesting to compare the measured (without ferrite core) C_{dist} to the computed value using the Medhurst formula.²⁴

$$C_{dist} = 0.29l + 0.41R + 1.94\sqrt{\frac{R^3}{l}} \quad [\text{Eq 19}]$$

where:

l = coil length in inches

R = coil radius in inches

Inserting the values for coil length and radius yields $C_{dist} = 1.2$ pF. The discrepancy of 0.7 pF between calculated and measured values can be attributed, at least in part, to the lead capacitance connecting the coil to the Q meter. Further, Medhurst's work assumes a specific geometry, where the coil is mounted vertically over a grounded chassis, a configuration significantly different than when the inductor is attached to a Q meter.

Simplified Inductance Calculation Approach

To avoid the complexity of the equations and adjustment factors presented in this paper, a simplified approach may prove adequate for Amateur Radio purposes. Ferrite and powdered iron toroidal are often designed using a simple equation, relating inductance, number of turns and the " A_L " factor. If we stick to the 7.5 inch \times 0.5 inch Type 33 and Type 61 cores, it is possible to define a similar equation, presented below.

$$\text{NumberTurns} = 100\sqrt{\frac{\text{Desired } L_{\mu\text{H}}}{A_L}} \quad [\text{Eq 20}]$$

Instead of a single value for A_L for Type 33 and Type 61 cores, however, the particular A_L value must be selected from the curves shown at Figure 20. The data markers are A_L points based on my measured coils, and the straight line are curve fitted. The results will be within 10 to 15% in most cases, and the calculations are much easier than the traditional methods covered earlier in this article.

Sample Calculation:

Desired Inductance: 200 μ H

Desired coil length: 6 inches (0.8 winding length to rod length ratio)

Core Material: Type 61.

From Figure 20 we read $AL = 520$. Hence the number of turns required is:

$$\begin{aligned} \text{NumberTurns} &= 100\sqrt{\frac{200}{520}} \\ &= 100\sqrt{0.385} = 62 \end{aligned}$$

62 turns, wound over 6 inches, or approximately 10 TPI, will yield 200 μ H when centered over the 7.5 inch long Type 61 core.

Conclusion

Our rambling excursion through the world of ferrite cores and antennas might lead to the expedient strategy of bypassing analysis completely and trying, more or less randomly, combinations of core materials and windings until an acceptable result follows. And, the complexity and contradictory nature of the limited information available may reinforce those desires. However, it's often said "a day in the library is worth a month in the lab," meaning that experiments guided by past learning are far more productive than random efforts.

If designing a ferrite rod antenna, my data shows a good starting point to be the large 7.5 inch \times 0.5 inch Type 61 material cores. For maximum performance, the windings should cover at least 80% of the core length, and reasonably large diameter wire should be used, such as AWG no. 18 to 16, depending on the number of turns required for the frequency band of interest. To determine the antenna inductance, one may start with the old rule of thumb of 1 to 2 pF of resonating capacitance per meter wavelength. From that capacitance, the inductance, and hence the number of turns can be determined from Equation 20 and Figure 20.

Table 1
Type X Core Configuration

ID	Configuration
28	1 Type X rod, 42 turns at 12 TPI
29	1 Type X rod, 67 turns at 20 TPI
30	2 Type X rods long, 70 turns at 10 TPI
31	3 Type X rods long, 85 turns at 8 TPI
32	4 Type X rods long, 112 turns at 8 TPI
33	1 Type X rod long, 5 rods in approx. cylindrical format, 32 turns at 10 TPI
34	2 Type X rods long, 3 rods in triangle (6 total rods) format, 70 turns at 10 TPI
35	3 Type X rods long, 2 rods side-by-side (6 total rods) format, 100 turns at 10 TPI
36	1 Type X rod, 35 turns at 10 TPI
37	1 Type X rod, 112 turns at 32 TPI
38	1 Type X rod, 168 turns at 48 TPI

Reference Configurations

21A	48 turns at 8 TPI, Type 61 core
21B	48 turns at 8 TPI, Type 33 core

Appendix 1

Adjustment for Space-Wound Inductors

The following is based upon an equation given in the *Radiotron Designer's Handbook*.²⁴ The method described yields results "suitable for slide rule computation."

Step 1 — Calculate the inductance using one of the standard formulas, such as Wheeler's equation.

$$L_0 = \frac{a^2 N^2}{9a + 10l}$$

where:

L_0 = inductance in μH

a = coil radius to center of wire, in inches

N = number of turns

l = length of coil, in inches

Step 2 — The correction factor applied to the result in Step 1 is:

$$L = L_0 - 0.0319 a N (A + B)$$

a, N as above

A, B as below

$$A \approx 2.3 \log_{10}(1.7 \cdot S)$$

$$B \approx 0.336 \left[1 - \frac{2.5}{N} + \frac{3.8}{N^2} \right]$$

$$S = \frac{D}{P}$$

where:

D = wire diameter

P = winding pitch

(D and P should be in the same units, such as inches)

Example:

48 turns, AWG no. 30 copper wire, wound at 8 turns/inch. The coil is wound on a paper core, consisting of 4 layers wound over a 0.500 inch diameter mandrel. The paper is standard typing paper, approximately 4 mils (0.004 inches) thick per sheet. AWG no. 30 copper wire has a diameter of 10 mils (0.010 inch).

Step 1 — Determine the parameters to use in the Wheeler formula and calculate L_0 :

$$a = \frac{0.500 + 2 \times 4 \times 0.004}{2} + \frac{0.010}{2}$$

$$= 0.271 \text{ inches radius to center of wire}$$

$$l = \frac{48 \text{ turns}}{8 \text{ turns / inch}} = 6 \text{ inches}$$

$$N = 48 \text{ turns}$$

$$L_0 = \frac{0.271^2 \times 48^2}{9 \times 0.271 + 10 \times 6} = 2.71 \mu\text{H}$$

Step 2 — Calculate the spaced winding correction

$$S = \frac{0.010}{0.125} = 0.080$$

$$A = 2.3 \times \log_{10}(1.7 \times 0.080) = -1.99$$

$$B = 0.336 \times \left[1 - \frac{2.5}{48} + \frac{3.8}{48^2} \right] = 0.319$$

$$L = 2.71 - 0.0319 \times 0.271 \times 48 \times$$

$$(-1.99 + 0.319) = 2.71 -$$

$$(-0.693) = 3.40 \mu\text{H}$$

In this example, the spaced winding correction increases the inductance by more than 25%.

Measurement Comparison

The inductor in this example was constructed and measured with a Boonton 260A Q meter at 7.9 MHz. The distributed capacitance, C_{dist} , of the coil was measured at 2.5 pF. The measured inductance, after correction for C_{dist} , the inductance of the lead wires connecting the coil with the Q meter and the residual inductance of the Q meter, was 3.55 μH . Based upon calibration with 2.5 μH and 5.0 μH Boonton 103A standard inductors, the Q meter is known to have an error of +2.6% at 7.9 MHz. Adjusting for this instrument error, the final measured L is 3.46 μH , representing a difference between the calculated and measured values of 1.8%.

Jack Smith, K8ZOA, has been licensed since 1961, first as KNSZOA, and has held an Amateur Extra Class license since 1963. He received a BSEE degree from Wayne State University in Detroit in 1968 and a JD degree magna cum laude from Wayne State University School of Law in 1976. Presently retired, he has enjoyed a career involving both engineering and telecommunication law. He is a co-founder of the telecommunications consulting firm TeleworX, and is the author of Programming the PIC Microcontroller with MBASIC (Newnes Publishing, 2005) as well as many articles published in 73 Amateur Radio magazine and QEX. His Web site is www.cliftonlaboratories.com.

Notes

¹Fair-Rite Soft Ferrites Catalog, 14th ed. (Fair-Rite Products Corp., Wallkill, NY, 2000), p 2: "During the 1930s research on 'soft' ferrites continued, primarily in Japan and the Netherlands. However, it was not until 1945 that J. L. Snoek of the Phillips Research Laboratories in the Netherlands succeeded in producing a 'soft' ferrite for commercial applications."

²For example, "The Optima 160/80-Meter Receive Antenna," R.Q. Marris, in *The ARRL Antenna Compendium*, Vol 6, R.D. Straw, ed., (ARRL, Newington, CT, 1999); *The ARRL Antenna Book*, R.D. Straw, ed.

(ARRL, Newington, CT, 1997), Chapter 14; *The ARRL Handbook for Radio Amateurs 2000*, R.D. Straw, ed. (ARRL, Newington, CT, 1999), Chapter 23; *Loop Antenna Handbook*, J.J. Carr (Universal Radio Research, Reynoldsburg, OH, 1999), Chapter 10; *The Low and Medium Frequency Radio Scrapbook*, 10th ed., K. Cornell (self-published, 1996).

³M.F. "Doug" DeMaw, *Ferromagnetic-Core Design and Application Handbook*, Section 2.2, (MFJ Publishing Co, Inc, Starkville, MS, 1996); R.D. Straw, ed., *The ARRL Antenna Book*, 18th Ed. (ARRL, Newington, CT, 1997), pp 5-6 through 5-8.

⁴J.D. Krause, *Antennas*, 2nd ed., (McGraw Hill, 1988), Section 6-12; W.L. Weeks, *Antenna Engineering*, Section 8.6.1, (McGraw-Hill Book Co., New York, NY, 1968); R.C. Johnson and H. Jasik, eds., *Antenna Engineering Handbook*, 2nd ed., (McGraw-Hill, New York, 1984) pp 5-5 through 5-9.

⁵The derivation of Equation 1 through Equation 9 is based upon several sources. Of particular interest is *Sensitivity of Multi Turn Receiving Loops*, by W.E. Payne, N4YWK, unpublished, but available at www.lwca.org/library/articles/ywk/looptheo.htm. See also the references cited at Note 4.

⁶One weber per square meter is also known as one Tesla. Because stating a "density" in terms of a value per unit area offers a more intuitive understanding, the discussion uses the older weber/m² terminology. It is simple to see that a uniform flux density of 5 webers/m² through a loop area of 2 square meters yields a total flux of 10 webers.

⁷Of more familiarity in radio engineering is the magnetic field strength, H, of an electromagnetic field, in amperes/meter, given by

$$H = \frac{E}{\eta_0}$$

where

η_0 is the intrinsic impedance of free space, 120π ohms. H is used, for example, to set safe exposure limits of low frequency signals where the biological effects of magnetic induction, not electric field coupling, is of concern. Of course, $B = \mu_0 H$ in free space and

$$\eta_0 = \sqrt{\frac{\mu_0}{\epsilon_0}}$$

where ϵ_0 is the relative permittivity of space, 8.85×10^{-12} F/m. Substituting, we find that

$$B = E \sqrt{\mu_0 \epsilon_0}$$

But we know

$$c = \frac{1}{\sqrt{\mu_0 \epsilon_0}}$$

Therefore,

$$B = \frac{E}{c} \text{ or } E = Bc.$$

⁸R. Dean Straw, N6BV, *The ARRL Antenna Book*, Equation 10, page 5-8. Note, however, that Johnson and Jasik, (op. cit Note 4) add an additional empirical correction factor F_v to the open circuit voltage, where F_v is an experimentally derived function of the ratio of the overall winding length to the core length. See Johnson and Jasik (op cit Note 4) Section 5-2, Figure 5-9 and Equation 5-15. F_v runs from 1.0 ($L_c/L_r = 0$ to 0.8 ($L_c/L_r = 1$, where L_c/L_r is the ratio of the winding (coil) length L_c to the ferrite

core length L_r). *The ARRL Antenna Book* has a similar correction factor, but of different magnitude, due to the "free end effect." Note, however, that *The ARRL Antenna Book* Equation 5-8 appears to erroneously invert L_c and L_r .

⁹M.F. "Doug" DeMaw, *Ferromagnetic-Core Design and Application Handbook*, Section 2.2, (MFJ Publishing Co., Inc., Starkville, MS, 1996).

¹⁰In general, adjustments in Q and L for distributed capacitance were not made, nor were adjustments made for the Boonton 260A Q Meter finite input impedance and other imperfections.

¹¹W.L. Weeks, *Antenna Engineering*, Section 8.6.1, (McGraw-Hill Book Co., New York, NY, 1968).

¹²I've emphasized the term "theoretical" since, as we see later, further adjustments are necessary to obtain even an estimate of the true relationship between the measured rod permeability and the material permeability.

¹³C. Chen, *Magnetism and Metallurgy of Soft Magnetic Materials*, Page 536, Table A3.1, (North-Holland Publishing Co., Amsterdam, 1977), reprinted by Dover Publications, Inc., New York, 1986, provides a table of "D" values versus rod geometry.

¹⁴M.F. "Doug" DeMaw, *Ferromagnetic-Core Design and Application Handbook*, Figure 2.2, (MFJ Publishing Co., Inc., Starkville, MS, 1996); R.C. Johnson and H. Jasik, eds., *Antenna Engineering Handbook*, 2nd ed., Figure 5-8, (McGraw-Hill, New York, 1984); *Fair-Rite Soft Ferrites Catalog*, 14th ed., page 131 (Fair-Rite Products Corp., Wallkill, NY, 2000).

¹⁵R. Dean Straw, N6BV, *The ARRL Antenna Book*, 18th Ed., op. cit., p 5-7 says "The Q of a short coil on a long rod is greatest at the center. On the other hand, if you require a higher Q than this, it is recommended that you spread the coil turns along the whole length of the core, even though this will

result in a lower value of inductance. (The inductance can be increased to the original value by adding turns.)" J.J. Carr (*Joe Carr's Loop Antenna Handbook*, 1st Ed., 1999, Universal Radio Research, Reynoldsburg, OH) makes a similar statement: "The Q is worst when the coil is concentrated in a small portion of the rod length. To improve Q , at the expense of overall possible inductance, then wind the coil over the entire length of the rod." No measured data or citation is advanced to support this statement.

¹⁶R. Dean Straw, N6BV, *The ARRL Antenna Book*, 18th Ed., op. cit., p 5-7, Eq. 8.

¹⁷F. Langford-Smith, ed., *Radiootron Designer's Handbook*, 4th ed., (Wireless Press, Sydney, Aust., 1953), reprinted by RCA Electronics Components, Harrison, N.J., 1968. A comprehensive discussion of the effect of spaced windings is given at Section 10.1(ii).

¹⁸Type 33 Material is described in catalogs and the literature as "permeability 800." See, for example DeMaw, Section 2.1. However, Fair-Rite, the manufacturer of Type 33 material, states, in Catalog no. 14, that it has an initial permeability of 600. Fair-Rite's graph of initial permeability versus frequency, how-

$$Q_i = Q_j \frac{C + C_d}{C}$$

ever, shows an initial permeability of 700 below about 750 kHz, increasing to 800 at 1 to 2 MHz. Fair-Rite specifies permeability within $\pm 20\%$.

¹⁹Ocean State Electronics, part no. LA-540. Ocean State Electronics, 6 Industrial Drive, P.O. Box 1458, Westerly, RI 02891, Order telephone number 1-800-866-6626, Web site: www.oselectronics.com.

²⁰Although the Type "X" rod is described in Ocean State Electronics' catalog as "tunes the broadcast band, 540 kHz - 1600 kHz," the Q performance leads to the suspicion that, in fact, the material is optimized for the long wave broadcast band, 200-400 kHz.

²¹F.E. Terman, *Electronic and Radio*

$$L_t = L_i \frac{C_d}{C + C_d}$$

Engineering, 4th Edition, (McGraw Hill, New York, 1955), Section 2.7.

²²Hewlett Packard provides the following correction factors in *Operating and Service Manual: Q Meter 4342A* (1983) at Pages 3-13 through 3-16:

Where:

Q_i is the true Q

Q_j is the indicated (instrument reading) Q

C is the instrument capacitance to achieve resonance

C_d is the inductor's distributed capacitance

where:

L_i is the true inductance

L_j is the indicated (instrument reading) Q

C and C_d are as above

Similar correction formulas are provided in the Instruction Manual for the Q Meter Type 260A, (undated) pages 19-21.

²³H.P. Westman, ed., *Reference Data for Radio Engineers*, 5th Edition, (Howard W. Sams, Indianapolis, 1970), Chapter 4, Table 25.

²⁴A different formulation of Medhurst's formula is presented in *Radiootron Designer's Handbook*, id, Chapter 11, Section 2(i), in which a table of coil length versus diameter must be used. I don't know the provenance of the formula presented — widely used by the Tesla coil builder fraternity — but it closely matches values computed using the tabular approach presented in the *Radiootron Designer's Handbook*. Of course, Medhurst's formula is based upon a vertically oriented coil, installed on a metal chassis and is not necessarily accurate for other configurations. However, it provides reasonable results for the examples that I investigated.

QEX

QEX

A Forum for Communications Experimenters

Subscription Order Card

QEX features technical articles, columns, and other items of interest to radio amateurs and communications professionals. Virtually every part of the magazine is devoted to useful information for the technically savvy.

Subscribe Today: Toll free 1-888-277-5289 • On Line www.arrl.org/QEX

Subscription Rates: 1 year (six issues)

ARRL MEMBER: for ARRL Membership rates and benefits go to www.arrl.org/join

US \$24.00 US via First Class \$37.00 Intl. & Canada by air mail \$31.00

NON MEMBER:

US \$36.00 US via First Class \$49.00 Intl. & Canada by air mail \$43.00

Renewal New Subscription

Name: _____ Call Sign: _____

Address: _____

City: _____ State: _____ ZIP: _____ Country: _____

Check Money Order Credit Card Monies must be in US funds and checks drawn on a US Bank

Charge to:    

Account #: _____ Exp. Date: _____

Signature: _____



Published by:
ARRL, 225 Main St,
Newington, CT 06111-1494 USA

Contact circulation@arrl.org
with any questions or go to
www.arrl.org

Web Code: QEC

Project #350

Some Thoughts on Crystal Parameter Measurement

Here is an automated way to measure a group of crystals to select units for a crystal filter.

If you have ever set about measuring crystal parameters for a large batch of crystals using some of the techniques suggested in the amateur literature you find that it gets tiresome very quickly. What one wants is some sort of instrument in which you put in the crystal and press a button!

Recently my friend Tom Allread, VA7TA, designed a new DDS module, called NimbleSig, which won the second prize in a contest sponsored by *Circuit Cellar* magazine.¹ NimbleSig has its own internal controller and covers the frequency range from zero to 175 MHz in 1 Hz steps. It can be amplitude or frequency modulated. It is controlled by a logic-level 115200 baud serial interface using simple ASCII commands. NimbleSig is a terrifically versatile signal source and it immediately motivated me to design a general purpose signal generator around it. I opted to use an external oven-controlled crystal oscillator as the clock for NimbleSig, so the output frequency should be accurate to a few Hz over this range. NimbleSig has a built-in AD8307 logarithmic detector IC, and I put a graphic liquid crystal display on the front panel of the signal generator so that I can easily sweep and adjust band-pass filters and other parameters. The signal generator uses an ARM7 microcontroller to handle all the signal processing, the display and to control the NimbleSig module and digital attenuator.

Having a very stable, flexible signal generator/power meter, one of the obvious operating modes to incorporate would be one to measure crystal parameters. In this article, I will briefly recap the general problem of measuring crystals and then describe how I implemented this mode.

Crystal Parameters

The simplest meaningful equivalent circuit for a crystal is that of a series R-L-C circuit in parallel with a single capacitance as shown in Figure 1. The motional inductance,

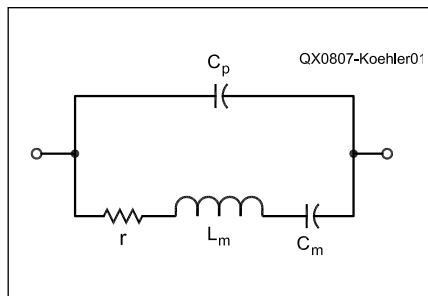
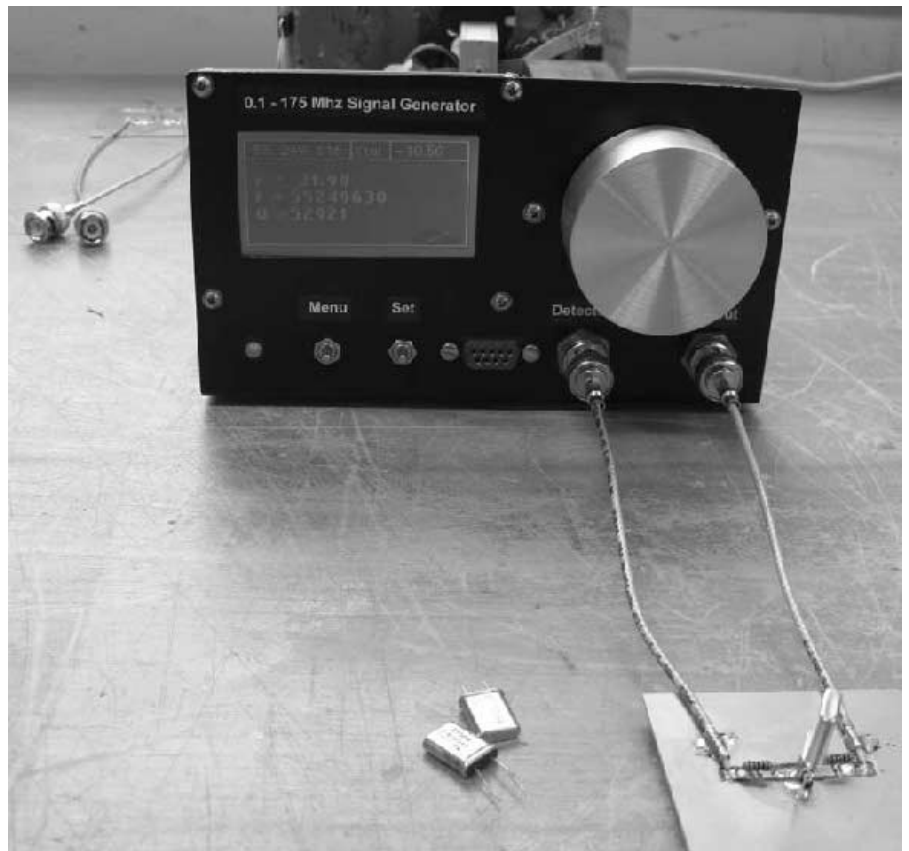


Figure 1 — This is a simple equivalent circuit for a piezoelectric crystal.

L_m and the series equivalent capacitance, C_m , are series-resonant at a frequency, f_s . The parallel capacitance, C_p , is a physical capacitance that results from the conducting plates on either side of the quartz crystal itself, plus whatever stray capacitance occurs from the construction of the unit. Typically, C_p is a few pF, and there is a parallel resonance at a somewhat higher frequency than f_s where the net inductive susceptance of the series circuit is equal to the capacitive susceptance of C_p . The loss element, r , is due to mechanical losses. More complicated equivalent circuits are possible to include, for example, the leak-

¹Notes appear on page 41.

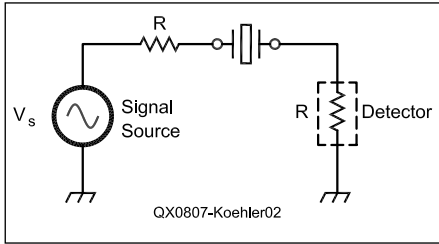


Figure 2 — The circuit of the conventional series circuit used to measure crystal parameters.

age resistance between the two terminals, the lead inductance, and so on, but these quantities are usually not significant for real crystals in the MHz region, which are well described by the simple model in Figure 1.

There have been many articles written in the ham literature about how to measure these four parameters to completely characterize a crystal.^{2,3,4} (The cited references are just a few of the many articles on this topic.) All the methods require manual intervention and, as mentioned before, become very tedious to use if one wants to measure a large number of crystals in order to select those needed for any particular filter. A very good comparative discussion of these techniques appeared recently in *QEX*, in an article describing the design and construction of two filters.⁵ In that article, Jack Smith admitted that he did the bulk of his measurements using an HP87510A wave analyzer, which has an automatic mode for crystal measurements. The HP87510A is a vector instrument and measures both resistive and reactive elements.

Not having an HP87510A or equivalent vector instrument (these are generally high cost items), the question becomes the following: Is there an accurate way of measuring the basic crystal parameters automatically using just a very stable and precise signal generator and a non-vector power detector? I hope to prove to you that there is.

Conventional Techniques

The most common technique used for measuring crystal parameters uses a circuit in which the crystal is in series between a low-impedance signal source and a low-impedance detector as shown in Figure 2. It is common for R to be 12.5 Ω but this is really quite arbitrary. This is the method used by the HP87510A, where a fixture is added to lower the source and detector impedance.

As the signal source is swept through the frequency range of the crystal series and parallel resonance, the amplitude response looks like that shown in Figure 3. The data for this figure was produced by my new signal generator and its AD8307 detector, using a fixture I made to emulate the circuit in Figure 2. (See Photo A.) To make this fixture and to have it

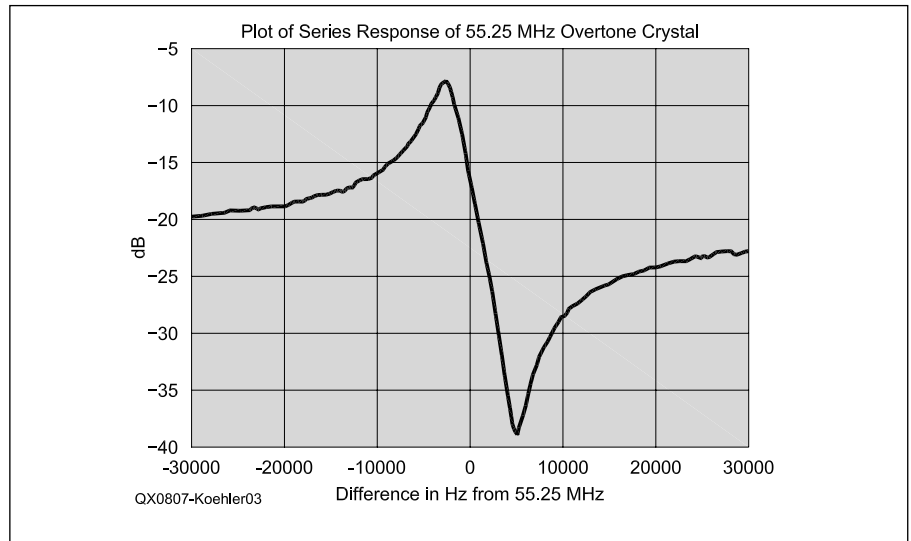


Figure 3 — The response of a 55.25 MHz overtone crystal as measured in the conventional series fixture.

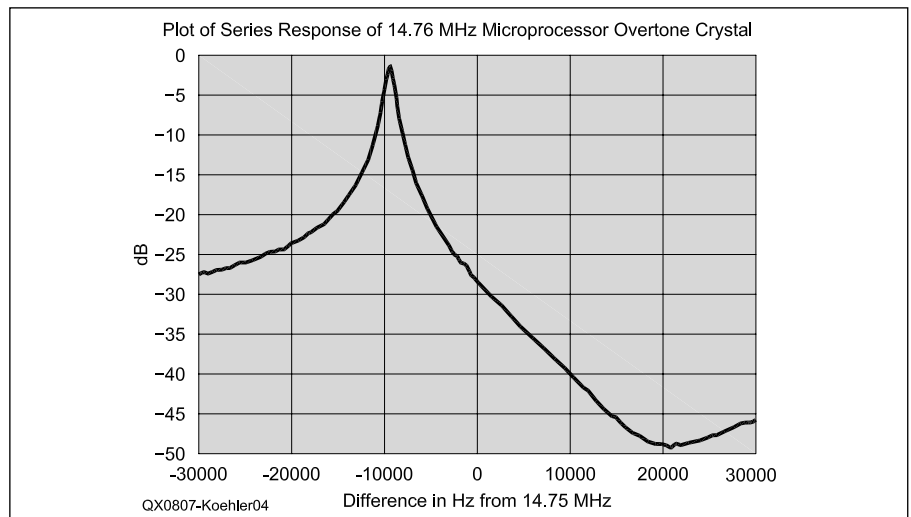


Figure 4 — The response of a 14.76 MHz microprocessor clock crystal as measured in the conventional series fixture.

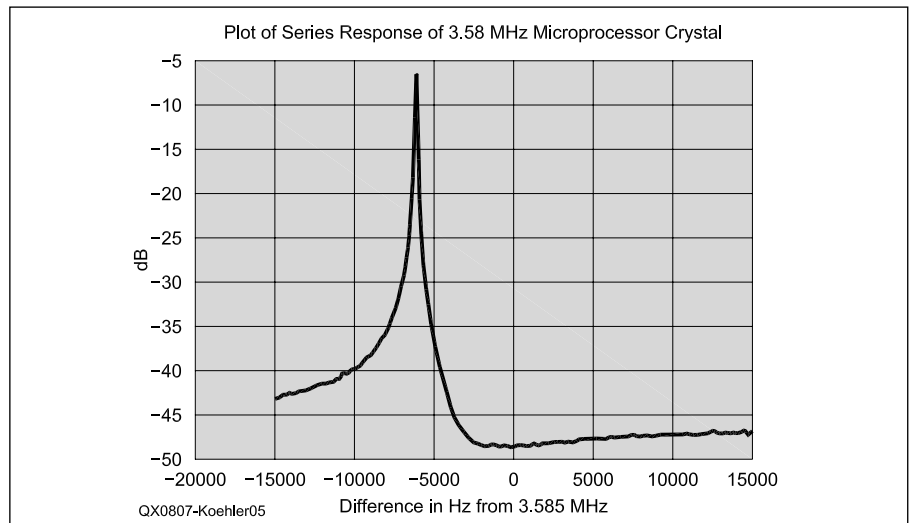


Figure 5 — The response of a 3.58 MHz crystal as measured in the conventional series fixture.

broadband enough to use with crystals from the entire range between a few hundred kHz and up to 100 MHz, I used broadband attenuators and small noninductive surface-mount resistors. A side effect of this was to reduce the sensitivity of the logarithmic detector. In my case, R was 25 Ω and the crystal measured in Figure 3 was a 55.25 MHz overtone crystal.

The peak occurs at the series resonant frequency, f_s , and the valley at the parallel resonant frequency. The magnitude of the attenuation at the series peak can be used to calculate the loss resistance of the crystal, r . There are two common ways of estimating the value of L_m .

One of these is to measure the bandwidth of the peak at the -3 dB points and use this to calculate the loaded Q (loaded by the source and detector) and hence the inductive reactance. This gives L_m and, by knowing f_s , then C_m . We can measure C_p with a capacitance meter. The second way is to measure C_p and then use it and the separation between the series and parallel resonance frequencies to estimate C_m . Then again knowing f_s , L_m can be calculated. As Jack Smith showed, even with careful measurements, these two methods or their variants often give slightly different results. To select crystals for a filter, however, the important quantities to know are f_s and crystal Q. Of course f_s can be measured with great precision in either of the two alternatives, and both give a measure of Q and L_m .

Before leaving the topic of the conventional method, it is worth discussing some of the problems associated with it. The measurement of r requires measuring the attenuation at the peak of the series resonance. This attenuation, as a voltage-ratio, A_0 , is related to the value of r and the resistance of the source and detector, R by:

$$A_0 = \frac{2R}{(2R+r)} \quad [\text{Eq 1}]$$

The higher the Q of the crystal, the lower the value of r and the resultant attenuation may be very low. Suppose r is, say, 5 Ω and R is 25 Ω. Then A_0 will be just 0.8333 which corresponds to -0.82 dB. One cannot measure attenuation with absolute precision and the lower the value of r , the more inaccurately it will be measured, in general. For example, if A_0 is measured to be -0.82 dB but we know that it is really somewhere between -0.9 and -0.7 dB, then r would be somewhere between 4.2 and 5.5 Ω; a difference of more than 20%. If r is large, then it is easier to measure it accurately, but crystals with large r are the ones we are least interested in. It is for this reason that low impedances for the source and the detector are desirable.

Another problem may occur if the method of frequency difference between series and parallel resonance is to be used to calculate C_m . Figures 4 and 5 show the response for two other crystals measured in

my setup. As you can see, the parallel resonance may be so broad that it is difficult to measure accurately. This broadness is caused by the limited dynamic range of the AD8307 detector, which, using my fixture, has a lower detection level of about -50 dB relative to the calibration level. This broadness is a problem for the 14.76 MHz crystal but even more so for the 3.58 MHz crystal.

In this conventional setup, the measured Q is the loaded Q due to a total resistance of $(2R + r)$ and, if R is accurately known, then L_m can be calculated. For this determination, it is an advantage to have a large R so that uncertainties in the calculated value of r are not as important.

The Shunt Method

There is another method of measuring crystal parameters, and that is to measure the crystal when it is in shunt (parallel), in a circuit between a signal source and a detector. This general configuration was suggested to me first by Paul Kiciak, N2PK, in an email he sent me after reading a previous article of

mine describing a Q meter. He asked why I hadn't just measured the Q of an inductor at resonance in shunt. My answer was that I hadn't thought of it! I did subsequently build yet another Q meter, in which I did use the shunt method and I have to say that it is a better instrument than my first. Hayward, Campbell and Larkin, in the section of their book dealing with crystals also briefly mention this method.⁶ The circuit used is shown in Figure 6A. The Thévenin equivalent circuit of this configuration is shown in Figure 6B.

Here, the crystal is inserted in shunt between a signal source and a detector. One would like to have the source and detector impedance, R, fairly large. I built a fixture (shown in Photo B) in which there were two 100 Ω resistors inserted in series between the 50 Ω signal generator and a 50 Ω detector, with the crystal connected to ground at the junction of the two resistors. For this setup, then, R' is 75 Ω.

The frequency response of this configuration, in the frequency region near f_s , is shown in Figure 7. This used the same 55.25 MHz

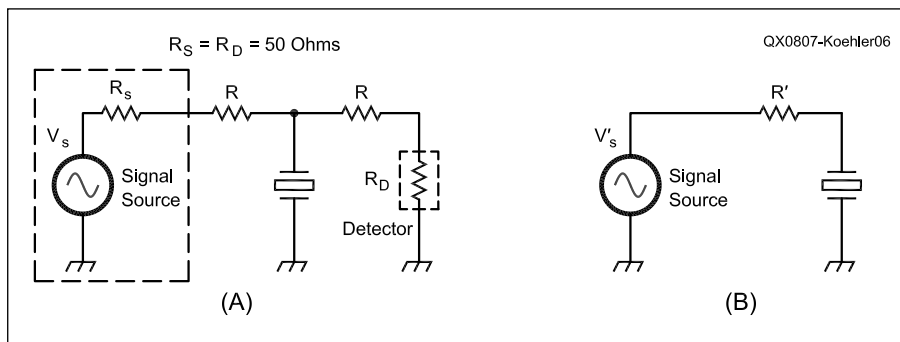


Figure 6 — Part A shows the circuit of the shunt fixture used to measure crystal parameters. Part B shows the equivalent circuit. R' in the equivalent circuit is equal to $R + R_s$ in parallel with $R + R_D$ in Part A.

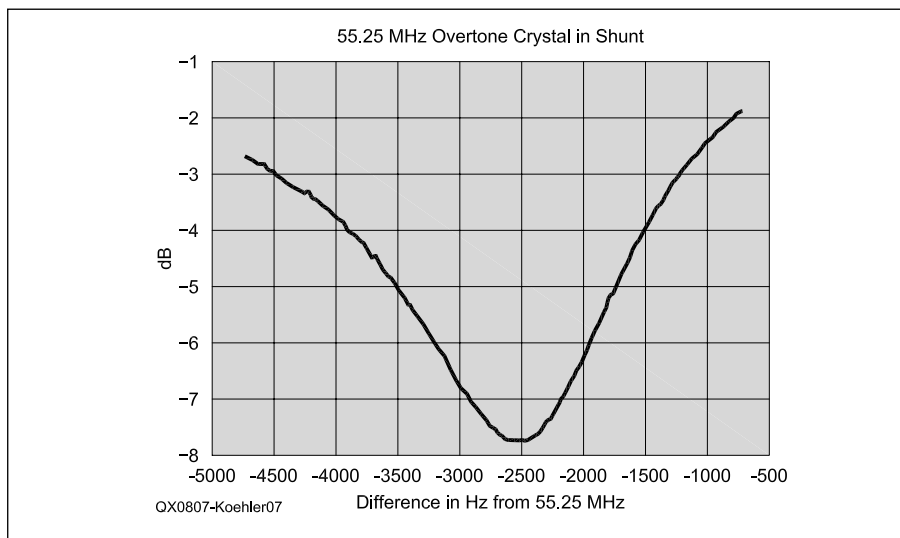


Figure 7 — The shunt response of the 55.25 MHz overtone crystal in the shunt fixture. The frequency range is smaller than that of Figure 3 to show the region near series resonance in greater detail.

overtone crystal used to make Figure 3. The parallel resonance is essentially undetectable but the series resonance causes a deep dip.

This configuration has one principal advantage over the conventional configuration. The smaller that r is, the deeper the dip, and hence it is easier to calculate accurate values for small r .

The attenuation at the deepest point, A_0 , is given by:

$$A_0 = \frac{r}{(R' + r)} \quad [\text{Eq 2}]$$

For example, as before where r is 5Ω , and with my setup value of R' of 75Ω , the attenuation would be -24.1 dB. Even an uncertainty as large as ± 1 dB in measurement (for example, if the measured attenuation was between -23 and -25 dB) the values of r would be between 5.7 and 4.5Ω . In the conventional setup, to get a similar accuracy would require an attenuation measurement precision of just a few tenths of a dB which might be difficult to achieve!

The bandwidth is not determined at 3 dB above the dip but, rather, at a different attenuation, A_1 , given by:

$$A_1 = A_0 \sqrt{\frac{2}{(1 + A_0^2)}} \quad [\text{Eq 3}]$$

To use this method to calculate crystal parameters, the response is first analyzed to determine the maximum attenuation, A_0 . This allows one to calculate r . One then calculates A_1 and measures the frequency difference between the two frequencies that have this attenuation; let this be Δf . Then the crystal Q (the “unloaded” Q of the crystal alone) is given by:

$$Q = \frac{f_s}{\Delta f} \quad [\text{Eq 4}]$$

L_m can be calculated from the known value of Q and, thus, also C_m . If you also need the value of the parallel capacitance, you can measure it with a capacitance-meter in the usual way. In practice, when measuring a large number of crystals in order to select some for a filter, you normally determine the parallel capacitance of one as accurately as possible and then assume all the rest in the batch have the same capacitance.

It goes without saying that in both the conventional series and the shunt method, the responses shown are normalized. That is, the responses are relative to a calibration. In the series mode, the calibration is done with the crystal replaced by a short circuit; in the shunt method, the calibration is the response with no crystal in the circuit (open circuit).

Automating the Measurement

After considering the alternatives, I decided that I would routinely use the shunt method to measure crystal parameters. It would be tedious in the extreme to measure

the response for each crystal, however, and then use a hand calculator to finally get C_m , L_m and r . So, what algorithm should we use to do these calculations inside the machine? For example, how do we actually measure the resonant frequency, f_s ? Do we just take that to be the frequency at which the lowest measured value (the greatest attenuation) occurred? Figure 8 shows the detailed measurements near the dip for the 55.25 MHz overtone crystal. These values of attenuation were measured at frequencies separated by about 30 Hz. As you can see, the value near +100 Hz from the center of the plot had the minimum value but it is off to the side of the axis of symmetry of the plotted points. The frequencies are precise but the measured amplitude has uncertainties, so, choosing just the lowest point is not a good way to best estimate the value of the series resonant frequency.

I plotted both the responses of many crystals in both the conventional and shunt modes and I noticed an interesting thing. If, instead of plotting the response, I plotted the difference between successive points of the response (in dB versus frequency) in the region near the resonance, the plot was close to a straight line. Mathematically, the fact that the differential of the response was a straight line or close to it suggests that the region of the response near resonance was a good approximation to a parabola. The solid line shown in Figure 8 is the best-fit of a parabola to the points in the graph. Because this parabola uses not just a single data point but all the points, the lowest point of the parabola will be a better estimate of the resonant frequency than using just a single piece of data.

The equation of a parabola is given by:

$$y = a + bx + cx^2 \quad [\text{Eq 5}]$$

where x is the independent variable (frequency), and y is the dependent variable

(measured attenuation). Using normal least-square-best-fit for a polynomial algorithm, the best values for a , b and c may be readily calculated from a set of data points. Looking at Figure 8, we can find $a = -7.74$, $b = 1 \times 10^{-30}$ and $c = 5.63 \times 10^{-6}$.

The values for a , b and c are not very useful in themselves, however. To determine the resonant frequency, for example, we want to know the value of x which gives the lowest value y . If we rewrite the previous equation as:

$$y = \frac{(x - x_0)^2}{a} + \beta \quad [\text{Eq 6}]$$

Then x_0 is the value of x at the minimum and β is the attenuation at that point. That is, x_0 is f_s and β is A_0 . These quantities may be related to the values of a , b and c determined from our least-square-best-fit by the following two relations:

$$f_s = \frac{-b}{2c} \quad [\text{Eq 7}]$$

And

$$A_0 = a - \frac{b^2}{4c} \quad [\text{Eq 8}]$$

For the graph of Figure 8, then, $A_0 = -7.74$ dB and $f_s = 0$ Hz, which means series resonance occurred at 55.24755 MHz for that crystal. Having determined A_0 and f_s in this way, we can immediately use Equation 2 to determine r . We can also calculate A_1 from Equation 3.

In Figure 8, by inspection, we see that A_0 is about -7.74 dB corresponding to a ratio of 0.410 and, from Equation 3, A_1 is then 0.537 or -5.40 dB. The maximum attenuation of 0.41 in my fixture means that r for this crystal is 52Ω . We could, of course, use the same technique for fitting a parabola to the peak of the response curve for the conventional

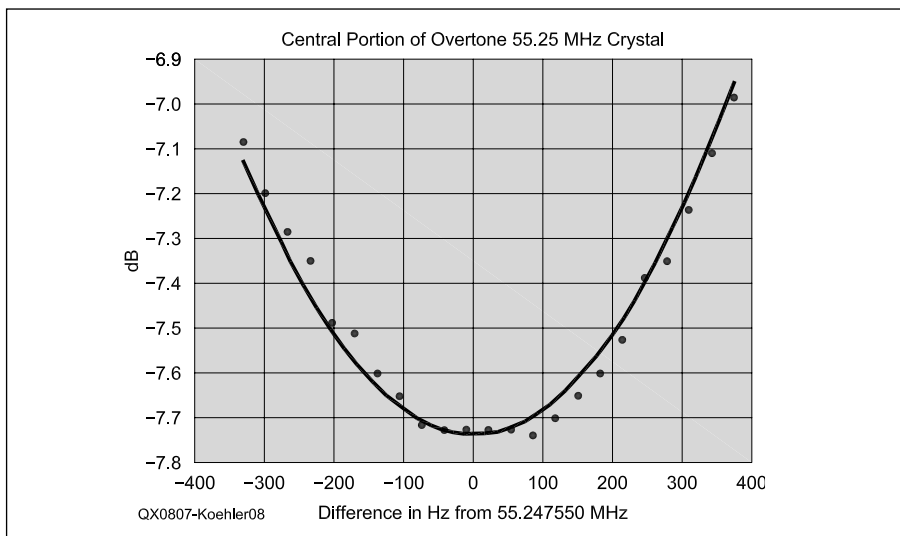


Figure 8 — The central region of the shunt response over a range of less than 800 Hz.

series method of method of measurement to obtain a value for r . I have done this and the values of r for this particular crystal were very comparable. It worked well because r for this crystal was quite large, so the series method gives a reasonably accurate result. The series method would not be as good if r were smaller.

Having calculated A_1 , we must then determine the bandwidth between points at this level. Looking at Figure 7, we see that the attenuation is varying rapidly with frequency in the vicinity of a level of -5.4 dB, so we would not be far out if we just simply found the upper and lower frequencies by simple interpolation between levels either side of -5.4 dB. However, having already written a routine to find the least-squares best-fit to a parabola, it makes sense to use it to improve the estimation of the frequencies of these levels.

If we select a dozen or so points on either side of the -5.4 dB value, we can again solve for a , b and c , which will be valid for that vicinity. This would result in an equation that gives us a value for the attenuation for any particular frequency. If we wished to find a frequency for which the attenuation is -5.4 dB, we would end up with having to solve another quadratic equation, which would give us two values, only one of which was appropriate. It would be better if we ended up with an equation that gives us frequency for any given attenuation because then we could simply substitute the desired attenuation and solve for frequency.

We may do this if we think of the attenuation as the independent variable and frequency as the dependent variable; that is, using frequency for y and attenuation for x . Then, we solve for a , b and c using our best-fit routine and then just substitute the desired attenuation for x , in this case -5.4 dB, and get the frequency directly. Figures 9 and 10 show plots of the points for the lower and upper frequency regions where the attenuation is -5.4 dB and the lines show the best fits. The bandwidth between the -5.4 dB points is then 1552 Hz, giving us an unloaded Q for the crystal of $55247550 / 1552$, which is about 35500 .

The Algorithm

The algorithm for determining the crystal parameters is very simple. With the crystal in the fixture, a relatively wide scan is done and the approximate location of the peak is found by simply looking for the minimum value. Next, a scan is made around this frequency with a much smaller frequency range to give good frequency resolution. Then, taking just the data points near the minimum up to an amplitude of about 0.5 to 0.7 dB greater than the observed minimum, the least-square best-fit solution to the parabola is calculated. From the coefficients in the solution, the maximum attenuation and the

resonant frequency can be calculated. From the maximum attenuation, A_0 , the value of A_1 can be calculated. Then, taking just the data points for frequencies less than the resonant frequency, data points with an attenuation of A_1 , plus or minus 1 dB, are selected and another least-square best-fit to a parabola is calculated using frequency as the y -values and attenuation as the x -values. Finally, we can solve for the lower bandwidth frequency. A similar process is then done for the upper bandwidth frequency.

Compared to the usual 8-bit microprocessors I have been using in my previous projects, the ARM7 used in this one (an NXP LPC2148) is blindingly fast! Without any optimization, the whole process just takes one or two seconds. The code was written in C and I used the GCC C compiler. All the mathematical calculations are done in double precision,

not because the accuracy is required, but because all the transcendental functions in ANSI standard C are done in double precision by default.

If the detector response in the conventional series mode were not as limited as mine was (that is, if the dynamic range of the detector was wide enough to clearly define the parallel resonance), another algorithm might be used to determine crystal parameters. There are only four variables needed to characterize any crystal, so one might write equations that completely describe the amplitude response of the crystal in terms of the four variables; C_m , L_m , r and C_p . Using this equation and the derivatives of it with respect to the variables, it is possible to find the best fit over the entire response curve for the variables using the Levenberg-Marquart method or one of its variants.⁷ The LM

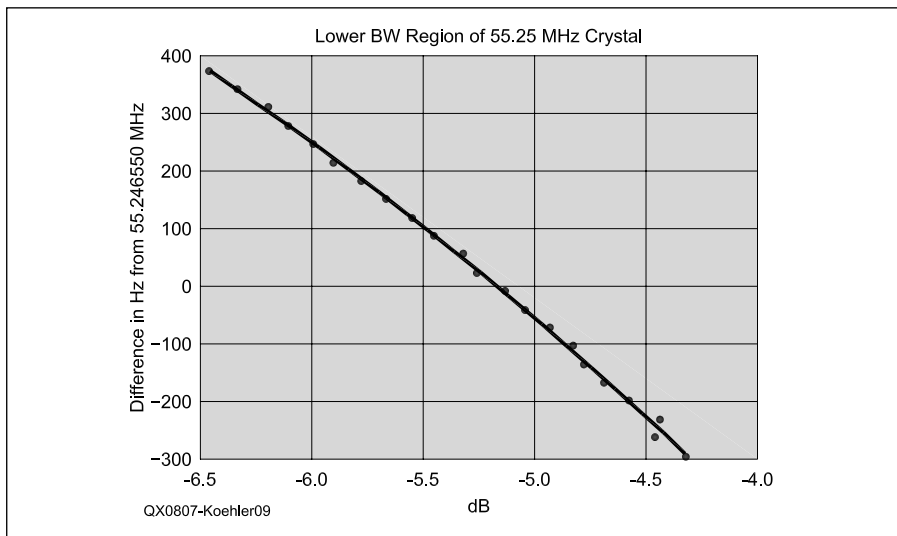


Figure 9 — The shunt response near the lower -5.4 dB region. The plot is of frequency in the Y-direction and attenuation in the X-direction.

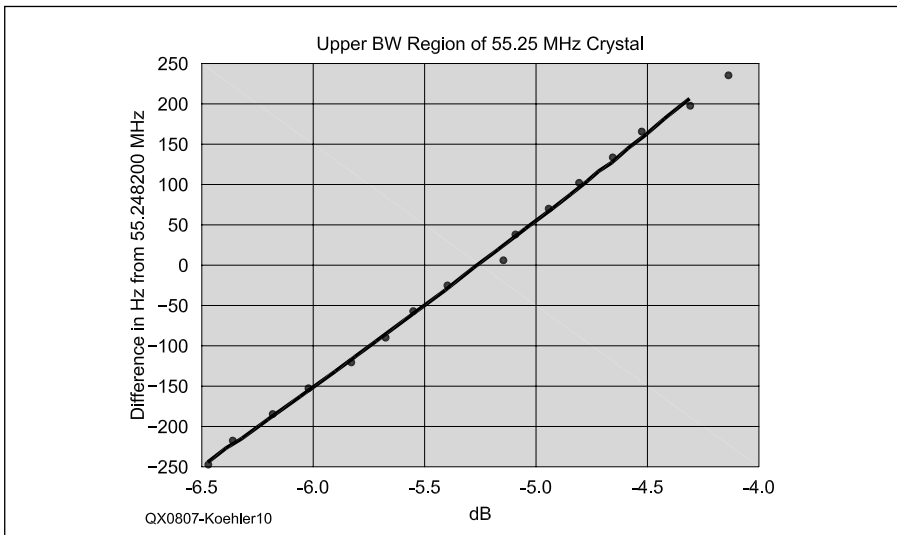


Figure 10 — The shunt response near the upper -5.4 dB region. The plot is of frequency in the Y-direction and attenuation in the X-direction.

method requires a first estimate of the value of the variables but these could easily be found using the techniques I have described here previously. It is worth commenting that it is important to make good initial estimates or the LM algorithm may not necessarily converge. The values obtained by the methods described here are likely to be good enough, however. Modern microprocessors such as the LPC2148 are sufficiently fast that even such complex calculations can be done very quickly.

Sources of Error and Limitations

For my signal generator, the principal limitation in a conventional series mode is due to the abbreviated dynamic range of the detector. This was caused by my choice to use attenuation to give a precise 25 Ω input and output resistance and could easily have been remedied by a post amplifier. I didn't want the additional complication and opted to use the shunt method instead because it worked well with just the simple circuit.

The principal source of error will be in the accuracy of the detector, since the frequency stability, frequency resolution and amplitude stability of the signal generator are of much higher precision. The AD8307 data sheet shows a graph of dc output versus RF input level. The graph is linear in dB but there are "ripples" in the response. From the very small graph in the AD8307 data sheet, it is difficult to estimate the magnitude of these ripples but it seems reasonable to say that the deviations from a straight line are at least 0.1 to 0.2 dB.

The slope of the line gives the relationship between input RF amplitude (in dB) versus output dc level. The A/D converter in the LPC2148 has a resolution of 10 bits. The maximum range of around 100 dB (from -80 to +20 dB) corresponds, roughly, to the 0 to 3.3 V range of the LPC2148, so that one bit is roughly 0.1 dB. I calibrated the detector by putting fixed attenuators in front of the detector with a steady 10 MHz signal source. The method was to insert five separate attenuators over about a 50 dB range, measure the value of the output A/D conversion for each of these attenuations and to then solve for the least-square best fit to a straight line. Then, using the values for the coefficients for this line, any subsequent A/D conversion can be quickly and simply converted to a level in dB. This is a much more satisfactory way to convert A/D measurements to a decibel value than interpolating.

For the AD8307, the data sheets show that the straight line output versus logarithmic input has a slope that is constant over a large frequency range even though the actual

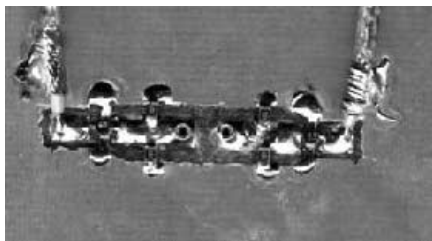


Photo A — A magnified view of the circuit implemented on a piece of double-sided circuit board material. The coaxial lines on either side go to a MiniCircuits 4 dB surface-mount attenuator and are shunted by two 100 Ω resistors on either side of the crystal. The net 50 Ω shunt along with the 50 Ω output resistance of the attenuators gives a source and detector resistance of 25 Ω .

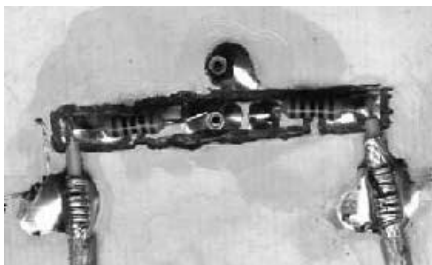


Photo B — The shunt fixture consists of two 100 Ω , 1% metal film resistors in series with the coaxial input and output lines. The crystal is mounted between the junction of the two resistances and the ground. The fixture was made from double-sided pc-board.

values may change with frequency. Since the response of the shunt fixture (at any frequency) is normalized, this means that the frequency sensitivity of the detector should not contribute to the errors.

There is the additional problem that the output of NimbleSig, as with any DDS source, contains spurious outputs at frequencies other than the fundamental. Since the AD8307 detector is very broadband, these spurs will add to the background and so raise the detected output level by a small amount dependent on the particular output frequency. In NimbleSig, there is a very sharp cut-off low-pass filter to reduce the outputs caused by aliasing and it is reasonable to assume that the total remaining spurious power is roughly — very roughly — constant, independent of the frequency to which the DDS is set. I do not think these spurs contribute significantly to the errors.

Many conventional signal generators have relatively high level harmonics of the fundamental in their output; sometimes just down 30 or so dB from the fundamental.

Such harmonics would be detected by the AD8307 and would contribute to the background and thus reduce the dynamic range. This is not a problem with NimbleSig.

In summary, I feel that the measurements are probably accurate to about 0.5 dB over the entire range of the detector. Over smaller ranges, the probable error is likely to be about 0.2 dB.

Acknowledgements

I would like to thank Tom Allread for designing NimbleSig and for constructing one unit and giving it to me. It made design and construction the rest of the signal generator very straightforward. I would like to thank NXP for making the LPC2148 ARM7 microprocessor. Having 512 KB of flash program memory and 32 KB of RAM makes programming a pleasure. The fact that it is about the same price as 8-bit microprocessors of much more limited speed and memory capacity is just a bonus! Finally, I would also like to thank Analog Devices for their wonderful series of logarithmic power detectors. Almost every project I have worked on in the last year or two seems to have one of these at the heart of it.

Notes

- ¹Thomas M. Allread, VA7TA, "NimbleSig, A Compact DDS RF Signal Generator," *Circuit Cellar*, Issue 208, Nov, 2007, p 22.
- ²Jack Hardcastle, G3JIR, "Quartz Crystal Parameter Measurement," *QEX*, Jan/Feb, 2002, p 7.
- ³Jim Kortge, K8IQY, "Simplified Tools and Methods for Measuring Crystals," *AmQRP Homebrewer*, No. 7, 2006, p 1.
- ⁴Wes Hayward, W7ZOI, "Refinements in Crystal Ladder Filter Design", *QEX*, June, 1995, p 16-.
- ⁵Jack Smith, K8ZOA, "Designing the Z90's Gaussian Crystal Filter," *QEX*, May/June, 2007, pp 16-26.
- ⁶Wes Hayward, W7ZOI, Rick Campbell, KK7B, and Bob Larkin, W7PUA, *Experimental Methods in RF Design*, ARRL Publication 208, 2003.
- ⁷William H. Press, Brian P. Flannery, Saul A. Teukolsky and William T. Vetterling, *Numerical Recipes in C*, Cambridge Press, 1988, p 542ff.

Jim Koehler was first licensed as VE5AL at age 15 in 1952. He attended university in Canada and Australia, and became a professor of physics and engineering physics at the University of Saskatchewan, retiring in 1996. He and his wife moved to Vancouver Island after retirement. He dabbles in photography, electronic design and generally enjoys the wonderful scenery and relaxed lifestyle.



From Spark Generators to Modern VHF/UHF/SHF Voltage Controlled Oscillators

Here is a brief overview of RF oscillators — from Heinrich Hertz's original apparatus to modern voltage controlled oscillators.

As we teach advances in the field of microwave oscillators, it may be fun to step back and look at the origin of oscillators. The very first one, invented by Heinrich Hertz in 1886, was generating RF energy based on a spark across a gap, and used a resonant dipole as a frequency determining element.

The original test circuit shown in Figure 1 is preserved at the Deutsche Museum in Munich, Germany. Figure 2 shows the current and voltage distribution along the dipole.^{1,2}

The iron balls at the end of the 2 wires, as shown in Figure 2, reduce the resonant frequency significantly. Today we call this capacitive loading, and this also makes the dipole bandwidth much narrower. Since the gap between the two poles produces a high impedance, the transmissions result in a highly damped waveform. A better way to show this and duplicate the result is by using a four-gap spark "transmitter" based on the 1914 work of Leimbach, as shown in Figure 3. Probably the most efficient of these "arcing" transmitters was the one built by Ludena in 1929, as shown in Figure 4.

These spark "oscillators" were driven by a modulated voltage, resulting in a hum-like sound at the receiving station.

Progress was made in the following years by the invention of an electron tube in about 1932 that was suitable for microwave applications. While the tube was one of the requirements of the oscillator, the resonant circuit was another important part of the circuit. In 1935, so called acorn tubes (miniature triode tubes) were developed, and probably the very first "crystal" triode transmitter was configured. This is shown in Figure 5.

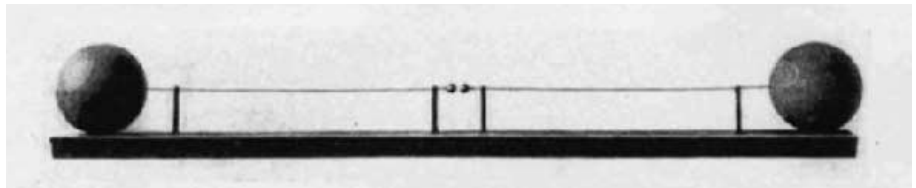


Figure 1 — Original dipole made by Heinrich Hertz in 1887 using balls at the end to form a capacitive load (Deutsches Museum, Munich) See Note 1.

Rather than getting the energy from a spark, the next generation of oscillators consisted of an amplifier with feedback, where a small amount of energy is used to start the oscillation, and then maintain the oscillation. Today, this is explained in terms of a negative resistance, which compensates for the losses, and can be expressed by concentrat-

ing them in the form of a loading resistor in parallel with the resonator (tuned circuit). By applying the right amount of feedback, the input (and/or output) of the amplifier shows a negative parallel impedance (or a transformed negative series impedance). Equation 1 is a simplified equation using the familiar Y-parameters, but can also be expressed in other forms, such as S-parameters. I prefer the Y parameters since they give more insight into the circuit than other forms.

$$Y^* = \frac{Y_{21} \times Y_{12}}{Y_{22} + Y_L}; \quad Y^* < 0$$

Y_{21} is the forward transconductance,
 Y_{12} is the reverse transconductance (internal and external feedback)
 Y_{22} is the output conductance, and
 Y_{11} is the input conductance of the active device (tube or transistor).
 Y_L is the output with load.

In the beginning, the capacitively loaded dipole determined the resonant frequency, and soon after discovering the piezoelectric effect, tourmaline crystals, of all things, were used to stabilize the oscillator frequency. This is shown in Figure 5. This is a photograph of probably the first stable "crystal controlled," slightly tunable 455 MHz oscillator. (See Note 1.)

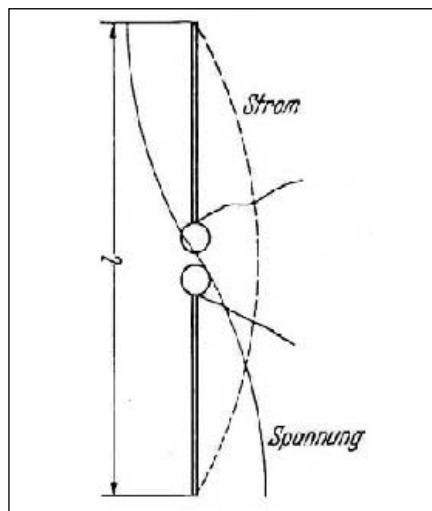


Figure 2 — A typical current (strom) and voltage (spannung) distribution along the length of the Hertz dipole. See Note 1.

¹Notes appear on page 45.

In the search for stable but tunable resonators, the principle of a quarter wave line was applied. By mechanically tuning the inner portion of a coaxial resonator, a high Q (Figure of merit, ratio of stored energy versus dissipated energy) oscillator with the novel mechanical arrangements shown in Figure 6 were invented. (See Note 2.) In the case shown in Part A, a screw allows fine tuning while in Part B the end can be mechanically set over a wide range. An actual circuit diagram is given in Figure 7, which shows how the tube is connected. (See Note 2.)

This system for obtaining very good resonators was applied to test equipment, where tuning the mechanical resonator set the oscillator frequency. This oscillator was used in the early Tektronix spectrum

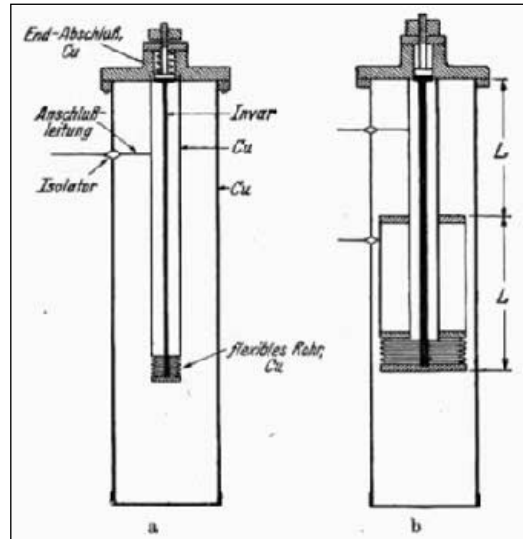


Figure 6 — Coaxial resonator oscillators. (See Note 2.) Invar refers to a type of steel used for the center conductor.

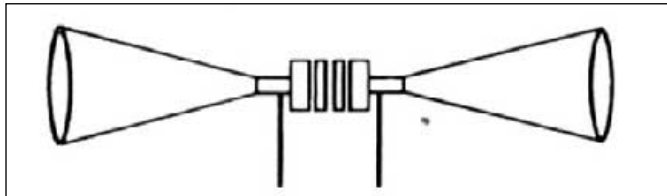


Figure 3 — Thick dipole formed by two conical resonators with spark gap (1914). See Note 1.

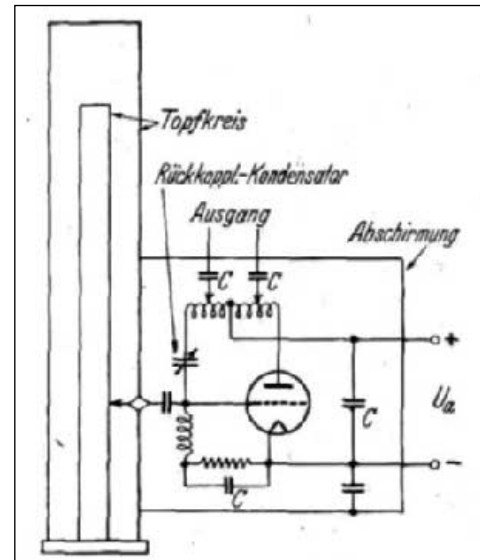


Figure 7 — Actual early tube oscillator circuit using a coaxial resonator. (See Note 2.) Topfkreis means coaxial resonator, Rückkopl-Kondensator refers to the tuning capacitor, Ausgang refers to output capacitors and Abschirmung is a shielding box.

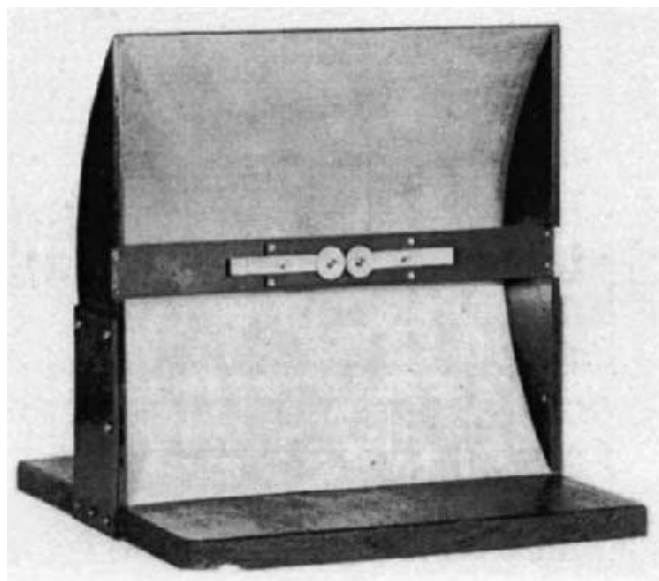


Figure 4 — Dipole oscillator with parabolic mirror (1929). (See Note 1.)

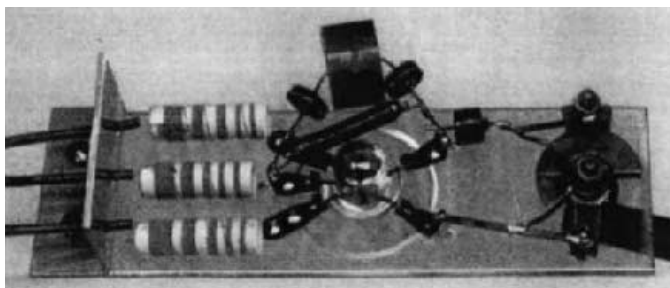


Figure 5 — 455 MHz crystal triode transmitter. (See Note 1.) The leads come out the sides of this "lighthouse" tube. Notice the three RF chokes on the left.

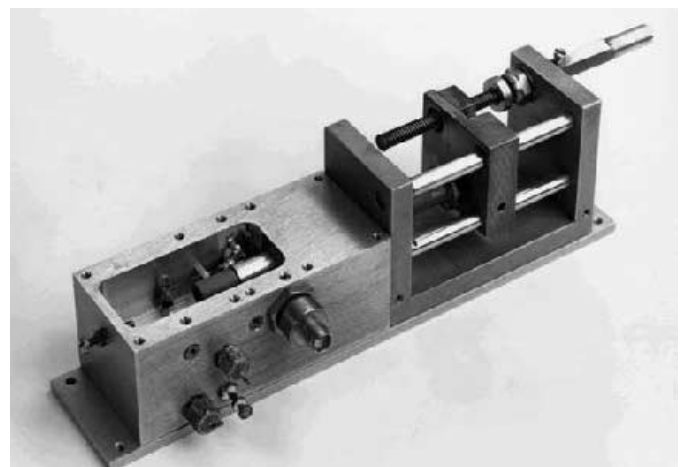


Figure 8 — Mechanically tuned 4GHz transistor oscillator.³ The tuning shift is on the right side.

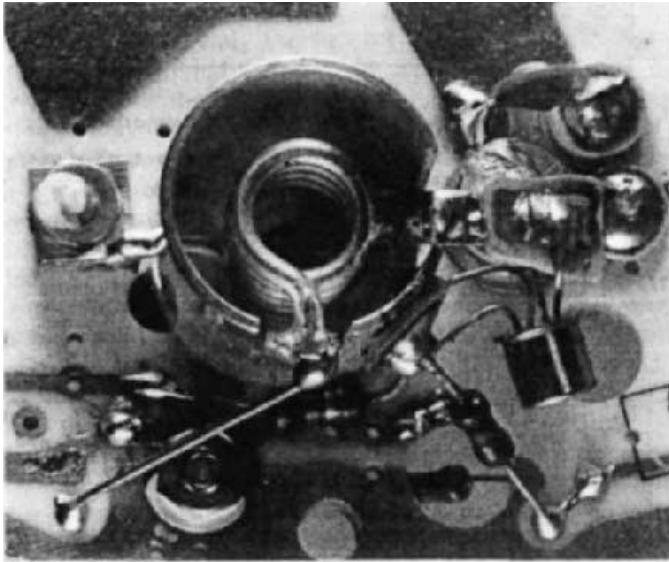


Figure 9 — High Q helical resonator oscillator (Rohde & Schwarz, SMDU).⁴ Notice the transistor hanging off the right side of the resonator.

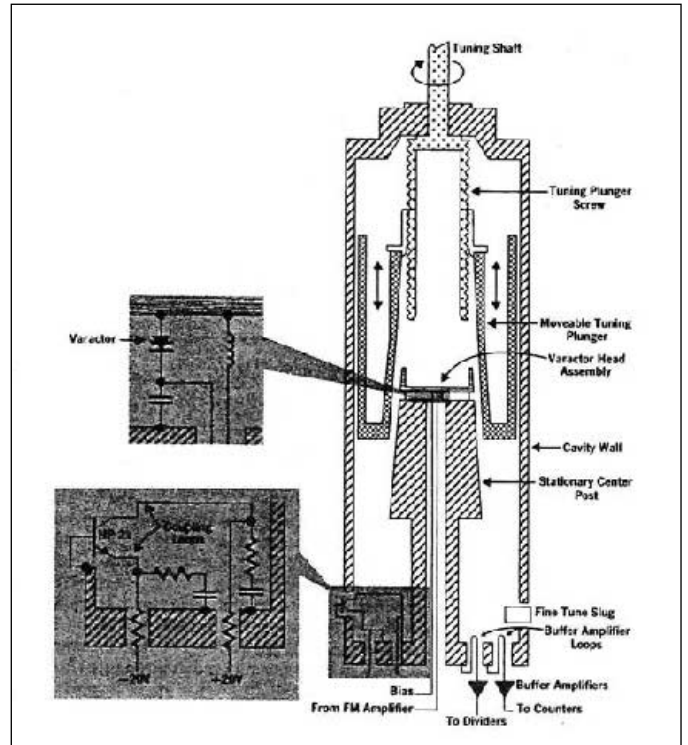


Figure 10 — Mechanically tuned 200 to 400 MHz Oscillator (Hewlett Packard HP8640).

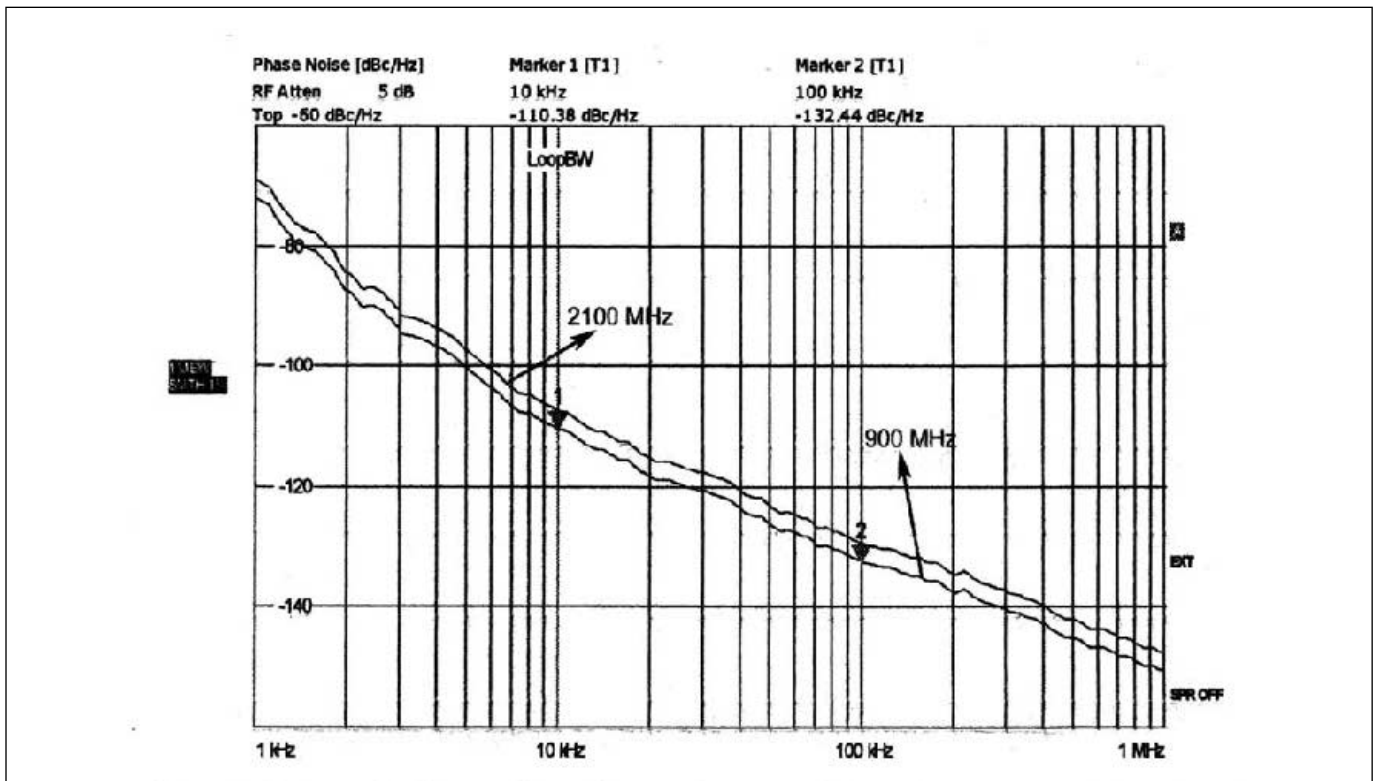


Figure 11 — Measured phase noise of a modern coupled mode resonator (line) based wideband VCO (900-2100 MHz) (Synergy Microwave Corp, USA).

analyzers, where the actual frequency was modulated as part of a phase locked loop control system, which stabilized the frequency against a standard. The photograph of Figure 8 shows the mechanically tuned resonator and the oscillator circuit. (See Note 2.)

A variation of this is the helical resonator, which has a high Q, low radiation and needs to be tuned electrically by some mechanical device — in this case an air variable capacitor. This was done in the vintage 1970 Rohde & Schwarz SMDU signal generator (Figure 9). Hewlett Packard — now Agilent — designed their HP 8640 signal generator around the tunable cavity, 200 to 400 MHz, and dividing the output frequency down for lower frequency in segments of 2:1. These were built when the spectral purity of a (wide) tunable oscillator became interesting. This parameter is called phase noise, expressed in dB below the carrier in different offsets referenced to 1 Hz bandwidth.

Today, with synthesized signal generators, these mechanical systems are replaced by voltage controlled oscillators (VCOs), using tuning diodes or varactors. These are reverse biased Si or GaAs diodes, which become voltage dependent semiconductor capacitors with a variation of up to 10 times change of the capacitance. These oscillators are built around printed circuits, which have a Q of about 50 for the resonators. By applying modern 3D field theory of coupled lines and resonators, these modern marbles now

realize a Q of up to 250, and compete well with the previous mechanical designs. They meet the stringent requirements of a modern wide tunable system with good phase noise. Figure 11 shows the measured phase noise of a modern coupled mode resonator (line) based wide band VCO and Figure 12 shows the phase noise of a 1960 vintage tube mechanically tuned oscillator (R&S). The layout of the modern printed resonator using this patented design is shown in Figure 13.^{5, 6, 7, 8, 9, 10}

For more details on these oscillators see the references and www.synergymwave.com.

Notes

- ¹H. E. Hollmann, *Physik und Technik der ultrakurzen Wellen*, Verlag von Julius Springer, Berlin 1936.
- ²H. Rothe and W. Kleen, *Elektronenöhren Als Schwingungserzeuger und Gleichrichter*, Akademische Verlagsgesellschaft Becker & Erler Kom.— GES, Leipzig, 1941.
- ³G. Vendelin, A. Pavio, U. L. Rohde, *Microwave Circuit Design Using Linear and Nonlinear Techniques*, Second Edition. John Wiley & Sons, Inc 2005.
- ⁴U. L. Rohde, *Microwave Wireless Synthesizers*, John Wiley & Sons, Inc, 1997.
- ⁵U. L. Rohde, A. K. Poddar, and G. Boeck, *Modern Microwave Oscillators for Wireless Applications: Theory and Optimization*, John Wiley & Sons Inc, 2005.
- ⁶U. L. Rohde and A. K. Poddar, "Technological Scaling and Minimization of 1/f Noise in Coupled Mode Oscillator For Wireless Systems," *Microwave Journal*, June 2007.
- ⁷U. L. Rohde, A. K. Poddar, and R. Rebel, "Integrated Low Noise Microwave Wideband Push-Push VCO," *US Patent No. 7,088,189*.
- ⁸U. L. Rohde and A. K. Poddar, "Noise Minimization Techniques for RF & MW Signal Sources

(Oscillators/VCOs)," *Microwave Journal*, Aug. 2007.

⁹A. Grebennikov, "Noise Reduction in Transistor Oscillators," *High Frequency Electronics*, May 2005. *Writer's Handbook*. Mill Valley, CA: University Science, 1989.

¹⁰J. S. Schaffner, "Simultaneous Oscillations in Oscillators," *IRE Transactions on Circuit Theory*, Vol 1, no. 2, Jun 1954, pp 2-8. T. Endo and S. Mori, "Mode Analysis of a Multimode Ladder Oscillator," *IEEE Transactions CAS-23*, Feb 1976, pp 100-113.

Ulrich L. Rohde studied electrical engineering and radio communications at the universities of Munich and Darmstadt, Germany. He holds a PhD in electrical engineering (1978) and an honorary ScD (1979) in radio communications, a Dr-Ing (2004) from the University of Berlin, Germany in Oscillator Circuits and several honorary doctorates.

He is President of Communications Consulting Corporation; Chairman of Synergy Microwave Corp, Paterson, New Jersey; and a partner of Rohde & Schwarz, Munich, Germany. Previously, he was the President of Compact Software, Inc, Paterson, New Jersey; and Business Area Director for Radio Systems of RCA, Government Systems Division, Camden, New Jersey. He is a Professor of RF Microwave Circuit Design at Cottbus and has held Visiting Professorships at several universities in the United States and Europe.

Dr. Rohde holds several patents and has published more than 60 scientific papers in professional journals, contributed a chap-

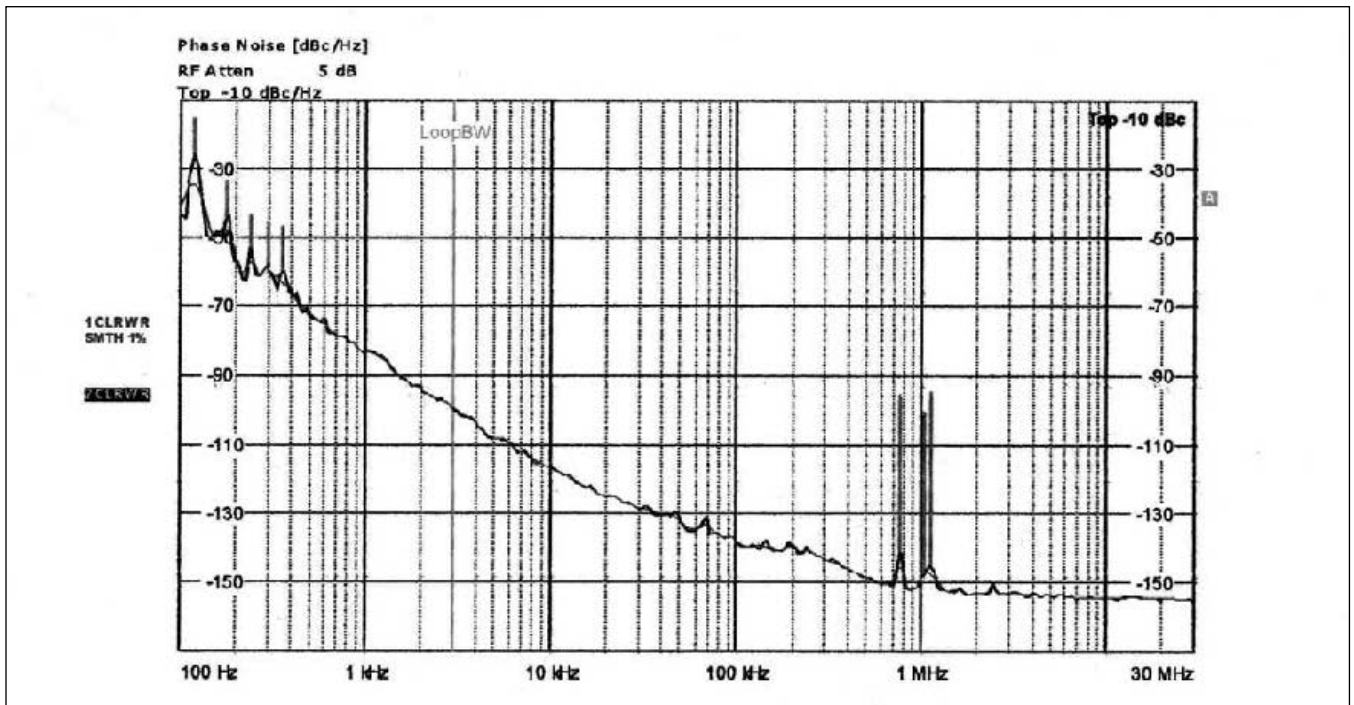


Figure 12 — Typical measured phase noise of a 1000 MHz 1960 vintage Rohde & Schwarz cavity stabilized tube oscillator. The two spurs shown are picked up from broadcasting stations.

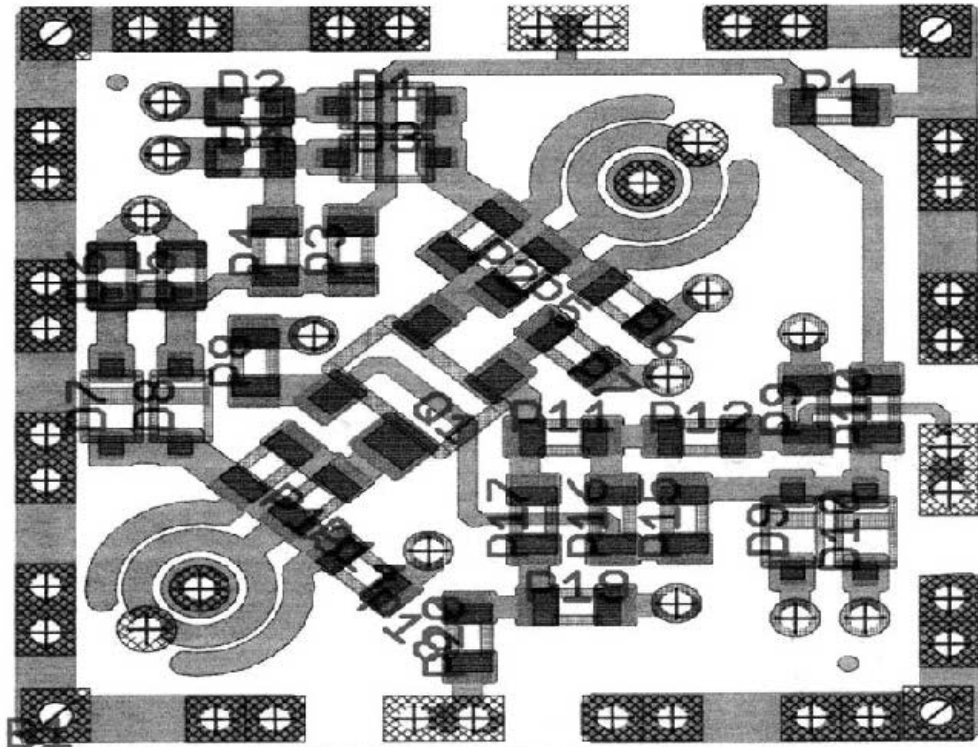
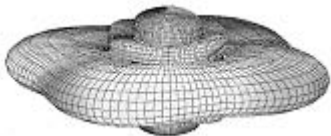


Figure 13 — Typical layout of the wideband VCO using modern printed coupled resonator (Synergy Microwave Corp, USA).

A picture is worth a thousand words...



With the

ANTENNA MODEL™

wire antenna analysis program for Windows you get true 3D far field patterns that are far more informative than conventional 2D patterns or wire-frame pseudo-3D patterns.

Describe the antenna in the program in an easy-to-use spreadsheet-style format, and then with one mouse-click the program shows you the antenna pattern, front/back ratio, front/rear ratio, input impedance, efficiency, SWR, and more.

An optional **Symbols** window with formula evaluation capability can do your computations for you. A **Match Wizard** designs Gamma, T, or Hairpin matches for Yagi antennas. A **Clamp Wizard** calculates the equivalent diameter of Yagi element clamps. **Yagi Optimization** finds Yagi dimensions that satisfy performance objectives you specify. Major antenna properties can be graphed as a function of frequency.

There is **no built-in segment limit**. Your models can be as large and complicated as your system permits.

ANTENNA MODEL is only \$90US. This includes a Web site download and a permanent backup copy on CD-ROM. Visit our Web site for more information about **ANTENNA MODEL**.

Teri Software
P.O. Box 277
Lincoln, TX 78948

www.antennamodel.com

e-mail sales@antennamodel.com
phone 979-542-7952

NATIONAL RF, INC.



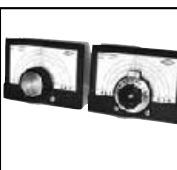
VECTOR-FINDER
Handheld VHF direction
finder. Uses any FM xcvr.
Audible & LED display
VF-142Q, 130-300 MHz
\$239.95
VF-142QM, 130-500 MHz
\$289.95



ATTENUATOR
Switchable,
T-Pad Attenuator,
100 dB max - 10 dB min
BNC connectors
AT-100,
\$89.95



TYPE NLF-2
LOW FREQUENCY
ACTIVE ANTENNA
AND AMPLIFIER
A Hot, Active, Noise
Reducing Antenna System
that will sit on your desk
and copy 2200, 1700, and
600 through 160 Meter
Experimental and Amateur
Radio Signals!
Type NLF-2 System:
\$369.95



DIAL SCALES
The perfect finishing touch
for your homebrew projects.
1/4-inch shaft couplings.
NPD-1, 3 1/8" x 2 3/4",
7:1 drive
\$34.95
NPD-2, 5 1/8" x 3 3/8",
8:1 drive
\$44.95
NPD-3, 5 1/8" x 3 3/8",
6:1 drive
\$49.95

NATIONAL RF, INC
7969 ENGINEER ROAD, #102
SAN DIEGO, CA 92111

858.565.1319 FAX 858.571.5909
www.NationalRF.com

ter entitled "Oscillators and Frequency Synthesizers" to The Handbook of Microwave and Optical Components, 2nd Edition; contributed a chapter entitled "Frequency Synthesizers" to The Wiley Encyclopedia of Telecommunications, as well as six books: Communications Receivers, Third Edition; RF/Microwave Circuit Design for Wireless Applications; Microwave and Wireless Synthesizers: Theory and Design; Microwave Circuit Design Using Linear and Nonlinear Techniques, with co-authors George Vendelin and Anthony M. Pavio; Communications Receivers: Principles and Design; and Digital PLL Frequency Synthesizers: Theory and Design.

Dr. Rohde is a member of the following: Fellow Member of the IEEE, Invited Panel Member for the FCC's Spectrum Policy Task Force on Issues Related to the Commission's Spectrum Policies, Eta Kappa Nu Honor Society, Executive Association of the Graduate School of Business-Columbia University, New York, the Armed Forces Communications & Electronics Association, fellow of the Radio Club of America, and former Chairman of the Electrical and Computer Engineering Advisory Board at New Jersey Institute of Technology. He holds German call signs, DJ2LR/DL1R since 1956, a Swiss call sign, HB9AWE and a US call sign, NIUL (formerly KA2WEU).



Tech Notes

The Goofy-Foot Yagi

Every time I have a brilliant idea, it seems someone has thought of it before. This is the bad news. The good news is that many of these previously discovered, not-my-own bright ideas have been long forgotten by most people who would otherwise care. I can shamelessly present them as new ideas because anyone who was around when they really *were* new ideas is probably retired, senile, or dead.

The real joy in dredging up old truths comes in the form of demolishing modern assumptions; of which Amateur Radio is replete. Assumptions like, "A director is always shorter than the driven element of a Yagi antenna," to name just one.

Einstein once said, "Everything should be made as simple as possible ... but not one bit simpler."

There is a disturbing little graph that bears out Einstein's assertion. It appears as Figure 22.64 in the 2008 edition of *The ARRL Handbook*, and has appeared in every previous edition since at least as far back as the mid 1940s.¹ (See Figure 1.) That graph haunts me. It's an annoying little thing that just refuses to go away. It is a continual reminder that the universe is not as simple as it seems, no matter how much we'd like it to be. It's like the number pi. It's so commonplace that it should be normal — but it's not. We call it an irrational number, even though it represents the most rational identity we're ever likely to encounter!

Now the graph in question shows us that a self-resonant parasitic element can act as either a director or a reflector, depending on its spacing from the driven element. The interesting point is that it works much better as a director, at least as far as maximum forward gain is concerned. It seems we can get just a gnat's eyebrow below 7 dB of gain with such an arrangement — not too shabby at all.

The reason I care is because I've been investigating the feasibility of a 40 meter Yagi at my QTH. Now, *all* 40-meter Yagis are monstrosities, but some are more monstrous monstrosities than others. A 40-meter Yagi with a reflector is one of the more monstrous monstrosities, with little advan-

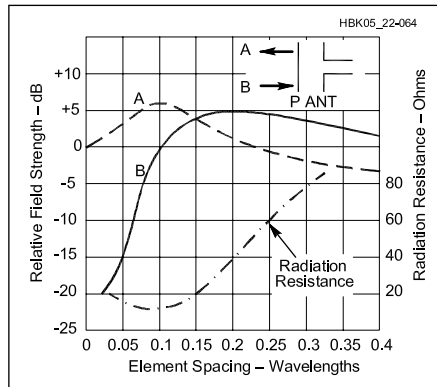


Figure 1 — Gain versus element spacing for a two element Yagi, having one driven and one parasitic element. The reference point, 0 dB, is the field strength from a $\frac{1}{2} \lambda$ dipole alone. The greatest gain is in the direction A at spacings of less than 0.14λ , and in direction B at greater spacings. The front-to-rear ratio is the difference in decibels between curves A and B. Variation in radiation resistance of the driven element is also shown. These curves are for the special case of a self-resonant parasitic element, but are representative of how a two element Yagi works. At most spacings, the gain as a reflector can be increased by slight lengthening of the parasitic element; the gain as a director can be increased by shortening. This also improves the front-to-rear ratio.

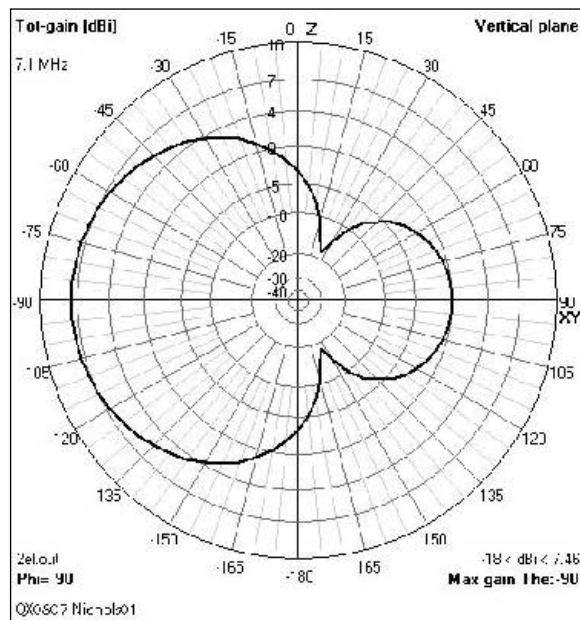


Figure 2 — This radiation pattern shows the NEC prediction for the Goofy Foot Yagi.

tage over lesser monstrosities, especially up here. Living in interior Alaska, in the Bermuda Triangle of radio propagation, *forward gain* is the only thing that matters. QRM just doesn't exist. We actually look forward to anything that might resemble QRM, because it means at least we have *some* propagation. Also, most low-band propagation is one-way into interior Alaska — nobody hears us, even when we hear them. Although a reflector might yield a bit more front-to-back ratio, it isn't very useful to me.

So, what this means is, for *my* purposes, at least, I should be able to quickly reach the point of diminishing returns with just two elements. Happy, happy, joy, joy!

Fortunately for me, I was able to confirm my suspicions on someone else's dime a few years ago. I was working at Hipas Observatory, and we were building a Doppler ionospheric sounder for one particular experiment at 4.53 MHz. We needed a good vertical incident antenna, and we needed it pretty fast. I had already known about that annoying chart, but never really had a reason to prove it or disprove it. We had a pair of towers that were just on the verge of being tall enough to build such a short-spaced vertical incident Yagi, using equal-length radiators in the director mode. I was also aware of the extremely low radiation resistance of this antenna, but we already had a partial solution in place; a couple of 6 inch diameter cage dipoles we had used for a previous experiment. We installed the two cage dipoles with the director on top, and the driven element probably a lot lower than it should have been. (Fortunately, our ground conductivity in interior Alaska is so bad; it's almost the same as free space. You can lay an 80 meter dipole on the ground and it works just fine).

At any rate, the antenna worked admirably, and our preliminary comparisons with one of our main "heater" dipoles showed that we were indeed getting close to 7 dB of gain. We might have had a certain amount of ground reflection contributing in our favor, but in any case, it worked so well, I believe that antenna is still standing. I have great confidence that a similar arrangement will

¹Notes appear on page 49.

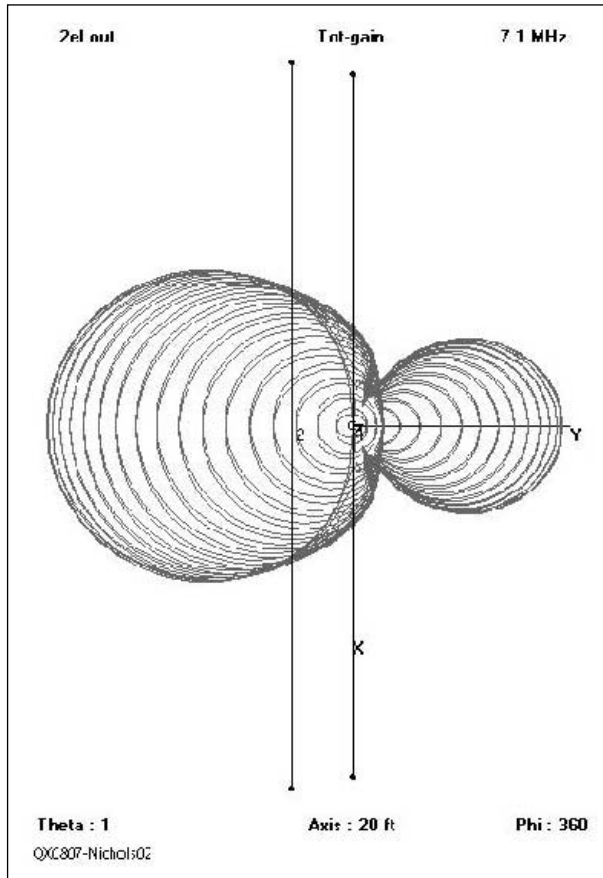


Figure 3 — A three-dimensional representation of the Goofy Foot Yagi antenna radiation pattern.

Feeding the Thing

If you're even a moderately experienced antenna person, you might suspect this thing has a really low value of feed point impedance, and you'd be right, as the output file of the NEC program indicates: 3Ω resistance with some spare change and about 62Ω capacitive reactance. Because the radiation resistance is so low, you definitely want to eliminate, as far as humanly possible, incidental losses. You probably don't have too much control over this, but don't make it any worse than you have to. I strongly recommend you read W8J1's excellent work on antenna efficiency. There is no magical way of feeding this thing that will reduce IR losses below what they are. As the modern vernacular goes, "It is what it is." You might consider "fattening" your conductors by using a cage-dipole arrangement for the elements, but you don't want to go too far in this direction, or your antenna will no longer be compact, which is one of the main points of this design.

As with any close-spaced antenna, this is a *narrow* bandwidth beastie; probably a lot touchier as far as dimensions go than any other antennas you've worked with. Don't be daunted! This is an *experimental* design, not the end all, be all! Be prepared to do some twiddling and pruning.

Now, with all that said, you're going to need about a 16:1 balun at the feed point of this antenna, if you're using standard 50Ω coax. You *can* put a couple of 4:1 transmission line baluns back to back to do this, or you can custom wind a conventional transformer. I recommend the latter for a couple of reasons. The main reason is that you still need to add some inductance in order to cancel out the capacitive reactance of the antenna. Why not kill two birds with one stone? Use a conservatively oversized powdered iron toroid — not a ferrite — and wind a conventional transformer. Use the extra leakage inductance to resonate your antenna. Since this is a narrow-band antenna anyway, there is no point in trying to build a broadband balun. You can actually get more efficiency out of a high-Q tuned one (the antenna itself supplying the necessary capacitive reactance). You can either use a single winding "autotransformer" configuration, or use two separate windings. The former is a bit more efficient, but a little trickier to tune. With two coils, you can independently "fiddle" with the reactance and the turns ratio a little more conveniently.

Again, this is an area for a bit of experimentation, but don't try to reinvent the wheel. There's lots of old literature on conventional-wound RF transformers, which are more than adequate for this application.

work just fine on 40 meters for me.

Only one thing remains.— to truly optimize those two elements for forward gain. It's probably a lot easier to do nowadays than when that mysterious, anonymous, truth-telling graph-maker of yore created that annoying chart.

Now, a little further investigation dredges up another obscure fact. Referring to the 16th Edition of *The ARRL Antenna Book* in Chapter 11, "Yagi Arrays," we find another buried gem.² On page 11-3, under the MAXIMUM GAIN subheading, we find these words.

"... At spacings greater than 0.25λ , the parasitic element must be shorter than a self-resonant length to operate as a reflector. The closer the spacing, the greater the detuning required..."

A few sentences later, we find more revelation.

"At spacings greater than 0.25λ , the parasitic element must be *shorter* than a self-resonant length to operate as a reflector. ... At less than 0.06λ spacing, the director must be tuned below resonance (*longer*

than a self-resonant length) to obtain the maximum gain..."

What heresy is this? Did I read that in the venerable *ARRL Antenna Book*? A director *longer* than a driven element? A reflector *shorter* than a driven element? Arrgh! My brain is about to explode!

Over the years, I've developed a great deal of confidence in NEC-2 antenna modeling software. I know what it *can't* do, but I also know what it *can* do. This comes from playing with a lot of antennas before I even knew what a computer was. Years ago, one of my mentors told me, "You'd better know what the answer is before you give it to a computer." This was very good advice. Antenna modeling programs work best for those who already know what the right answer is — then the computer can give you a "more righter answer." And a lot more quickly, I might add.

The bottom line is that careful NEC modeling confirms the heresy encountered in those hidden paragraphs.

A few years ago, my teenage son and his friends, to their collective astonishment, learned I could skateboard. They also

informed me that I was a "goofy-foot," a fact of which I had been previously unaware. A goofy-foot places his "passive foot" at the rear of the skateboard and pushes with his other one to get moving, then places his pusher foot in *front*. This always seemed perfectly natural to me, but my son's friends informed me it was a highly-prized skill in skateboard-dom, for reasons I've yet to fathom.

And so, in this far-stretched analogy, we learn that this "goofy-footed," backward-firing Yagi should be a pretty good performer for a lesser-grade monstrosity.

Now, here's a bit of a surprise. Once I have the Goofy-Foot optimized, the addition of either a reflector or an additional director totally destroys the thing! I've yet to find any combination thereof that actually improves either the gain or the front-to-back ratio. It's almost as if it's in a class of its own, and doesn't want to let anyone else in.

This is not really a problem; all it means is that once you've decided to go for this thing, you're committed to only two elements. So, as they said in the Old West, "choose your ruts well."

I'm fairly sure that nameless, faceless, annoying graph maker is laughing in his grave, saying, "I knew all that." Fortunately, he's not around to make me feel so dumb in public.

As soon as the snow clears and I can find my back yard, I'll be able to build my mini-monstrosity and see if everything I've modeled is really true. I have no reason to question it. The jury is still out, but I'm expecting great things from this antenna experiment. I plan to make a full report by

next winter. Stay tuned.

Eric P. Nichols, KL7AJ has been licensed since 1972, and has held the call sign KL7AJ since 1977. He has written numerous articles for QST, QEX, and other Amateur Radio publications since 1983. He is also the author of the novel, Plasma Dreams, and is currently marketing the prequel to that book, Steel Stonehenge. He has worked many years in broadcast engineering and ionospheric research/auroral modification.

Notes

¹Mark Wilson, K1RO, Editor, *The ARRL Handbook*, 2008 Edition, ARRL, 2007, p 22.34. ARRL publications are available from your local ARRL dealer, or from the ARRL Bookstore. Telephone toll-free in the US 888-277-5289, or call 860-594-0355, fax 860-594-0303; www.arrl.org/shop; pubsales@arrl.org.

²Gerald (Jerry) Hall, K1TD, Editor, *The ARRL Antenna Book*, 16th Edition, ARRL, 1991, pp 11-3, 11-4.



Chicago – “Your Kind of Town” for the 2008 ARRL/TAPR Digital Communications Conference

September 26-28



Chicago plays host to the largest gathering of Amateur Radio digital enthusiasts in the country. Make your reservations now for three days of education and camaraderie, including a Sunday seminar on Software Defined Radio by **Phil Harman, VK6APH**.

See the Digital Communications Conference site on the Web at www.tapr.org/dcc/ or call TAPR at **972-671-8277** to make your reservations today.

Antenna Options

In Memoriam—L. B. Cebik, W4RNL

L. B. Cebik, W4RNL, ARRL Technical Adviser and antenna authority, passed away in late April 2008, of natural causes. He was 68. An ARRL Life Member, Cebik was known to many hams for the numerous articles he wrote on antennas and antenna modeling. He had articles published in most of the US ham journals, including *QST*, *QEX*, *NCJ*, *CQ*, *Communications Quarterly*, *Ham Radio*, *73*, *QRP Quarterly*, *Radio-Electronics* and *QRPP*. L. B. was probably the most widely published and often read author of Amateur Radio antenna articles ever to write on the subject.

Cebik lived in Knoxville, Tennessee and wrote more than a dozen books on antennas for both the beginner and the advanced student. Among his books are a basic tutorial in the use of *NEC* antenna modeling software and compilations of his many shorter pieces. A teacher for more than 30 years, Cebik was retired, but served as Professor Emeritus of philosophy at the University of Tennessee, Knoxville. Cebik served his country in the US Air Force from 1957-1961, specializing in air traffic control.

Former ARRL Senior Assistant Technical Editor Dean Straw, N6BV, and editor of *The ARRL Antenna Book*, said, "LB will be greatly missed by the thousands of hams he's helped through his incredibly prolific — and invariably proficient — writing about antennas. LB helped me personally in numerous ways while I worked on antenna matters at the League, always communicating with a gentle, scholarly attitude and a real eye for detail. I'm in shock at the news of LB's passing. May his soul rest in peace."

Licensed since 1954, Cebik served as Technical Editor for *antennex*

Magazine (www.antennex.com). Cebik also maintained a Web site — www.cebik.com — a virtual treasure trove to anyone interested in antennas. Besides a few notes on the history of radio work and other bits that Cebik called "semi-technical oddities," the collection contains information of interest to radio amateurs and professionals interested in antennas, antenna modeling and related subjects, such as antenna tuners and impedance matching. Cebik said that his notes were "geared to helping other radio amateurs and antenna enthusiasts discover what I have managed to uncover over the years — and then to go well beyond." Cebik's Web site had been hosted by *antenneX* publisher Jack Stone, and he has taken steps to ensure that the content remains available to everyone. Simply go to www.cebik.com and create a log-on password.

That Web site also contains information on antenna modeling. His book, *Basic Antenna Modeling: A Hands-On Tutorial* for Nittany-Scientific's *NEC-Win Plus* NEC-2 antenna modeling software, contains models in .NEC format for over 150 exercises. For more advanced modelers using either NEC-2 or NEC-4, Cebik wrote an additional volume, *Intermediate Antenna Modeling: A Hands-On Tutorial*, based on Nittany-Scientific's *NEC-Win Pro* and *GNEC*. The volume includes hundreds of antenna models used in the text to demonstrate virtually the complete command set (along with similarities and differences) used by both cores.

I learned that I could count on L. B. to offer clear, concise comments on any submitted article dealing with antennas. He was always a friendly

voice on the other end of my phone line when I needed to talk to an expert, and I came to expect a quick e-mailed response to any antenna questions that I sent him. L. B. was so much more than an antenna author, though. He was one of the first ARRL Educational Advisors I ever had the pleasure of working with when I became editor of the ARRL study materials. He played a key role in helping develop the concept of online courses when ARRL began to study the idea of the Continuing Education Program; his *Antenna Modeling* course has been one of the most popular offerings in the program. L. B. leaves a legacy of friendly advice and Amateur Radio wisdom. I will miss him as a friend and as an advisor. (Much of this information was taken from an ARRL Web story posted April 25, 2008 by S. Khrystyne Keane, K1SFA, ARRL News Editor.)

In this issue we publish "AO19," the 19th column by W4RNL. The column appeared in nearly every issue since the July/August 2004 issue, with an issue skipped only occasionally for space or other consideration, but never because L. B. didn't have a column ready to be published. That's an awesome track record! In e-mail correspondence I had with L. B. shortly before his passing, he told me that he had written eleven more Antenna Options columns for *QEX*. He always sent the next column as soon as one issue had gone to the printer. At this point I have not been successful in obtaining the files for the extra columns he had written. If we are able to retrieve those files, the Antenna Options column will continue. Otherwise, this may be L. B.'s last column. — *Larry Wolfgang, WR1B*

One Wavelength Loops

Antennas based on the $1\text{-}\lambda$ loop present us with some interesting shape options, ranging from a triangle with 60° corner angles to a circle, which is really a continuous curve. The lore of antennas employing $1\text{-}\lambda$ loops instead of linear elements, however, is fraught with claims that do not quite logically align. For example, I have read that a resonant circular loop has more bidirectional gain than the resonant square loop that we might find commonly used in the HF region. Presumably, gain increases as we gradually decrease the corner angles, since we may view a circular loop as a polygon with an indefinitely large number of sides. Unfortunately, this interpretation does not quite square away with claims that an equilateral delta (triangular) loop has just as much bidirectional gain as a square loop. Of course, the delta's angles are much more acute than the angles of a square loop.

I have two goals for this set of Antenna Options notes. One aim is to discover whether we might settle the logic of loop gain versus loop shape. To that end we shall look at a number of delta, square, and circular loops, along with some reference antennas. We shall eventually pose two questions. First, do we find any numerically significant gain differences? The answer to this question is not only

important to comparative modeling, but may also shed light on what we may expect from two-element driver-reflector beams using various loop shapes. Second, do any gain differences that we find make enough operational difference to dictate loop-beam construction?

My second goal emerged in the course of exploring the elements of the first one. Antenna modeling is the most straightforward way of settling the first question, but the technique turns out to have a number of challenges. Since many readers also model antennas for either design or analysis, examining the challenges and ways to overcome them may prove instructive.

The One λ Loop and Its Models

To determine whether there is a significant difference in the bidirectional gain of $1\ \lambda$ loops, we might model various loop shapes. Since 1 meter equals $1\ \lambda$ at 299.7925 MHz, that frequency is a convenient test frequency. The wire diameter is arbitrary, so long as we use the same diameter for all models. Let's use 2-mm diameter lossless (or perfect) wire for our exercise. Free-space is a completely adequate modeling environment for our comparisons. We shall bring each model to resonance within $\pm j1\ \Omega$ in order to compare both dimensions and operating characteristics.

The only step left is to select the loop shapes that can give us a good sense of what occurs as we alter the polygon's structure. For reference, we need a linear dipole. At the far end of the scale, we need a circle. NEC and MININEC models create close structures from straight lines. If we use enough short straight lines, however, we can simulate a shape that is electrically indistinguishable from a circle. For this task, 45 segments are sufficient. This level of segmentation also coincides with the level of segmentation for our triangles and squares.

We shall use two forms of the square: the ordinary form with "level" sides and the diamond with vertical and horizontal points. In free space, of course, the 45° tilt between the two forms is immaterial, except for one feature. We normally feed the level square at the mid-point of one side. The diamond, we feed at a point. Figure 1 shows the collection of shapes that we shall review, including the two deltas, one with mid-side feed, the other with point feed.¹

The figure also shows one additional shape: a diamond loop with two feed points. A $1\text{-}\lambda$ loop is actually two dipoles with their tips connected. The two dipoles are in phase with each other and separated by an average distance of about

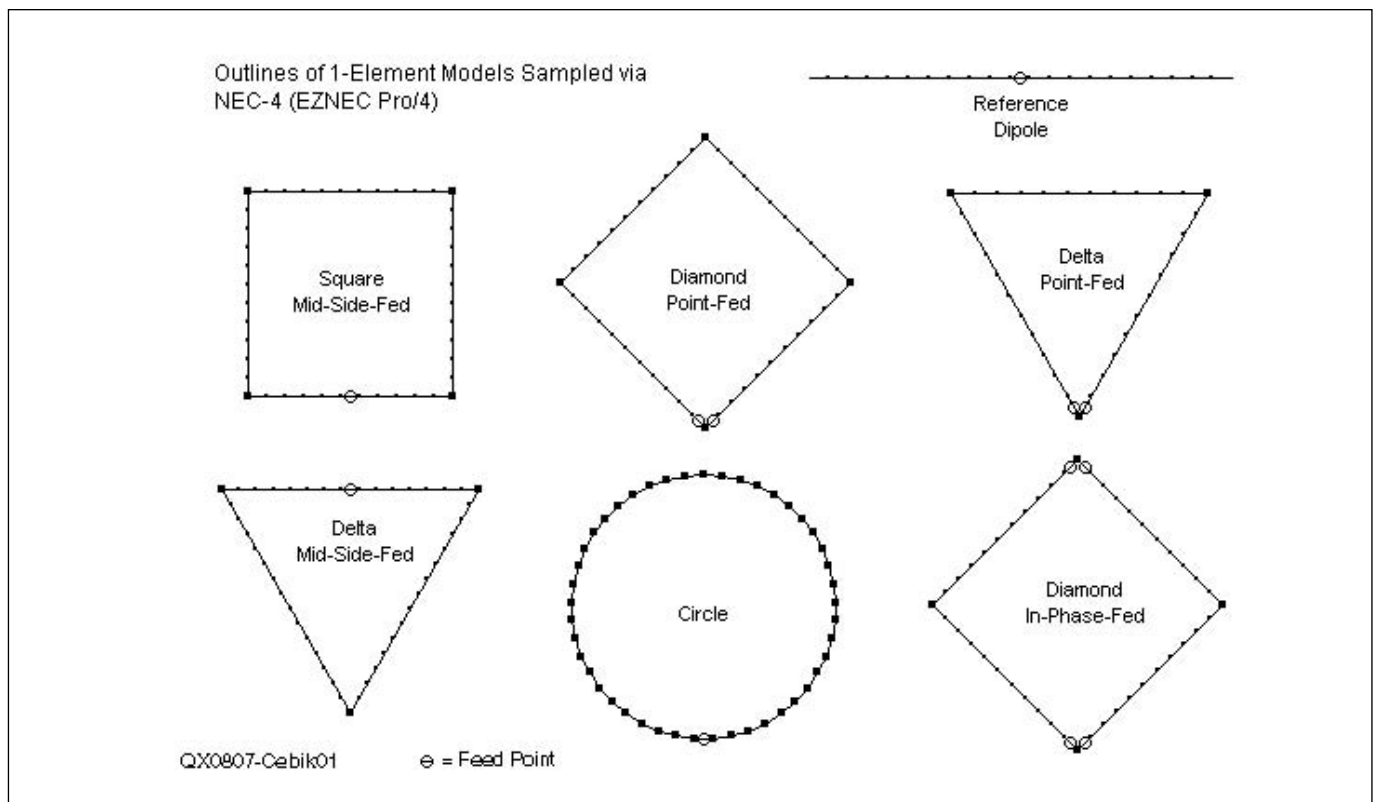


Figure 1 — Outlines of one-element loop models sampled via NEC-4 (EZNEC Pro/4).

Table 1
Single (1-λ) Resonant Loop Elements
NEC-4 Models (EZNEC Pro/4): Free-Space Environment, 0.002 m Zero-Loss Wire, 299.7925 MHz

Antenna	Circumference (λ)	Gain (dBi)	AGT	Cor. Gain (dBi)	Feed Impedance (Ω)	Cor. Resistance (Ω)
Reference dipole	0.4746	2.13	1.000	2.13	71.9 + j0.3	71.9
Square, mid-side fed	1.0944	3.40	1.004	3.38	130.5 - j0.0	131.0
Diamond, point fed	1.0963	3.23	0.962	3.40	136.8 + j0.8	131.6
Triangle (delta), point fed	1.1160	2.76	0.936	3.05	134.6 + j0.2	126.0
Triangle (delta), mid-side fed	1.1070	3.06	1.004	3.04	121.4 + j0.6	121.9
Circle (45 segments)	1.0631	3.67	0.999	3.67	142.2 - j0.1	142.2
Diamond, phase-fed	1.0940	3.24	0.962	3.41	68.3 + j0.0 (x2)	65.7 (x2)

Notes
 Dipole "circumference" = dipole length.
 Cor. = corrected value based on AGT score.

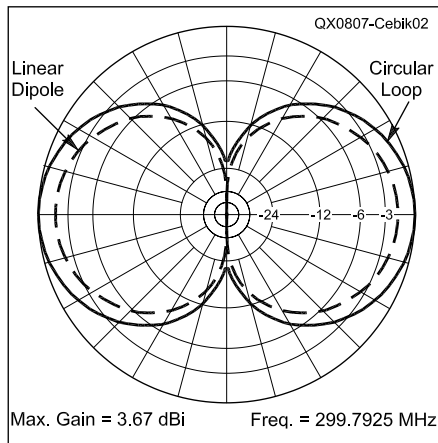


Figure 2 — Comparative free-space E-plane (azimuth) patterns for a linear dipole and a circular 1-λ loop.

$\frac{1}{4} \lambda$. (Actually, the average separation varies over a small range, depending upon the loop shape. Since the current varies along each dipole, a strict geometric averaging of the separation does not quite capture the electrical separation.) Table 1 lists the data collected from all of our sample antennas. Note that the circumference of the phase-fed loop is greater than 1λ . The length increase is largely a function of the mutual coupling between the two dipoles, and therefore requires a longer length for each one to achieve resonance. The ultimate impedance for each feed point is $\frac{1}{2}$ the value shown for a single feed point for the diamond.

While examining the circumference values, we may also see a trend or two. The deltas have similar circumference values, as do the two squares. More generally, as we move from the triangle toward the circle, the required circumference diminishes. The amount is small, but noticeable.

When it comes to performance, the modeling data becomes more complex. Let's jump to the corrected gain and feed

point impedance values. As we reduce the corner angles from 60° to the circle's continuous curve, the feed point impedance climbs a small amount. (The 45-segment circle actually changes by 8° per segment so that the angle between segments is 172° .) The amount is operationally small — about 20Ω overall — but again it is noticeable. For example, a $\frac{1}{4}\lambda$ matching section for a delta might use a 75Ω cable, while a circular loop might use a 93Ω cable.

With respect to bidirectional gain, the $1\text{-}\lambda$ loop has a distinct advantage over a linear dipole, as shown by the comparative E-plane patterns in Figure 2. Within the collection of loops, however, we find only a 0.6 dB difference between the delta and the circle. The circle's gain advantage is small enough that other construction factors are likely to carry more weight in the decision as to which loop shape to use. Squares and diamonds are far more practical in the HF range than circles (or other more complex polygons in the progression). In the UHF range, loops composed of straps hold their shape well with only single-point fastening. This fact simplifies construction. We shall have further comments on the circle's gain later on in these notes.

Next, let's examine the intermediate columns that list the uncorrected NEC reports and the average gain test (AGT) scores. Within NEC — and assuming adherence to the guidelines — the chief measure of model adequacy is the average gain test (AGT), which we have discussed extensively in past columns. Ideally, a free-space lossless model should show an AGT of 1.000 (2.000 for models using a perfect ground). There are no absolute rules for when an AGT score other than 1.000 renders a model inadequate. The more rigorous and systematic a modeling exercise is, the closer to 1.000 that we require the AGT values to validate comparisons among models.

The AGT rests upon performing a full spherical far-field scan for a model in free space (a hemisphere over perfect

ground). Using sufficient and equally spaced (angularly, of course) increments for the sample, the average far-field gain should equal the reference gain so that the ratio is 1.000. As we examine more complex geometries, we should reduce the increment between each sampled point on the sphere to obtain the most accurate average value. (Automated AGT scans offered by some implementations of NEC often use 5° increments, which is normally adequate for linear elements in various arrays. Changing the increment to a lower value, however, is a good check to ascertain the best value to use in a given exercise.) We may often obtain corrected values for raw NEC gain reports by converting the reported AGT value into dB. The conversion consists of taking the log of the reported AGT value and multiplying by 10. A reported AGT score of 1.010 converts to 0.04 dB. Since the AGT score is greater than 1, we subtract the converted value from the reported gain. Hence a raw gain report of 5.00 dBi becomes 4.96 dBi. Reported AGT values below 1.000 result in increases to the raw far-field gain report. An AGT report of 0.960 becomes -0.18 dB. Had the gain report been 5.00 dBi, the corrected gain value would be 5.18 dBi.

We may also correct the resistive component of the reported source impedance using the AGT directly. The correction works best when the impedance is close to resonant, that is, has a relatively low reactive component. (Results with high reactive components appear to be mixed, with some results appearing to coincide with range test results and some appearing to diverge considerably.) To correct the impedance value, simply multiply the AGT score times the resistive component. Assume a reported value of 150Ω . An AGT score of 1.01 would convert this value to 151.5Ω . An AGT value of 0.960 would correct the reported resistance to 144Ω . How significant these corrections are depends upon the terms of the modeling exercise. If I were building an antenna with a target feed point impedance

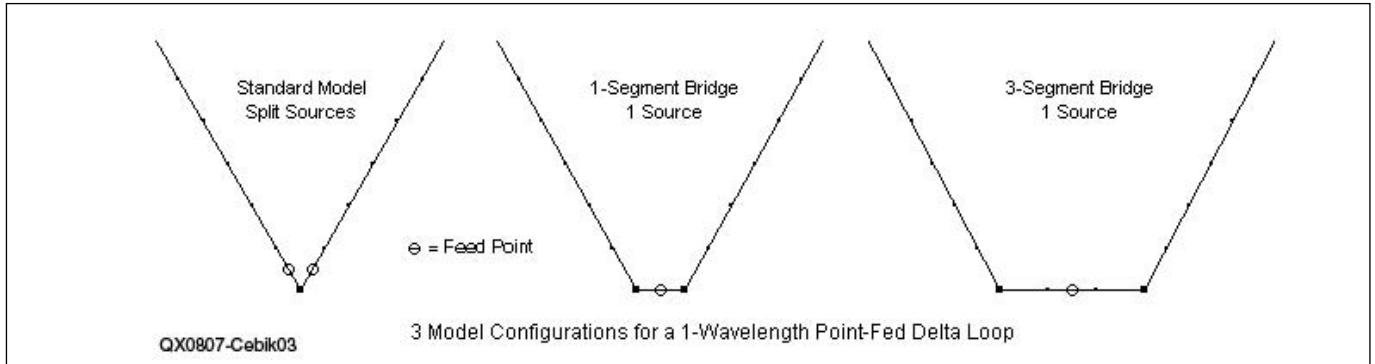


Figure 3 — Outlines of three model configurations for a 1-λ point-fed delta loop.

of 150 Ω, I might expect construction variables to outweigh the range of variation within the example. For a sequence of modeled antenna geometry variations, however, I might wish to use corrected source impedance values in order to obtain a reasonable sequence of values associated with the variations, especially if each variation produces a different AGT value.

The two models fed at points make use of a common work-around for NEC's inability to place a source precisely on a point, that is, on the end of a segment. The split-source technique places a source on the segments adjacent to the point and sums their values. Even using this modeling method, we obtain AGT values that are far from adequate. Therefore, the table uses the AGT score to correct the values. The remaining question is whether the corrections themselves are adequate. To test the technique, I reconstructed the delta loop with its highly angular wire junctions. The angle plays a role in the AGT inadequacy, but not just because the wires meet at 60° angles. The mid-side-fed version of the model shows an excellent AGT value. Rather, the combination of feed point placement and the angular junction together form the basis for the poor AGT score. (As we open the angle, as we do in the point-fed diamond, the AGT improves, but not to a level sufficiently adequate to let us accept the uncorrected results for model comparisons.)

Figure 3 shows the outlines of methods used to overcome the problems just

described. This sequence of models uses 33 segments per side for a uniform segment length of 0.011 λ. The center example uses a single bridge segment on which to place the source. Its length is the same as the segments on the adjacent angular wires. The third example uses a three-segment wire so that the source segment has adjacent segments in the same plane before the junction with the angular delta sides. Table 2 shows the results of the experiment, with a mid-side-fed delta for reference. The single-segment bridge wire is insufficient to correct the AGT score very much, although we see some improvement. The three-segment wire yields an acceptable AGT value, however, within the context of this exercise. The impedance of this quasi-point-fed model coincides most closely with the impedance of the mid-side-fed version. (The gain climbs a small amount due to the slight "squaring" of the delta, but less than a third of the way to the typical gain of a full square.)

The lessons that we learn from the exercise are numerous. First, the impedance of a point-fed and a mid-side-fed loop are very similar for any loop shape. Second, the use of NEC is fraught with limitations, most of which we may detect by paying close attention to the AGT value. Moreover, most entry-level NEC software has automated the process of obtaining an AGT value. In general, gain and impedance corrections based on the AGT value are quite reliable when making fairly fine comparisons among antenna shapes, the core of this exercise.

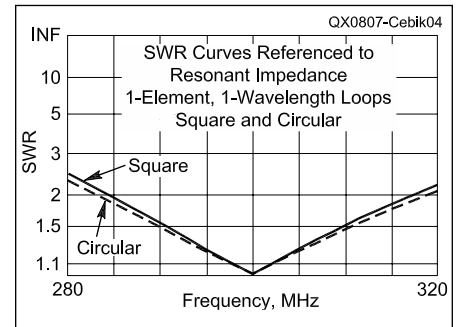


Figure 4 — Comparative SWR curves referenced to the resonant feedpoint impedance values for 1-λ square and circular loops.

Finally, for a large number of cases, we can find work-arounds that will yield more acceptable AGT values.

As significant as our modeling exercise may be, it does not alter our original conclusions about 1 λ loops. As we move from the triangle to the circle, we obtain small additions to the gain, an increase in the feed point impedance, a slight decrease in the overall circumference for a given wire size, and (as shown in Figure 4) a very slight broadening of the SWR curve when taken with respect to the resonant feed point resistance. Nevertheless, the improved performance is — for most antenna-building projects — too small to override structural considerations for the operating frequency.

Table 2
Revised "Point-Fed" Triangles (Deltas)
Models Use 33 Segments Per Side, With All Segments 0.011 λ Long.

Antenna	Circumference (λ)	Gain (dBi)	AGT	Cor. Gain (dBi)	Feed Impedance (Ω)	Cor. Resistance (Ω)
Mid-side fed (reference)	1.1082	3.06	1.002	3.05	121.8 - j0.5	122.0
Point fed	1.1202	2.60	0.901	3.05	141.2 - j0.5	127.2
1-segment bridge wire	1.1192	2.86	0.947	3.10	131.3 + j0.8	124.3
3-segment bridge wire	1.1220	3.19	1.006	3.16	120.7 - j0.1	121.4

Two-Element Driver-Reflector Loop Beams

One wavelength loop elements are a critical component of loop (or quad) beams using any number of elements. Although monoband HF loop beams rarely exceed five elements, UHF beams of this design type may have 40 elements or more. Available space will restrict our investigation to two-element beams using a driven loop and a reflector loop.

We might bring to the investigation any number of questions, but one in particular seems most relevant. In the 1980s, it was popular to make somewhat excessive claims for beam designs. The pre-modeling-era practice seemed to have a justifi-

cation. Long practice had established that certain antenna embellishments might add x -dB to a basic element. Another improvement might add y -dB to the same element. If we combine the two enhancements, then our gain ought to increase by $(x+y)$ dB. Adding a reflector to a 1λ loop adds almost 4 dB to the forward gain. According to the formula, if we change the loop from a delta or a square to a circle, we might gain as much as a half dB in the process. If we also make the reflector a circle, we may add another half dB. Hence, a circular quad beam ought to have at least a full dB gain over a delta or square version of the same beam.

To examine this dose of optimism, I

created a number of driver-reflector loop beams, as shown in Figure 5. The square and diamond models derive from some past optimizing that I did in developing an algorithm set to design such beams to achieve the broadest possible operating bandwidth for the front-to-back ratio and the SWR, since quad beams tend to have narrower beamwidths in these categories of performance than Yagis.² I then extended the technique for this exercise to delta beams with different feed points and to a circular beam. The data for the exercise appears in Table 3. The columns provide the raw reports and the corrected values based on the AGT values. Although we find revised values for the for-

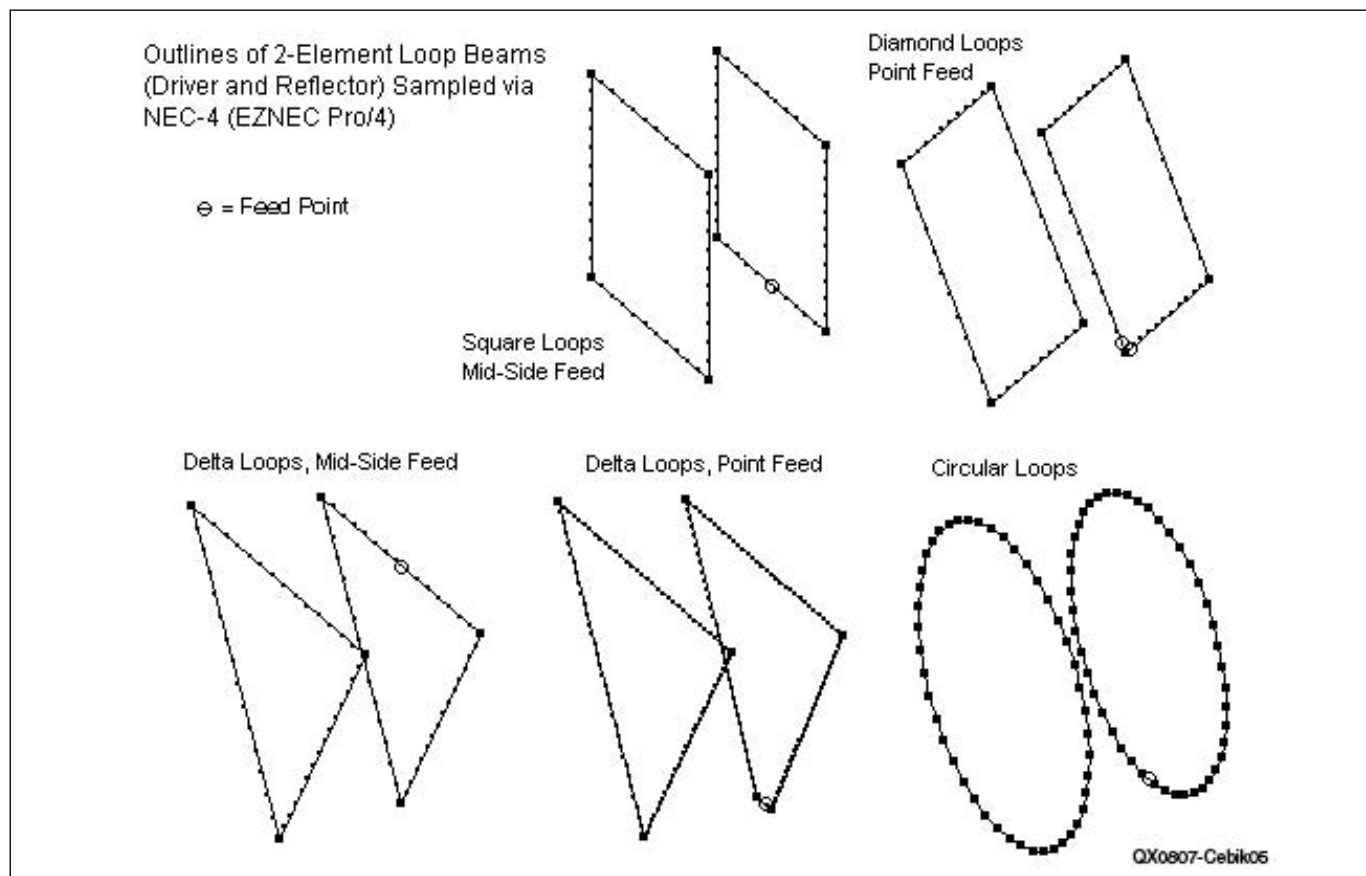


Figure 5 — Outlines of two-element loop beams using drivers and reflectors as sampled via NEC-4 (EZNEC Pro/4).

Table 3

Two-Element Driver-Reflector Loop Beams

NEC-4 Models (EZNEC Pro/4): Free-Space Environment, 0.002-m Zero-Loss Wire, 299.7925 MHz

Antenna	Circumference (λ)	Spacing (λ)	Gain (dBi)	AGT	Cor. Gain (dBi)	Front-Back Ratio (dB)	Feed Impedance (Ω)	Cor. Resistance (Ω)
Square loops	1.023/1.116	0.166	7.16	1.004	7.14	55.32	142.5 - j0.1	143.1
Diamond loops	1.024/1.116	0.166	7.00	0.962	7.17	45.94	151.0 - j0.4	145.3
Delta loops, mid-side fed	1.040/1.134	0.155	6.89	1.003	6.88	32.99	116.7 - j0.4	117.1
Delta loops, bridge point fed	1.053/1.128	0.150	7.05	1.008	7.02	40.89	118.0 + j0.9	118.9
Circular loops	0.990/1.084	0.169	7.36	0.999	7.36	45.59	161.9 + j0.2	161.7

ward gain and the feed point impedance, the front-to-back ratio is not generally susceptible to distortion by virtue of a poor AGT value.

All of the sample beams have 180° front-to-back ratios greater than 30 dB, which suggests that the comparison is likely quite general. Dimensionally, we may notice the same trends that occur with single elements. The more angular the junction between loop wires or sides, the larger the circumference. The circular beam requires the smallest set of element circumference values. In contrast, as the elements become more circular, the required spacing becomes wider.

With respect to performance, the beams show a relatively small range of variation. The deltas show the lowest gain, while the circular beam shows the highest value. The difference is less than a half dB, however. Figure 6 compares the E-plane (azimuth) patterns for the poorest and the best performers in the group, and the difference is too slight for anyone to notice in operation. As we discovered for single-loop antennas, the feed point impedance of two-element loop beams increases as the elements become more circular.

Unfortunately, the optimistic gain calculations that derived from the 1980s prove to have no foundation. In fact, the entire idea of a quagi — a hybrid array consisting of a quad-loop driver and reflector, but with linear directors — rests on there being no significant difference in performance between parasitic linear elements having different shapes. J. Appel-Hansen established this situation in “The Loop Antenna with Director Arrays of Loops and Rods” in July, 1972 (*Transactions of the IEEE on Antennas and Propagation*, p 516). In a parasitic array, the gain improvement of the circular loop accrues only to the driver when compared to delta and square drivers. As well, we obtain the benefit, as small as it is, only if we optimize the beam element spacing to account for the differences in mutual coupling between loop elements having different shapes. Alas, early claims for quagi performance far exceeded reality. The actual benefit of the quagi, in its era, was to provide an approximate 50-Ω feed

point impedance at a time when most Yagi designers used closely spaced reflectors and contended with very low-impedance drivers. Most 21st century VHF and UHF Yagi techniques allow 50 Ω drivers.

The circular loop beam does have one small advantage over its straight-sided counterparts: a slightly broader SWR passband. Figure 7 compares the SWR curves for beams using delta, square, and circular elements when each sweep is adjusted to the resonant impedance of

the beam. The region of greatest improvement, however, occurs in a frequency region in which the beam’s front-to-back ratio is already seriously degraded relative to the design-frequency performance.

Before we close our investigation of two-element loop beams, we likely should look at one more epidemic temptation that confronts quad builders: the search for magic cutting formulas. Casual treatments of quad designs repeat a set of formulas based on a single three-element quad design from the 1980s, and builders use the set of equations in whole or part, depending on how large a beam they are constructing.

Cutting formulas are a good way of generating a very poor loop-based beam. The required circumference and element spacing are functions of the element diameter. Figure 8 graphs the dimensions of two-element square quad beams over a very wide range of element diameters, when we treat the diameters as a fraction of a wavelength. The X-axis increments actually employ a log scale to avoid radical slopes to the curves. The element spacing has been multiplied by 10 for greater visibility. Table 4 provides the data that goes with each coordinate point on the graph. Note that the dimensions shown apply to square quad beams designed to achieve specific goals — namely, broader operating bandwidths for both the SWR and front-to-back performance. Other designs with different goals are certainly possible.

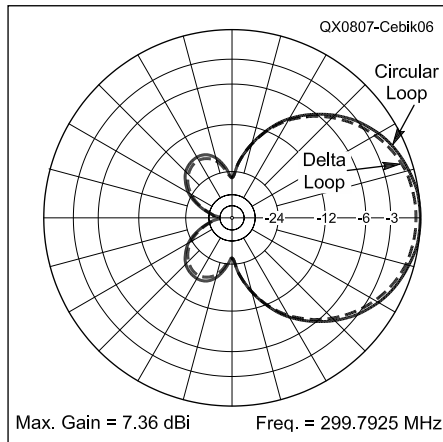


Figure 6 — Comparative free-space E-plane (azimuth) patterns of two-element driver-reflector loop beams with circular and delta loop elements.

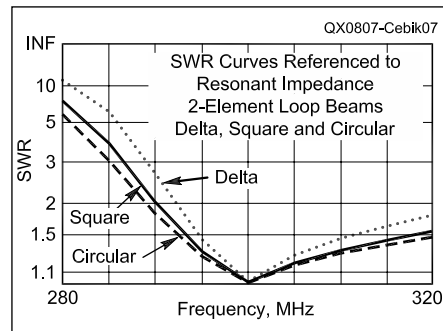


Figure 7 — Comparative SWR curves referenced to the resonant feed point impedance values for two-element driver-reflector loop beams using delta, square and circular elements.

Conclusions

Our exploration of loop elements has touched on the main options for element construction, ranging from triangles to circles. In one direction, we uncovered a number of cautions that we must observe in modeling these shapes in order to assure ourselves that we develop adequate models with reliable output data. Those cautions do not touch upon the pitfalls that we may encounter when building a physical implementation of a loop element. Most square loops, for example, use a non-conductive set of cross braces to support the element at the corners. Introducing any form of conductive ring

**Table 4
Wire Diameter Versus Two-Element Driver-Reflector Quad Beam Dimensions**

Wire Diameter (λ)	\log_{10} of Diameter	Driver Circumference (λ)	Reflector Circumference (λ)	Spacing (λ)
1.0×10^{-5}	-5	1.0077	1.0435	0.1078
3.1623×10^{-5}	-4.5	1.0061	1.0523	0.1421
1.0×10^{-4}	-4	1.0103	1.0653	0.1557
3.1623×10^{-4}	-3.5	1.0149	1.0803	0.1605
1.0×10^{-3}	-3	1.0192	1.0995	0.1635
3.1623×10^{-3}	-2.5	1.0278	1.1302	0.1673
1.0×10^{-2}	-2	1.0501	1.1843	0.1699

Note: Dimensions apply to square loop elements with a mid-side feed point.

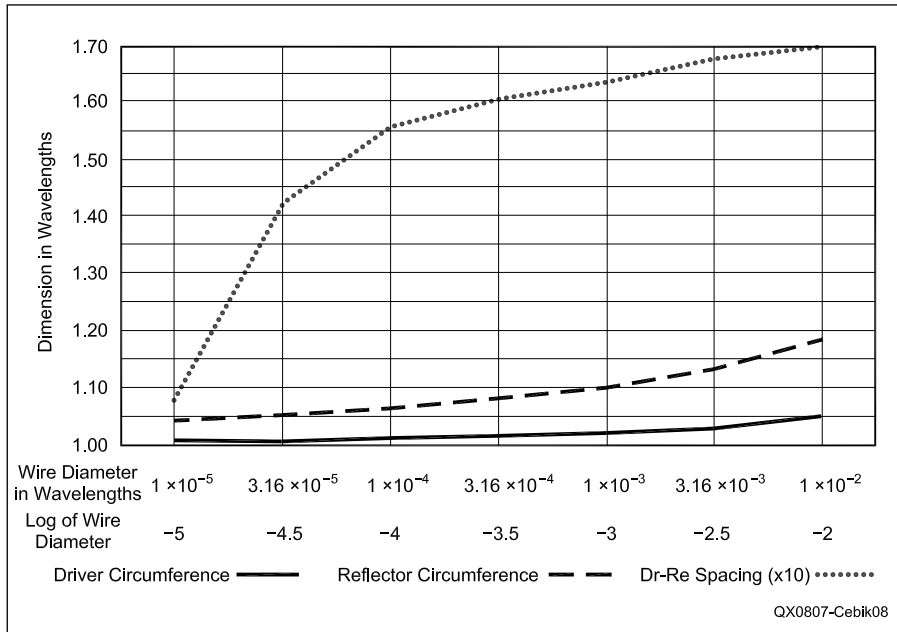


Figure 8 — Dimensions of two-element driver-reflector loop beams as a function of changes in wire size, shown as a function of wavelength. Read the spacing value as $\frac{1}{10}$ the value shown on the X-axis.

clamp — whether or not insulated from the element wire — can detune the element by introducing a one-turn coil at four points around the loop circumference. Such fasteners do not degrade loop performance, but they do alter the loop resonant frequency. We must be prepared to make adjustments relative to models that do not include them.

In the other direction of exploration, we did uncover a progression of gain improvements and feed point impedances increases as we moved from triangles to circles. However real these phenomena, their operational significance is marginal at best and hardly worth notice at worst. In the end, from an operational perspective, deciding among the options for loop construction hinges more on structural considerations than on performance differences.

Notes

¹Models for the antennas discussed in these notes are available for download in EZNEC format at the ARRL Web site. Go to www.arrl.org/qxfiles and look for the file **07x08_AO.zip**.

²The spreadsheet (called ant-design) is available in both *Excel* and *Quattro Pro* formats at the ARRL web site. The files are included in the zip file listed in Note 1.

QEX

Down East Microwave Inc.

We are your #1 source for 50MHz to 10GHz components, kits and assemblies for all your amateur radio and Satellite projects.

Transverters & Down Converters, Linear power amplifiers, Low Noise preamps, coaxial components, hybrid power modules, relays, GaAsFET, PHEMT's, & FET's, MMIC's, mixers, chip components, and other hard to find items for small signal and low noise applications.

We can interface our transverters with most radios.

Please call, write or see our web site www.downeastmicrowave.com for our Catalog, detailed Product descriptions and interfacing details.

Down East Microwave Inc.
19519 78th Terrace
Live Oak, FL 32060 USA
Tel. (386) 364-5529

1010 Jorie Blvd. #332
Oak Brook, IL 60523
1-800-985-8463
www.atomictime.com

ATOMIC TIME



ADWA101 - \$49.95

14" LaCrosse Black Wall WT-3143A \$21.45
This wall clock is great for an office, school, or home. It has a professional look, along with professional reliability. Features easy time zone buttons, just set the zone and go! Runs on 1 AA battery and has a safe plastic lens.

Digital Chronograph Watch ADWA101 \$49.95
Our feature packed Chrono-Alarm watch is now available for under \$50! It has date and time alarms, stopwatch backlight, UTC time, and much more!



WS-8248 - \$49.95

LaCrosse Digital Alarm WS-8248U-A \$49.95
This deluxe wall/desk clock features 4" tall easy to read digits. It also shows temperature, humidity, moon phase, month, day, and date. Also included is a remote thermometer for reading the outside temperature on the main unit. approx. 12" x 12" x 1.5"

1-800-985-8463
www.atomictime.com
Quantity discounts available!



WT-3143A - \$21.45



WT-5720U - \$24.95

LaCrosse WT-5720UU Clock \$24.95
This digital projection clock is great for travel and fits in a small space. Shows 12 or 24 hour time, time zone, and alarm time. Size 5.25" x 1.25" x 4"

Tell time by the U.S. Atomic Clock - The official U.S. time that governs ship movements, radio stations, space flights, and warplanes. With small radio receivers hidden inside our timepieces, they automatically synchronize to the U.S. Atomic Clock (which measures each second of time as 9,192,631,770 vibrations of a cesium 133 atom in a vacuum) and give time which is accurate to approx. 1 second every million years. Our timepieces even account automatically for daylight saving time, leap years, and leap seconds. \$7.95 Shipping & Handling via UPS. (Rush available at additional cost) Call M-F 9-5 CST for our free catalog.

Letters to the Editor

A Software Controlled Radio Preselector (May/June 2008)

Dear Readers,

I sincerely apologize to Juan Jose de Onate, MØVWA, and to all of you for typing Juan's call sign incorrectly for the cover text and also for the "About the Cover" description at the top of the Table of Contents page.

— 73, Larry Wolfgang, WR1B, QEX Editor;
lwolfgang@arrl.org

A High-Efficiency Filament Regulator For Power Tubes (Nov/Dec 2006)

Dear Larry,

In response to a number of inquiries, the following additional notes are offered here to clarify the operation of the circuitry contained in my previous article "A High-Efficiency Filament Regulator For Power

Tubes" (Nov/Dec 2006 QEX). The "output" stage in that circuit is very unorthodox in operation despite its simplicity, and the following details will explain how it actually works. [The original schematic diagram from this article is reprinted here as Figure 1 — Ed.]

A key feature of this design is the use of very low R_{ds} N-channel devices, with on resistances of 5 mΩ or less. This is necessary in order to avoid the use of heat sinks below about 20 A, and very small heat sinks above that. Conventional circuits, which will switch an ac waveform using only N-channel MOSFETs are considerably more complex than this one, which is why it was conjured up for this application.

To understand its operation, first visualize that the circuit is running in steady state, with a typical PWM duty cycle of 50-80% being applied to the input of U2 on each half-cycle (symmetrically). The bootstrapping capacitor C5 will be charged up to very nearly the peak value of the ac voltage.

Also, initially consider that Q1 is a "short" on the negative half-cycle and Q2 is likewise a short on the positive half-cycle due to the action of the internal body diodes. (This is shown clearly on any MOSFET data sheet.) This then allows the phototransistor in U2 to apply this voltage across C5 to both gates while their sources are, at the beginning of the cycles, at ground. Both transistors turn ON and current flows into the load. As the load voltage rises with the ac voltage, the bottom side of C5 rises simultaneously, which maintains the full gate-source voltage to hold them in heavy saturation (required for low loss). C5 charges on the negative half-cycle with D4 providing a current path for the charging current, most of which happens near the negative peak of the supply and load voltage. The large size of C5 holds the gate supply voltage constant during the succeeding positive half cycle, during which it discharges only minutely through R9.

There is one seemingly apparent problem with this circuit, however. Despite the above explanation, which is valid during

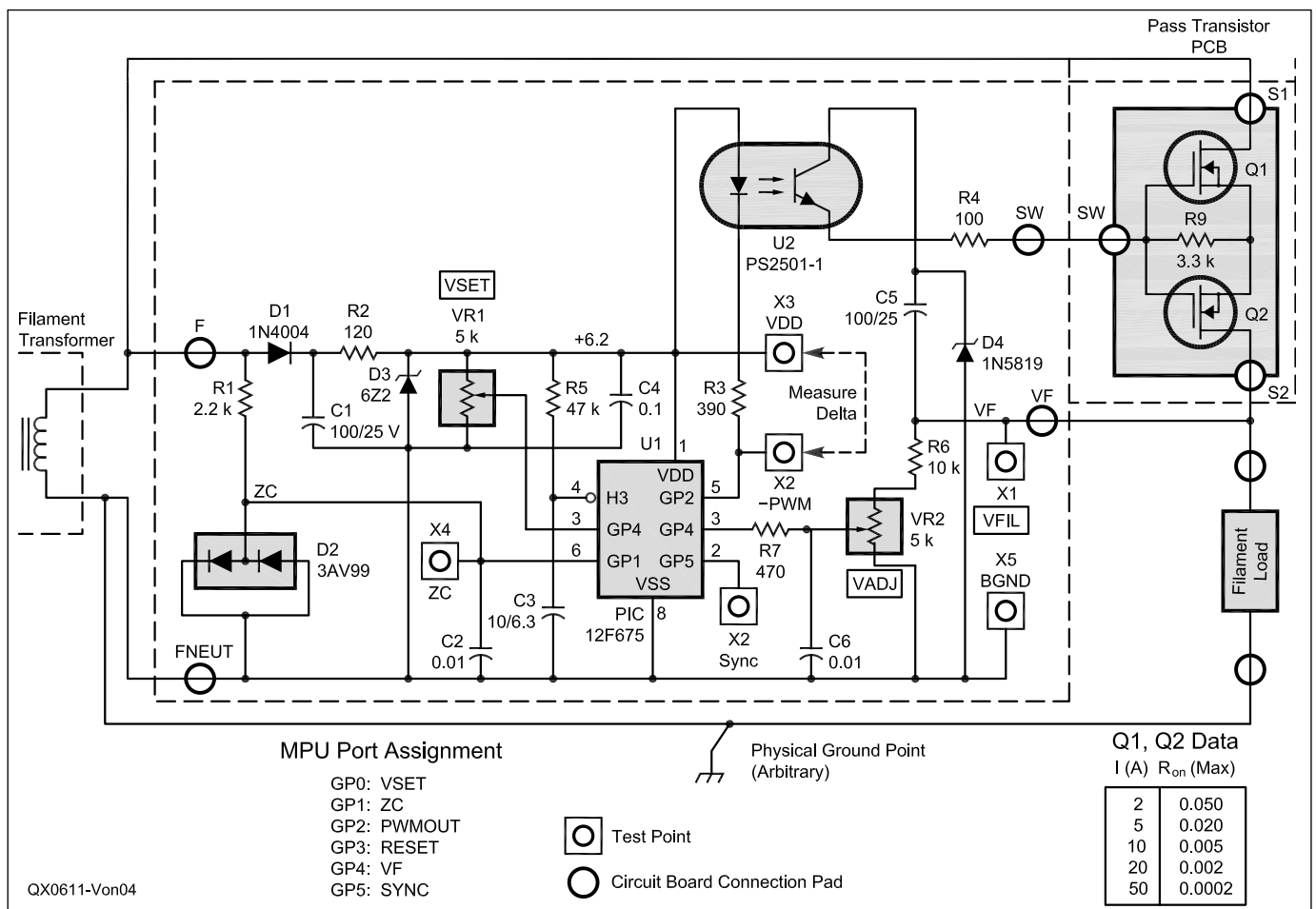


Figure 1 — This schematic diagram appeared with the original article by K8LV in the Nov/Dec 2006 issue of QEX. We have reproduced it here for the convenience of our readers.

steady state, there is no obvious mechanism to start it up — in other words, how does C5 initially obtain enough charge to start Q1 and Q2 conducting, after which the bootstrapping action will maintain C5?

To understand the “startup,” note that the common-source node of Q1 and Q2 effectively follows the ac line S1 during the negative cycle. It will begin to swing negative and current will flow up from ground through D4, U2, and R4, causing a positive voltage drop across R9. As soon as this voltage reaches the ON threshold of Q2 (~2 V) current starts to flow in the load and S2, the actual output terminal, starts its negative swing. Since the top side of C5 is clamped at 0.3 V below ground by D4, the capacitor will start to charge as its bottom end follows the output voltage in its negative swing. It will quickly charge up to a value equal to the peak of the ac line minus the 0.3 V drop due to D4. It is large enough to hold almost all of its charge during the positive cycle and provide turn-on gate voltage for Q1.

The primary limitation of this circuit is that C5 cannot be allowed to charge up to higher than 20 to 30 V because this is the gate voltage limitation of typical MOSFETs. This limits the circuit to use with ac supply voltages of less than about 20 V RMS. That is adequate for the most popular transmitting tubes. At very low voltages (<6 V peak) the bootstrapped voltage across C5 may become too low to fully saturate Q1 and Q2 and power dissipation will increase. Both of these factors must be properly considered for a given project.

— 73, Eric von Valtier, K8LV, 6793 Big Trail, Holly, MI 48472; k8lv@comcast.net

Hi Eric,

Thanks for sending the detailed explanation of the start-up conditions for your circuit. I hope the explanation helps our readers understand how the circuit works.

— 73, Larry, WR1B; lwolfgang@ar1.org

A Low-Cost Atomic Frequency Standard (Nov/Dec 2007)

Dear Larry,

Inspired by the article “A Low-Cost Atomic Frequency Standard” in the Nov/Dec 2007 issue of QEX, I decided to build my own Rubidium Oscillator.

I have included some pictures so you can see what I have done. I made the measurements at the institute “Physikalisch-Technische Bundesanstalt (PTB)” in Braunschweig, where the official German time is “created.” The accuracy of the frequency standard they use in their laboratory is better than 1×10^{-14} . As you can see, my Rubidium Frequency Standard is about 3.5×10^{-11} .

The cabinet is $20 \times 25 \times 8$ cm (about $8 \times 10 \times 3$ inches). It also has connectors for an external 24 V dc power supply. Total cost of



Photo A — DJ7GP built this version of John Raydo’s rubidium atomic frequency standard.

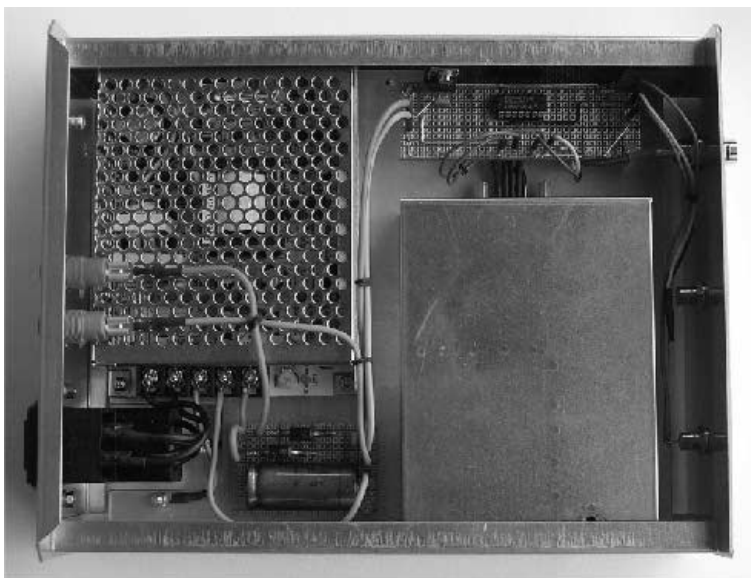


Photo B — This view shows the inside of DJ7GP’s rubidium oscillator from the top. The rubidium oscillator is in the box at the bottom right. There is a 5-V regulator board at the top right.



Photo C — This view shows the inside of DJ7GP’s rubidium oscillator from the rear panel.

my Rubidium Oscillator was less than 300 € (\$430).

I am now building a GPS Disciplined Frequency Standard based on a "ThunderBolt GPS Disciplined Clock" from Trimble Navigation Ltd.

Thanks to John S. Raydo, KØIZ, and thanks to you all for the always very interesting QEX!

— 73, Peter-J. Goedecke, DJ7GP; peter.goedecke@gmx.de

Dear Peter,

Thank you for finding me at the Dayton Hamvention! I enjoyed meeting you and talking with you about your rubidium oscillator project. Your project looks beautiful, and the graphs of your measurements are interesting. Congratulations on your project.

— 73, Larry, WR1B; lwolfgang@arrl.org

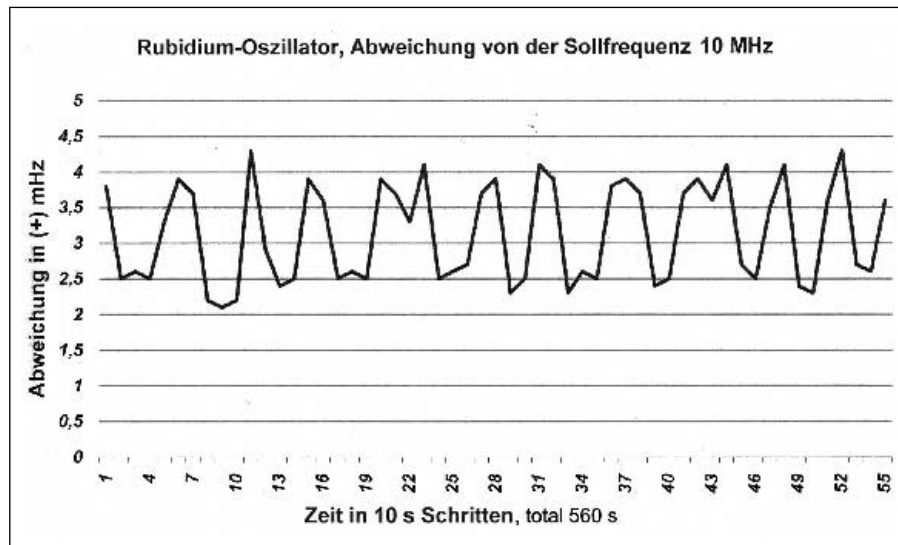


Photo D — This graph shows the oscillator output. The vertical axis represents frequency variations in millihertz and the horizontal axis represents time in 10 second increments.

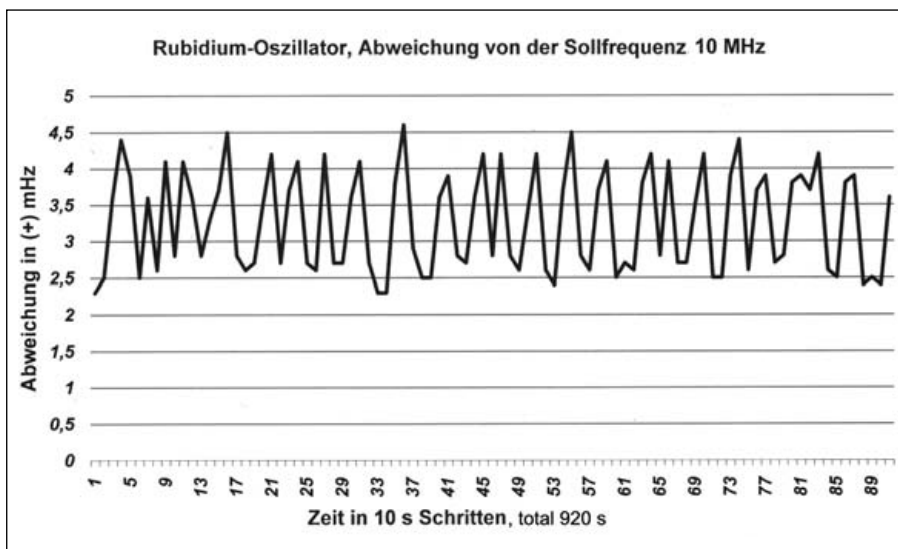


Photo E — This graph represents a second, longer, measurement that DJ7GP made on his rubidium oscillator.

from **MILLIWATTS to KILOWATTS™**
More Watts per Dollar

Quality Transmitting & Audio Tubes

- COMMUNICATIONS
- BROADCAST
- INDUSTRY
- AMATEUR

Immediate Shipment from Stock

3CPX800A7	3CX15000A7	4CX5000A	813
3CPX5000A7	3CX20000A7	4CX7500A	833A
3CW20000A7	4CX250B	4CX10000A	833C
3CX100A5	4CX250BC	4CX10000D	845
3CX400A7	4CX250BT	4CX15000A	866-SS
3CX400U7	4CX250FG	4X150A	872A-SS
3CX800A7	4CX250R	YC-130	5867A
3CX1200A7	4CX350A	YU-106	5868
3CX1200D7	4CX350F	YU-108	6146B
3CX1200Z7	4CX400A	YU-148	7092
3CX1500A7	4CX800A	YU-157	3-500ZG
3CX2500A3	4CX1000A	572B	4-400A
3CX2500F3	4CX1500A	807	M328/TH328
3CX3000A7	4CX1500B	810	M338/TH338
3CX6000A7	4CX3000A	811A	M347/TH347
3CX10000A7	4CX3500A	812A	M382

— TOO MANY TO LIST ALL —

VISA **MasterCard** **Discover**

ORDERS ONLY:
800-RF-PARTS • 800-737-2787
Se Habla Español • We Export

TECH HELP / ORDER / INFO: 760-744-0700
FAX: 760-744-1943 or 888-744-1943

An Address to Remember:
www.rfparts.com

E-mail:
rfp@rfparts.com

RF PARTS™ COMPANY
Since 1967

All the information you need to design your own complete antenna system.

The ARRL

The ARRL
ANTENNA BOOK

21st Edition

ANTENNA BOOK



21st Edition

ARRL Order No. 9876

Only **\$44.95***

*shipping \$10 US/\$15.00 International

The *ultimate* reference for Amateur Radio antennas, transmission lines and propagation



Fully searchable
CD-ROM included!



ARRL The national association for
AMATEUR RADIO

SHOP DIRECT or call for a dealer near you.
ONLINE WWW.ARRL.ORG/SHOP
ORDER TOLL-FREE 888/277-5289 (US)

QEX 7/2008

Upcoming Conferences

ARRL/TAPR Digital Communications Conference

September 26-28, 2008
Chicago, IL

Technical papers are solicited for presentation at the ARRL and TAPR Digital Communications Conference for publication in the Conference Proceedings. Annual conference proceedings are published by the ARRL. Presentation at the conference is not required for publication.

The ARRL and TAPR Digital Communications Conference is an international forum for radio amateurs to meet, publish their work, and present new ideas and techniques. Presenters and attendees will have the opportunity to exchange ideas and learn about recent hardware and software advances, theories, experimental results, and practical applications. Topics include, but are not limited to:

- Software defined radio (SDR)
- Digital voice (D-Star, P25, WinDRM, FDM DV, DRMDV, G4GUO)
- Digital satellite communications
- Global position system
- Precise Timing
- Automatic Position Reporting System (APRS)
- Short messaging (a mode of APRS)
- Digital Signal Processing (DSP)
- HF digital modes
- Internet interoperability with Amateur Radio networks
- Spread spectrum
- IEEE 802.11 and other Part 15 license-exempt systems adaptable for Amateur Radio
- Using TCP/IP networking over Amateur Radio
- Mesh and peer to peer wireless networking
- Emergency and Homeland Defense backup digital communications in Amateur Radio
- Updates on AX.25 and other wireless networking protocols
- Topics that advanced the amateur radio art

Submission of papers are due by July 31st, 2008 and should be submitted to:

Maty Weinberg, ARRL, 225 Main Street, Newington, CT 06111 or via the Internet to maty@arri.org.

For further details about submitting papers, and for Conference registration information, see the TAPR Web page at www.TAPR.org/dcc.htm.

Microwave Update 2008

October 17-18, 2008
Bloomington, MN

Call for Papers

Microwave Update 2008 will be held on Friday, October 17 through Saturday, October 18 in Bloomington, Minnesota. Technical papers are currently being solicited for publication in the ARRL's *Microwave Update 2008 Conference Proceedings*. You do not need to attend the conference nor present your paper to have it published. Strong preference will be given to original work and to those papers that are written and formatted specifically for publication rather than as a presentation visual aid.

This is a microwave conference, so papers must be on topics for frequencies above 900 MHz. Examples of such topics include microwave theory, construction, communication, deployment, propagation, antennas, activity, transmitters, receivers, components, amplifiers, communication modes, LASER, software design tools, and practical experiences. Authors retain the basic copyright, and by submission, consent to publication in the *Proceedings* and possible publication of the *Proceedings* in CD/DVD format. If you are interested in submitting a paper please contact Jon Platt, W0ZQ, at w0zq@aol.com for additional information. The deadline for papers is Sunday, August 31, 2008. If you are interested in presenting at Microwave Update please contact Barry Malowanchuk, VE4MA, at ve4ma@shaw.ca.

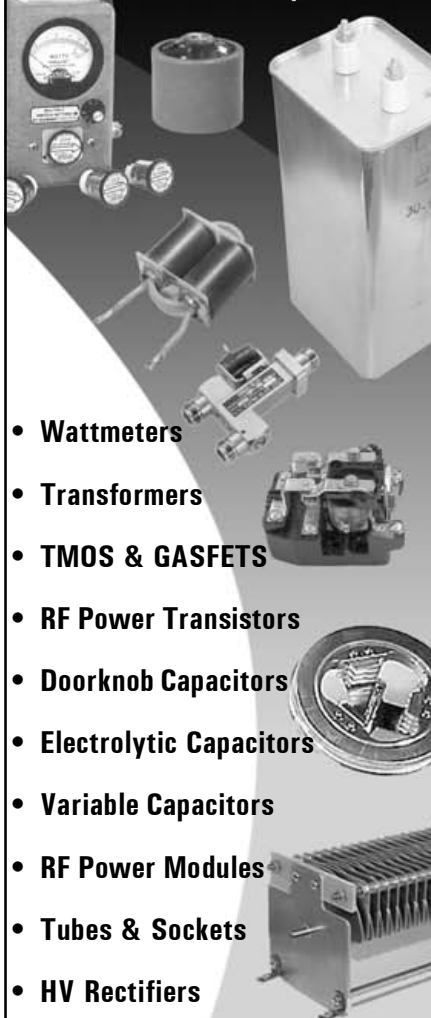


In the Next Issue of QEX

Bertrand Zauhar, VE2ZAZ, presents The Rechargeable Battery Cycler. This project will periodically discharge and recharge a battery pack for hand-held or other radios. It is much more than a battery charger, though! It supports two battery packs with distinct configurations for each pack. It will work with NiCd or Ni-MH batteries, with cells of capacity between 500 mAh and 5000 mAh and from one to ten cells per battery pack.

If all that isn't enough to catch your interest, Bertrand has also added *Windows* configuration software to set up the controller. The software can also collect battery data during the charge/discharge cycle and plot a graph of voltage versus time. If you use batteries in your Amateur Radio operation, you won't want to miss this one!

From
MILLIWATTS
to **KILOWATTS**
More Watts per Dollar



- **Wattmeters**
- **Transformers**
- **TMOS & GASFETS**
- **RF Power Transistors**
- **Doorknob Capacitors**
- **Electrolytic Capacitors**
- **Variable Capacitors**
- **RF Power Modules**
- **Tubes & Sockets**
- **HV Rectifiers**



ORDERS ONLY:

800-RF-PARTS • 800-737-2787

Se Habla Español • We Export

TECH HELP / ORDER / INFO: 760-744-0700

FAX: 760-744-1943 or 888-744-1943



An Address to Remember:
www.rfparts.com

E-mail:
rfp@rfparts.com



RF PARTS
COMPANY



ARRL PUBLICATIONS

SHOP DIRECT or call for a dealer near you.

ONLINE WWW.ARRL.ORG ORDER TOLL-FREE 888/277-5289 (US)



License Study Materials

Technician Class

Exam: 35-question Technician test (Element 2)

The ARRL Ham Radio License Manual. All you need to become an Amateur Radio Operator. For Technician exam study.
Order No. 9639 **\$24.95**



The ARRL Ham Radio License Course. Register at www.arrl.org/cep and complete all of your ham radio license training online. Registration includes *The ARRL Ham Radio License Manual*, a one year ARRL membership, and graduate support. **Book with online course \$69 100% Guaranteed!**

ARRL's Tech Q & A. 4th Edition. Review questions and answers from the entire Technician question pool. Includes brief, clear explanations for all the questions. Order No. 9647 **\$17.95**

Ham University. Quiz yourself using this feature-packed easy-to-use software. **Technician/General Edition**, Order No. 8956 .. **\$24.95**

HamTestOnline™. Web-based training for all three written exams. Order No. 9571 **\$49.95**

Ham Radio for Dummies. Order No. 9392 **\$21.99**

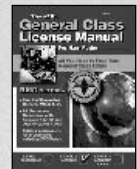
The ARRL Instructor's Manual for Technician and General License Courses. 4th Edition. Order No. 1263 **\$19.95**

General Class (upgrade from Technician)

Exam: 35-question General test (Element 3)

ARRL General Class License Manual—6th Edition
Order No. 9965 **\$24.95**

ARRL's General Q & A—3rd Edition
Order No. 9957 **\$17.95**



Extra Class (upgrade from General)

Exam: 50-question Extra test (Element 4)

ARRL Extra Class License Manual—9th Edition
All you need to pass your Extra Class Exam! All the exam questions with answer key, for use July 1, 2008 to June 30, 2012. Order No. 1352 **\$24.95**



NEW!

ARRL's Extra Q & A—2nd Edition
Includes the latest question pool and brief, clear explanations for all questions. Order No. 1379 **\$17.95**

NEW!

Ham University. Quiz yourself using this feature-packed easy-to-use software. **Complete Edition (Tech, Gen, Extra, and Morse code)**. Order No. 8735 **\$39.95**

Operating and Reference

The ARRL Operating Manual. 9th Edition.
Order No. 1093 **\$29.95**

ARRL Repeater Directory®—2008/2009 Edition. The authoritative source of VHF/UHF repeater listings. Over 20,000 listings!

- Pocket-sized** (3.75" x 5.25"), Order No. 1271 **\$10.95**
- Desktop Edition** (6" x 9"), Order No. 1298 **\$15.95**

TravelPlus for Repeaters™—2008-2009 Edition. It's like having the power of *The ARRL Repeater Directory* on your COMPUTER! CD-ROM, version 12.0. Order No. 1301 **\$39.95**

The ARRL DXCC List (February 2008 ed.) Order No. 1212 .. **\$5.95**

ARES Field Resources Manual. Order No. 5439 **\$12.95**

The ARRL Emergency Communication Handbook.
Order No. 9388 **\$19.95**

The ARRL DXCC Handbook. Order No. 9884 **\$19.95**

DXing on the Edge—The Thrill of 160 Meters. Book with audio CD! Order No. 6354 **\$19.95** ~~\$29.95~~

RF Exposure and You. Order No. 6621 **\$22.95**

Hints & Kinks. 17th Edition. Order No. 9361 **\$17.95**

Low Profile Amateur Radio. 2nd Edition. Order No. 9744 **\$19.95**

FCC Rules and Regulations for the Amateur Radio Service
Order No. 1173 **\$5.95**

Getting Started with Ham Radio. A guide to your FIRST Amateur Radio station. Order No. 9728 **\$19.95**

The ARRL Software Library for Hams. Quick access to utilities, applications and information.
CD-ROM, version 2.0, Order No. 9825 **\$19.95**

Ham Radio FAQ. Order No. 8268 **\$9.95** ~~\$14.95~~

Amateur Radio on the Move. Order No. 9450 **\$19.95**

ARRL's Vintage Radio. Order No. 9183 **\$19.95**

Your Introduction to Morse Code. Learn code at 5 words-per-minute. Order No. 8314 **\$9.95** ~~\$14.95~~

The Radio Amateur's World Atlas.
Order No. 5226 **\$12.95**

ARRL Map of North America. 27 x 39 inches. Includes grids!
Order No. 8977 **\$15**

ARRL Map of the World (Azimuthal). 27 x 39 inches.
Order No. 7717 **\$15**

ARRL Map of the World (Robinson). 26 x 34.5 inches.
Order No. 8804 **\$15**

ARRL Worked All States (WAS) Map. 11 x 17 inches.
ARRL Frequency Chart on reverse side. Order No. 1126 **\$3**

MAPS

CD-ROM Collections

QST on CD-ROM!

ARRL Periodicals CD-ROM is a compilation of all *QST*, *QEX* and *NCJ* issues on one CD. **\$19.95 per set.**

- | | |
|--------------------------------------|--------------------------------------|
| 2007 Edition , Order No. 1204 | 2002 Edition , Order No. 8802 |
| 2006 Edition , Order No. 9841 | 2001 Edition , Order No. 8632 |
| 2005 Edition , Order No. 9574 | 2000 Edition , Order No. 8209 |
| 2004 Edition , Order No. 9396 | 1999 Edition , Order No. 7881 |
| 2003 Edition , Order No. 9124 | 1998 Edition , Order No. 7377 |

1997 Edition, Order No. 6729 **1995 Edition**, Order No. 5579
1996 Edition, Order No. 6109

Radio Amateur Callbook CD-ROM. Thousands of worldwide call sign listings. Requires Microsoft *Windows* or MS-DOS. Summer 2008 Edition. Order No. 1129 **\$49.95**

NEW!

HamCall™ CD-ROM. Thousands of worldwide call sign listings.
Order No. 8991 **\$49.95**

Antennas and Transmission Lines

The ARRL Antenna Book—21st Edition

The ultimate reference for Amateur Radio antennas, transmission lines and propagation. Fully-searchable CD-ROM included (for Windows and Macintosh). Softcover, Order No. 9876 **\$44.95**

International Antenna Collection. Fixed and mobile antenna designs from 136 kHz to 1.3 GHz.

Volume 1, Order No. 9156 **\$19.95**
Volume 2, Order No. 9465 **\$21.95**

Antenna Zoning. Order No. 8217 **\$40 Web Special**..... **\$49.95**

ON4UN's Low-Band DXing. Antennas, equipment and techniques for DXcitement on 160, 80 and 40 meters. Fourth ed. with CD-ROM. Order No. 9140 **\$39.95**

ARRL's Yagi Antenna classics. Order No. 8187 **\$17.95**

Simple and Fun Antennas for Hams. Order No. 8624 **\$22.95**

ARRL's Wire Antenna Classics. Order No. 7075 **\$14**

More Wire Antenna Classics—Volume 2. Order No. 7709 **\$17.95**

More Vertical Antenna Classics. Order No. 9795 **\$17.95**

Vertical Antenna Classics. Order No. 5218 **\$12**

ARRL's VHF/UHF Antenna Classics. Build your own portable, mobile and fixed antenna designs. Order No. 9078 **\$14.95**

ARRL Antenna Compendium series—Practical antenna designs, and other articles covering a wide range of antenna-related topics.

Volume 7. Order No. 8608 **\$24.95** **Volume 4.** Order No. 4912 **\$20**

Volume 6. Order No. 7431 **\$22.95** **Volume 3.** Order No. 4017 **\$14**

Volume 5. Order No. 5625 **\$20** **Volume 2.** Order No. 2545 **\$14**

Volume 1. Order No. 0194 **\$20**

Practical Circuits and Design



The ARRL Handbook—2008

The Standard in applied electronics and communications.

Operating activities, electronics and communications concepts, radio propagation and antenna theory, practical projects, repair techniques, references and more. Includes **The ARRL Handbook CD**—the complete and fully searchable book on CD-ROM (version 12.0).

Softcover, Order No. 1018 **\$44.95**

Basic Radio—Understanding the Key Building Blocks. An introduction to radio for everyone. Includes build-it-yourself projects. Order No. 9558 **\$29.95**

Understanding Basic Electronics. Order No. 3983 **\$29.95**

Digital Signal Processing Technology.

Order No. 8195 ~~\$34.95~~ **\$44.95**

ARRL's Hands-On Radio Experiments. Basic electronics instruction from the pages of *QST*. Order No. 1255 **\$19.95**

NEW! **Hands-On Radio Parts Kit.** Order No. 1255K **\$79.95**

The ARRL RFI Book. 2nd Edition. Practical cures for radio frequency interference. Order No. 9892 **\$29.95**

Experimental Methods in RF Design. CD-ROM included.

Order No. 8799 **\$49.95**

L/C/F and Single-Layer Coil Winding Calculator. A slide rule for the experimenter. Order No. 9123 **\$12.95**

Introduction to Radio Frequency Design.

Order No. 4920 **\$39.95**

ARRL's RF Amplifier Classics. Find practical designs and construction details for classic tube and solid-state amplifiers at power levels from 5 W to 1.5 kW. Order No. 9310 **\$19.95**

Emergency Power for Radio Communications. Plan alternative means for electric power generation. Order No. 9531 **\$19.95**

More QRP Power. More equipment, accessories and antennas for low power radio operating! Order No. 9655 **\$19.95**

W1FB's QRP Notebook. Order No. 3657 **\$10**

ARRL's Low Power Communication. 3rd edition. Build and operate low-power radio gear—the QRP way!

Book. Order No. 1042 **\$19.95**

Book with Cub CW Transceiver Kit. Order No. 1042K **\$99.95**

Digital and Image Communications

ARRL's VHF Digital Handbook. 1st Edition. Dive into the digital radio universe! Order No. 1220 **\$19.95**

ARRL's HF Digital Handbook. 4th Edition. Use your computer to talk to the world! Order No. 1034 **\$19.95**

VoIP: Internet Linking for Radio Amateurs.

Order No. 9264 **\$17.95**

GPS and Amateur Radio. Order No. 9922 **\$18.95**

The ARRL Image Communications Handbook. See and talk with other hams! CD-ROM included with software utilities.

Order No. 8616 ~~\$19.95~~ **\$25.95**

Space and VHF/UHF/Microwave Communications

The Radio Amateur's Satellite Handbook.

Order No. 6583 **\$24.95**

The ARRL Satellite Anthology—5th Edition. Includes specific satellite operating details. Order No. 7369 **\$15**

The ARRL UHF/Microwave Projects CD. CD-ROM includes Volumes 1 and 2 of *The ARRL UHF/Microwave Projects Manuals*.

Order No. 8853 **\$24.95**

Shipping and Handling Information

In the US, add the following amounts to your order to cover shipping and handling (S/H). Add an additional \$5.00 to the US rate for shipment outside the US. US orders will be handled via ground delivery service. International Air and other specialty forwarding methods are available. Please call or write for information. Sales Tax is required for shipments to CT 6% (including S/H), VA 5% (excluding S/H), CA (add applicable tax, excluding S/H), Canadian Provinces NS, NB and NF add 14% HST, all other Provinces add 6% GST (excluding shipping/handling).

Amount of Order	Add	Amount of Order	Add
\$10.00 or less	\$6.00	40.01 - 50.00	10.00
10.01 - 20.00	7.00	50.01 - 75.00	11.00
20.01 - 30.00	8.00	Over \$75.00	12.00
30.01 - 40.00	9.00	CD-ROM only	6.00



We accept the following major credit cards: American Express, MasterCard, Visa and Discover. Prices and product availability are subject to change without notice.

If you'd like a complete publications listing or would like to place an order, please contact us:

- To order or obtain the address of an ARRL Dealer near you, call toll-free (US): 1-888-277-5289 (non-US call 860-594-0355) 8 AM-5 PM Eastern time, Monday-Friday.
- Fax 1-860-594-0303 24 hours a day, 7 days a week.
- By mail to: ARRL, 225 Main St, Newington CT 06111-1494
- Visit our World Wide Web site: <http://www.arrl.org/shop>

Join or Renew!



Public Service



Advocacy



Education



Technology

Benefits that keep you
On The Air.



Membership

www.arrl.org

Membership Application

Name _____ Call Sign _____

Street _____

City _____ State _____ ZIP _____

E-mail _____

Sign up my family members, residing at the same address, as ARRL members too! They'll each pay only \$8 for a year's membership, have access to ARRL benefits and services (except QST) and also receive a membership card.

Family Member Name _____ Call Sign (if any) _____

Sign up _____ family members @ \$8 each = \$ _____.

Total amount enclosed, payable to ARRL \$ _____.

Enclosed is \$ _____ (\$1.00 minimum) as a donation to the Legal Research and Resource Fund.

Charge to: VISA MasterCard Amex Discover

Card Number _____ Expiration Date _____

Cardholder's Signature _____

If you do not want your name and address made available for non-ARRL related mailings, please check here.

Please check the appropriate one-year¹ rate:

- \$39 in US.
- Age 65 or older rate, \$36 in US*.
- Age 21 or younger rate, \$20 in US (see note**).
- Canada \$49.
- Elsewhere \$62.

*Please indicate date of birth _____.

(US funds drawn on a bank in the US).

¹ 1-year membership dues include \$15 for a 1-year subscription to QST. International 1-year rates include a \$10 surcharge for surface delivery to Canada and a \$23 surcharge for air delivery to other countries.

Other US membership options available: Blind, Life, and QST by First Class postage. Contact ARRL for details.

**Age 21 or younger rate applies only if you are the oldest licensed amateur in your household.

International membership is available with an annual CD-ROM option (no monthly receipt of QST). Contact ARRL for details. Dues subject to change without notice.

Call Toll-Free (US)
1-888-277-5289

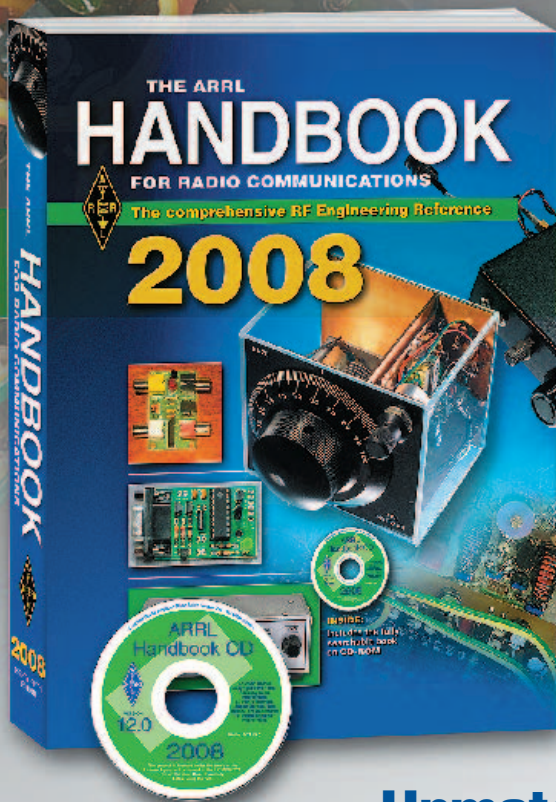
Join Online
www.arrl.org/join
or Clip and send to:



ARRL The national association for
AMATEUR RADIO

225 Main Street
Newington, CT 06111-1494 USA

QEX 7/2008



The ARRL Handbook —2008 Edition

- **The ARRL Handbook**—2008 edition. Up-to-date and always revised!
- **The ARRL Handbook on CD-ROM**—version 12.0 included with every book.

Unmatched Excellence

This 85th edition is both a useful introduction to radio communication and a source for answers to questions about every aspect of the state-of-the-art. Topics include Amateur Radio licensing requirements and operating activities, fundamental and advanced electronics and communications concepts, radio propagation and antenna theory, practical projects, repair techniques, references and much more. **The Handbook** includes descriptions for new and emerging wireless technologies involving digital signal processing (DSP) innovations, and radio applications utilizing software and the Internet. New projects include:

- **MKII updated universal QRP transmitter**
 - **MicroR2 receiver and MicroT2 transmitter**
 - **ID-O-Matic**—10-minute ID timer for individual, repeater or beacon control
 - Simple computer-to-transceiver **serial port interface** and **USB interface**
 - **Keying adapter** to interface vintage radios with modern gear (CW keying or amplifier TR keying)
- Plus**, new filter theory and design examples, including a **HF/6 meter high-power low-pass filter project** and revised and expanded RF safety content.

CD-ROM Included! This edition is bundled with **The ARRL Handbook CD (version 12.0)** – includes the fully searchable text and illustrations in the printed book, as well as companion software, PC board templates and other support files.

Order Today www.arrl.org/shop
or Toll-Free **1-888-277-5289** (US)

2008 ARRL Handbook (Softcover). Includes book and CD-ROM
ARRL Order No. 1018 **\$44.95***

*shipping: \$10 US (ground)/\$15.00 International



ARRL The national association for
AMATEUR RADIO

225 Main Street, Newington, CT 06111-1494 USA

SHOP DIRECT or call for a dealer near you.

ONLINE WWW.ARRL.ORG/SHOP

ORDER TOLL-FREE 888/277-5289 (US)

KENWOOD

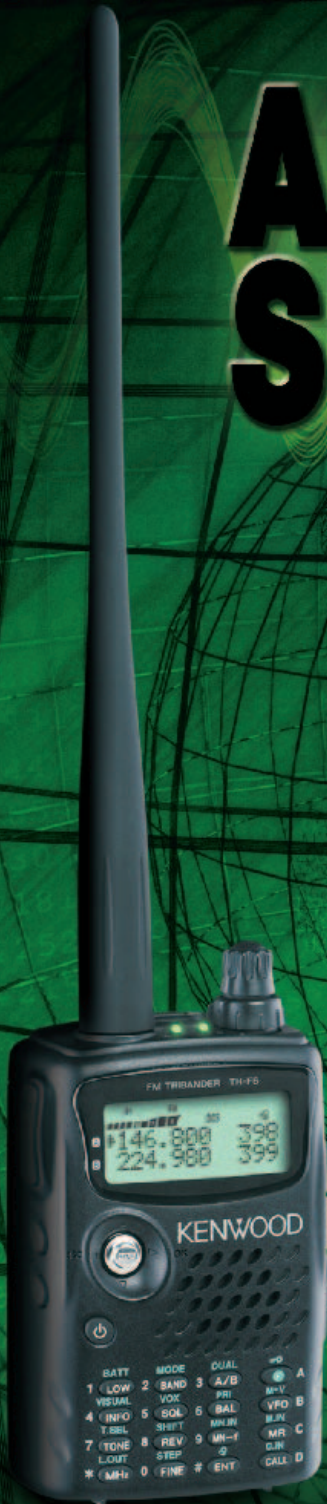
Listen to the Future

AIRWAVE SUPERIORITY

Never before has a compact HT offered as many features, and such high powered performance as the TH-F6A. Arm yourself with one today and gain your own airwave superiority.

- Triband (144/220/440 MHz)
- Receives 2 frequencies simultaneously even on the same band
- 0.1~1300MHz high-frequency range RX (B band)¹
- FM/FM-W/FM-N/AM plus SSB/CW receive
- Bar antenna for receiving AM broadcasts
- Special weather channel RX mode
- 435 memory channels, multiple scan functions
- 7.4V 1550mAh lithium-ion battery (std.) for high output² and extended operation
- 16-key pad plus multi-scroll key for easy operation
- Built-in charging circuitry for battery recharge while the unit operates from a DC supply
- Tough construction: meets MIL-STD 810 C/D/E standards for resistance to vibration, shock, humidity and light rain
- Large frequency display for single-band use
- Automatic simplex checker
- Wireless remote control function
- Battery indicator • Internal VOX • MCP software

¹Note that certain frequencies are unavailable. ²5W output



TH-F6A

TRIBANDER

KENWOOD U.S.A. CORPORATION

Communications Sector Headquarters

3970 Johns Creek Court, Suite 100, Suwanee, GA 30024

Customer Support/Distribution

P.O. Box 22745, 2201 East Dominguez St., Long Beach, CA 90801-5745

Customer Support: (310) 639-4200 Fax: (310) 537-8235



www.kenwoodusa.com
ADS#21408



JQA-1205 091-A
ISO9001 Registered
Communications Equipment Division
Kenwood Corporation
ISO9001 certification